COTTON ROOT ROT IDENTIFICATION & DELINEATION BASED ON UAV PLATFORM

A Dissertation

by

TIANYI WANG

Submitted to the Office of Graduate and Professional Studies of
Texas A&M University
in partial fulfillment of the requirements for the degree of

DOCTOR OF PHILOSOPHY

Chair of Committee,	J. Alex Thomasson
Committee Members,	Thomas Isakeit
	Stephen W. Searcy
	Marian Eriksson
Head of Department,	Stephen W. Searcy

August 2020

Major Subject: Biological and Agricultural Engineering

ABSTRACT

Cotton Root Rot (CRR) is a severe cotton disease in Texas and the southwestern U.S. It kills cotton and other dicotyledonous plants so quickly that the death of the plant may be the first observable symptom. CRR cannot be cured within season, but spraying flutriafol fungicide next to the seed during planting controls the disease effectively. A previous study indicated that CRR typically reoccurs at the same location in fields, so historical location information can guide the grower on where to apply the fungicide more efficiently and to minimize environmental risk. Manned aircraft remote sensing has been proven capable of providing CRR location distribution information.

Because image data from manned aircraft tend to be expensive and have low spatial resolution compared to images from unmanned aerial vehicles (UAVs), three studies were undertaken to develop the capability of UAV remote sensing to determine CRR location in cotton fields so that fungicide can be applied in a precise manner. Study I was conducted to explore the possibility of using the UAV based remote sensing data to delineate CRR-infested areas and generate a prescription map. The result demonstrated that UAV remote sensing can be used effectively for this purpose, and can significantly reduce the amount of fungicide applied.

Study II was conducted to develop methods to improve the image processing methods used to identify CRR in UAV remote sensing data in an effort to take advantage of their inherently high spatial resolution. Conventional classification methods used with manned-aircraft data do not work well on UAV data, because the higher resolution

results in additional classes of image pixels like bare soil and shadows between crop rows. In this study, two new regional classification methods were developed which can accurately and automatically identify CRR-infested areas with high-resolution UAV remote sensing data. The results demonstrated that the new proposed methods are superior for CRR detection in UAV images compared to conventional classification methods.

Study III was an attempt to make further use of the high resolution of UAV data by creating a plant-by-plant level CRR identification method. The desire is to make fungicide application as precise as possible, even potentially at the level of individual plants, so as to minimize the amount applied, saving cost and reducing environmental risk. The results of this study illustrated that the plant-by-plant image classification method can identify individual plants and determine whether they are infected or not with high accuracy.

All of these studies were funded by Cotton Incorporated, Cooperative Research Agreement number 16-233.

DEDICATION

I dedicate this dissertation to those people who love and care about me. You let me feel not alone in this world.

To Grandma,

who just passed away and loved me the most in this world.

To my wife,

who just married me and dedicated her happiness of rest life to me.

To Mom and Dad,

who gave me a chance and always offered me endless supports to understand this world.

ACKNOWLEDGMENTS

I would like to thank all my committee chair and members, Dr. Alex Thomasson, Dr. Chenghai Yang, Dr. Thomas Isakeit, Dr. Stephen W. Searcy, and Dr. Marian Eriksson for their kindly guidance on this research,

I would like to give a special thanks to my advisor, Dr. Alex Thomasson, for leading me into this research area that I'm interested in, always inspiring me, and offering me help patiently.

Thanks also go to my friends and colleagues who helped me a lot in my study experience at Texas A&M University.

Last but not least, thanks to my family for their unrequited supports.

CONTRIBUTORS AND FUNDING SOURCES

Contributors

This work was supervised by a dissertation committee consisting of Professor J. Alex Thomasson [advisor], Professor Stephen W. Searcy, and Professor Chenghai Yang of the Department of Biological and Agricultural Engineering and Professor Thomas Isakeit of the Department of Plant Pathology and Professor Marian Eriksson of the Department of Ecosystem Science and Management.

The 2015 data in Chapter 2 were collected with the help of Professor Dale Cope, and the 2017 data in Chapters 2,3, and 4 were collected with the help of my colleagues. The fungicide effectiveness plot-test in Chapter 4 was conducted with the help of Professor Thomas Isakeit and Ryan Collett.

All other work conducted for the thesis (or) dissertation was completed by the student independently.

Funding Sources

Graduate study was supported by an assistantship from Texas A&M University.

This work was also made possible in part by Cotton Incorporated under Cooperative Research Agreement Number 16-233.

NOMENCLATURE

AGL	Above ground level
CH	Chase
C-U	combined-unsupervised
G_i	total number of pixels classified as Class i in ground-truth data
i	class number
KM	k-means
k	kappa coefficient
MD	minimum distance
MHD	Mahalanobis distance,
ML	maximum likelihood,
N	total number of pixels
PA	proposed automatic
PBP	plant-by-plant
P_i	total number of pixels classified as Class i in the predicted data
S	supervised
SH	School House
$t_{i,i}$	correctly classified number of pixels in Class i
U	unsupervised
WP	West poncho

TABLE OF CONTENTS

Page

LIST OF FIGURES

LIST OF TABLES

Page

1. INTRODUCTION

1.1. Background

Cotton is a shrub plant of the genus Gossypium belonging to the family Malvaceae that originally grew in the subtropics and tropical regions of the Americas, India, China, etc. In its reproductive stage, flowers appear on the plant and then wilt, and a small green capsule called the cotton boll remains where a flower was situated. Cotton seeds are produced inside the cotton boll. As the boll matures, small fibers begin to protrude from the surface of the seed. These white fibers gradually fill the boll, which opens when fully mature, leaving the cotton fiber to dry in the air. The fiber, en masse, is a very important raw material for producing cloth for garments, carpet, and other knit goods. The use of cotton fabric can be dated to 5000 BC. Since that time, cotton has promoted the progress of human civilization and greatly influenced the culture.

The U.S. is one of the top cotton-producing countries in the world and is the largest cotton exporting country. According to the final 2017 USDA crop estimates (2017-18), the U.S. produced 20.92 million 480-lb bales, ranking 3rd after India and China (Figure 1.1). The production value of U.S. cotton was 7.22 billion in that year [1].

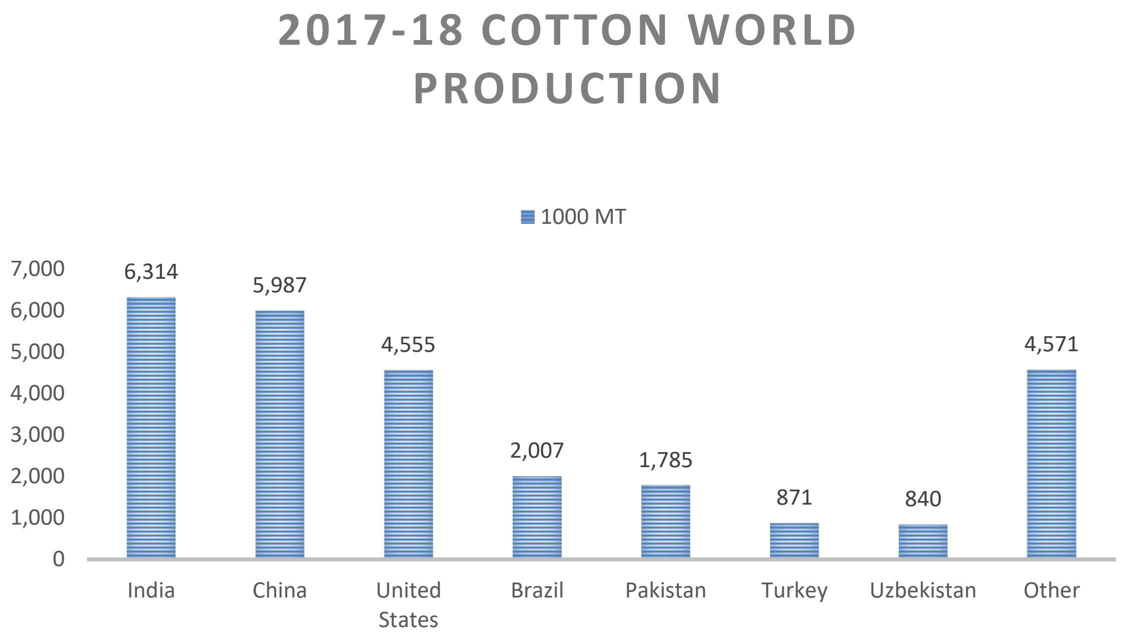

Figure 1.1 Cotton production by country worldwide in 2017/2018 in 1,000 metric tons [2] **(referred from USDA-NASS https://downloads.usda.library.cornell.edu/usda-esmis/files/kp78gg36g/4q77fw02f/hx11xk098/cotton.pdf)**

The state of Texas is located in the so-called "Cotton belt" of the U.S., which is known for its high production of cotton from the 18th to the 20th century. From the 2017 USDA-NASS (National Agricultural Statistics Service) report [1]. of Texas agriculture overview, the state of Texas produced 9.523 million bales of cotton, ranking 1st in the U.S. in 2017 [1]. This amount is approximately 44.4 % of U.S. cotton production; Georgia produced 2.23 million bales, ranking second (Figure 1.2). Texas's cotton production amounted to around 3.40 billion U.S. dollars that year. In sum, cotton is a very important commercial crop in the U.S. as well as in the state of Texas.

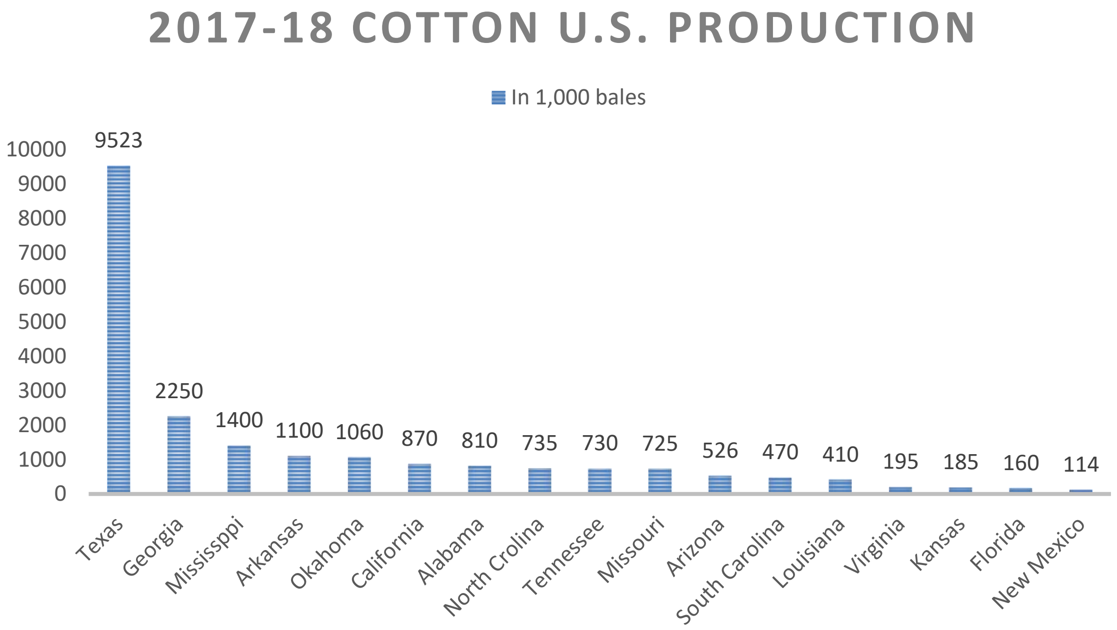

Figure 1.2 Leading 10 U.S. states for cotton production in 2017 in 1,000 bales [2] **(referred from USDA-NASS https://downloads.usda.library.cornell.edu/usda-esmis/files/k3569432s/f4752k06n/th83m180b/CropProdSu-01-12-2018.pdf)**

One of the greatest obstacles to cotton production in Texas is a disease called cotton root rot (CRR) or Texas root rot, which is caused by the soil-borne fungus Phymatotrichopsis omnivora, and is a very destructive plant disease throughout the southwestern region of the U.S. It was first observed in 19th century by Pammel [3]. CRR has been studied extensively and was first observed in Arizona in September 1928 [4]. Annual losses associated with CRR have been reported to be as high as $29 million in Texas [5].

The Phymatotrichopsis fungus is thermophilic and more common in alkaline soils (PH:7.2-8.5) and high moisture environments. When ammonium salts have been used as a crop nitrogen source in the solution, the growth of the fungus has been notably restricted, because both the mycelial and sclerotial stages of the fungus were killed by short exposure to the gas [6]. Most of the infected plants were dicotyledonous.

The fungus is a soil-borne organism, not restricted to living roots, but having independent means of over-wintering and spreading. It spreads through root contact between plants and growth of mycelia in the soil [7].

The sclerotia can survive in soil up to 7 feet deep for many years. In suitable environmental conditions, the sclerotia germinate and eventually contact the roots of the plants [5].

The fungus usually kills the plant within ten days [8] of infection. If the disease occurs at the early stage of growth, the plants will die before bearing fruit. Otherwise, the disease will reduce the cotton yield and lower the quality of the lint. Based on the observations, the area of cotton infected with CRR increased 10%-50% from the border of the initial infected area through the season (Aug to Sept.). Control practices have been neither economical nor effective (Ron Smith, 2004). However, since CRR occurs in roughly the same field locations each year, zones of infection can be predicted.

It is impossible to get adequate information about the extent of CRR infection from the ground because of the large size of infected areas and their irregular shapes. Therefore, remote sensing (RS) technology has been applied to CRR detection research [9]. Multispectral and hyperspectral imaging have both been used to distinguish infected areas from non-infected areas, but 3-band multispectral images work well and thus appear to be appropriate because they are less expensive and more widely available [9].

1.2. Literature Review

1.2.1. Aerial and satellite remote sensing (RS) may be options for detection

In agricultural fields, RS may involve aerial or satellite images. RS data including visible, near-infrared (NIR), and shortwave infrared (SWIR) have been studied widely to understand many crop phenomena [10].

Aerial RS has been used to estimate crop yield. Read et al. used remote sensing to study the relationship between potential cotton yield and soil properties [11]. The experiment was conducted on a 104-acre dryland field in east-central Mississippi with an annual average of 1422 mm precipitation. The field was in a soybean-cotton rotation, with 50,000 seed/acre seeding rates in the cotton-growing seasons of 2001 and 2002. Multispectral images were obtained from two third-party companies in June 2001 and June 2002. The manned aircraft surveyed at 3650-m altitude and achieved 2 m^2 /pixel spatial resolution in 2001. The aircraft carried a 3-band multispectral camera that was sensitive to green (540 ± 20 nm), red (695 ± 20 nm), and NIR (840 ± 20 nm) band reflectance. A better resolution 0.5 m2 /pixel was obtained at 1824 m altitude in 2002. The camera system was also sensitive to green (550 ± 5 nm), red (650 ± 5 nm), and NIR (850 ± 10 nm). NDVI maps, derived from the multispectral images, indicated a strong relationship between plant growth and lint yield. Yang and Everitt (2012) also used a hyperspectral system to help estimate crop yield variation[12]. The charge-coupled device (CCD) camera collected spectral data containing 102 usable bands from

457.2 nm to 921.7 nm bandwidth with a 3.63 nm interval. Two-band and three-band hyperspectral vegetation indices (VIs) were derived from the hyperspectral image data to characterize crop variation. The results indicated VIs derived from a green and NIR combination, and a NIR and red edge combination performed better than traditional a red and NIR combination on yield prediction.

Research has also indicated that RS is able to monitor weed infestations. Sui et al. developed a ground-based proximal weed mapping sensing system, and RS was used to test the system[13]. The study was conducted on the 13-ha cotton field at Stoneville, Mississippi. The image was collected by a 3rd party company (Geodata Inc.) at 1300-m altitude. The camera system included red (450nm), green (550nm), red (650nm), and NIR (850nm) bands with 0.5m spatial resolution. The image was mosaicked in Erdas imagine software. NDVI maps were generated from multispectral image data. The research not only demonstrated that crop canopies and weeds between rows have a strong relationship to RS images, but also indicated that RS could detect the differences from different land covers. The ability to distinguish between cotton and weed is sufficient for distinguishing between healthy cotton and CRR-infested cotton.

Aerial and satellite RS have also been used to assess cotton. Gogineni and Thomasson used satellite and airborne remote sensing data with a cotton growth model [10]. Landsat 7 satellite data consisting of blue, green, red, and NIR bands with 30 m spatial resolution were used. Aerial images were obtained biweekly from May 12th to September 15th with a multispectral sensor sensitive to blue, green, red, and NIR bands and had 0.5m spatial resolution per pixel. The multispectral images were georectified, and NDVI maps were derived from them. The NDVI maps were used as a proxy for plant height in a cotton yield prediction model. With feeding RS derived plant height information, the yield prediction model got improvement. Yang (2011) used a 3-CCD camera composite color-infrared (CIR) system to survey 105-ha, and 55-ha center-pivot irrigated cotton fields in Corpus Christi, TX. The ground resolution of the aerial images was 0.2 to 0.3 m/pixels. The results indicated that aerial CIR RS data can monitor the status of cotton crops in the field and was more efficient and reliable than ground-based reflectance data on assessing cotton defoliation and regrowth control.

Aerial and satellite RS have previously been used to detect disease in the field. Chen (2007) used Landsat satellite data to detect take-all disease in wheat, which causes considerable wheat yield decreases in China. The chlorophyll level of infested plants affects the spectral reflectance. Compare to the spectral reflectance curve of healthy wheat, the reflectance of NIR decreases, and then no ‘red edge’ is evident in the spectral curve, and the reflectance peak in the NIR will disappear. The result indicated that the NDVI derived from RS image is able to detect the root disease. One of the symptoms of take-all disease is stunting and yellow leaves, which is similar to CRR. Calderon used high resolution airborne multispectral (450, 490, 530, 570, 670 and 800 nm), hyperspectral (260 bands at 1.85 nm/pixel), and thermal RS (8–12 μm) to early detect *Verticillium* wilt (VW) of olive, which like CRR is also caused by a soil-borne fungus [14]. It indicates that physiological hyperspectral indices and canopy temperatures are more related to physiological stress caused by VW, while structure indices such as NDVI were more related to structural damage caused by VW. Apan et al. used Hyperion satellite hyperspectral imagery to detect the orange rust disease in sugarcane [15]. The visible near-infrared based indices such as Structure-Insensitive Pigment Index (SIPI) have significant separability for orange rust disease infected sugarcane.

In addition to foliar pathogen diseases, some root diseases are also able to be detected with RS. Fletcher et al. used CIR (NIR, red, green) airborne digital imagery taken from 3.7m AGL height to detect Phytophthora root rot infection of citrus trees, which leads canopy defoliation, leaf yellowing, and twig dieback [16]. Cook et al. used airborne CIR video to detect Phymatotrichum root rot (PRR) and the root-knot nematode of kenaf. The result indicates the NIR band had the potential to identify and monitor the progression of PRR [17].

It is clear that aerial and satellite remote sensing has been widely studied for uses in agricultural production. The VIs derived from spectral imagery is useful for yield estimation, crop status monitoring, and field management. Most satellite images used in agricultural studies have from 5 to 30m/pixel resolution. Many are available free of charge, and historical data may be easily acquired. On the other hand, satellite remote sensing is limited by temporal resolution and cloud coverage. There is a risk that clouds may obscure the satellite's view when it is taking images over a certain area. Satellite images also commonly have low temporal resolution, and image collection frequency is reduced whenever cloud cover impairs image collection on a particular day. Aerial RS makes an excellent compensation on this. Imagery collected with aerial RS can be obtained the weather permits anytime, and cloud cover often does not obscure aerial RS, but it does create problems with shadows in the images. Aerial RS data can be from 0.2 to 2.0 m/pixel resolution, depending on flight altitude.

Image errors can be caused by numerous problems, including those introduced during the mosaicking of the images or the attitude of aircraft during flight [10]. Green, red, NIR, and red edge are popular spectral bands used in agricultural study. The VIs derived from combinations of these spectral bands are commonly used in agriculture. Plant height, leaf-area index (LAI), and evapotranspiration (ET), also can be developed from RS data.

1.2.2. CRR has been documented with remote sensing

Taubenhaus et al. were the first to report using remote sensing for the study of cotton root rot. An infected cotton field was photographed from an airplane with a handheld camera [18]. The aircraft flew between 10:00 A.M. and 3:00 P.M. local time at 250 to 500 ft altitude. A commercially available black and white (B&W) panchromatic film camera was used. The results indicated that ground-based photographs were challenging to use for monitoring damage from cotton root rot, but aerial photographs could provide views of cotton root rot infection over a large area.

Nixon et al. introduced CIR film photography to the tasks of documenting the distribution of cotton root rot infection and detecting the effect of chemical treatment for root rot [19]. The film was sensitive to NIR, visible light, and UV light. Four CIR photos were shown in the results. All of the photos were captured from an airplane between 11:30 A.M. and 3:00 P.M. local time. The flying above ground level (AGL) heights used were 15000, 2000, 800, and 500 ft. All the images could be used to delineate cotton root rot well. A multispectral video image of cotton root rot was evaluated in 1987 [20]. They used for cameras that are sensitive from 400nm to 1500nm waveband at 900m and 1800m altitude height. The result indicated that Infrared and red band images showed the infested area better than the green band. The infrared band also showed an infested area better than the red band image. However, the reflectance of infrared may be impacted by exposing more shadows and soil, which were caused by drooping of foliage.

Yang et al. began to consider the possibility of precision application of fungicide to mitigate CRR only in the infected zones of a field [21]. They used remote sensing to observe cotton root rot disease on a 105-ha center-pivot irrigated cotton field and a 39-ha rainfed cotton field located near Corpus Christi, TX. An 8-bit 3-CCD digital camera system was used. This camera system could observe the crop in green (555-565 nm), red (625-635 nm), and NIR (845-857 nm) bands. A single-engine manned aircraft carried the sensor at 3000m altitude and surveyed the field between noon and 2:00 P.M. local time. The ground resolution was 1.3m/pixel. Raw images were geographically registered and rectified, and then assessed with ERDAS IMAGINE software. As a result of the larger reflectance difference between healthy and infected plants in the red band relative to the green band, Yang pointed out that the red band performed better than the green in cotton root rot detection. Overall, the CIR images could easily distinguish the CRR infested area from the healthy cotton area. An unsupervised 2-class classification was made based on aerial images. The results indicated that highly accurate CRR detection could be achieved with aerial remote sensing in the absence of other biotic and abiotic factors. It has been reported that CRR can spread at a speed of 1.5 to 9 m per season [7]. Thus, when Yang et al. developed preseason fungicide-application maps based on remote-sensing data from a prior year, they added a buffer area around the CRR zones in the field.

Yang et al. used remote sensing to map cotton root rot again in 2015 [22]. They used a sensor system composed of four individual charge-coupled device (CCD) digital cameras with a PC. Each camera was able to provide 12-bit image data with 2048 x 2048 pixels corresponding to sensing blue (430-470mm), green (530-570mm), red (630-670mm), and near-infrared (810-850mm) bands. The image data were collected from a single-engine airplane at 3050m altitude. The ground resolution was 0.9 m/pixel.

Yang et al. used three imaging systems in this study. Besides a 2-camera system (RGB, NIR), they also used the 3-camera (G, R, NIR) and 4-camera (R, G, B, NIR) imaging systems mentioned above to capture the multispectral images at 3050 m AGL altitude height from a single-engine aircraft [23]. All captured images were resampled into 1m resolution. An NDVI ISODATA classification map was derived from the 1.0 to 1.3 m ground resolution images. A 3 to 12 m distance buffer area proved to be appropriate based on this level of resolution. Two classification maps of two dates were overlaid to detect changes. The results indicated that CRR occurred in the same general area, even after ten years. This finding illustrates that historical remote sensing data can be helpful in predicting the CRR infection area.

Hyperspectral RS could be used for CRR detection. In 2010, Yang et al. compared airborne hyperspectral to multispectral imagery for mapping CRR. A 97.7-ha semicircular field and a 54.5-ha circular field located near Edroy, TX, were studied [9]. The camera system used for multispectral data collection was the same as described above in the Yang 2005 study. A SuperVGA Sensicam digital CCD camera was used to capture the 12-bit depth hyperspectral image data in 128-bands (457 – 922 nm). Yang et al. (2011) used the same hyperspectral camera to collect data in Corpus Christi, TX, in 2001 and 2002 [24]. The systems were carried by manned aircraft flying between 11:30 A.M. and 2:30 P.M. local time under sunny conditions. The multispectral images had 0.2 to 1.2 m/pixel spatial resolution, while the hyperspectral images had 2.4m/pixel resolution. Results indicated that both multispectral and hyperspectral remote sensing could be used to delineate CRR. Yang found multispectral remote sensing was more suitable for CRR detection because of its lower cost and more convenient processing.

Satellite remote sensing has also proven useful in detecting CRR. Song et al. used a 10m resolution Sentinel-2A multispectral instrument (MSI) images [25]. These images contain 13 bands, including visible, NIR, and SWIR. They used blue, green, red, and NIR image bands and conducted ISODATA unsupervised classification was used to analyze the data. They were able to detect CRR for large zones of the disease. However, the method sometimes misclassified zones of CRR as non-CRR and small healthy zones surrounded by CRR because of the low image resolution. Wu et al. also used Sentinel-2 data to monitor the progression of CRR within the season [26]. The result indicates that NDVI is a useful index for monitoring the progression of CRR.

Previous research has indicated that airborne and high-resolution satellite multispectral imagery can be used successfully to detect CRR infected areas in both dryland and irrigated fields. However, the ground spatial resolution of these data is generally from 1 to 10 m, not high enough to enable plant by plant-level mapping. The flying height of the sensor platform affects the image resolution. The higher required altitudes for these platforms, thus, degrade the resolution. No literature is currently available about low-altitude RS, such as with a UAV, for CRR delineation.

Yang et al. used the four-camera multispectral imaging system mentioned above to monitor CRR as it progressed in a field. This study revealed that multispectral imagery, along with unsupervised classification is useful for monitoring CRR infection in the field [27].

Wu et al. used Sentinel-2 satellite data to monitor the progression of CRR within the season [26]. They used a fusion method called improved spatial and temporal data fusion approach (ISTDFA) to combine the 250-m Moderate Resolution Imaging Spectroradiometer (MODIS) NDVI image and the 10-m Sentinel-2 NDVI image to generate time series map and improve the spatial and temporal resolution of the data. The result indicated that the ISTDFA had a good correlation coefficient on combining the time series MODIS and Sentinel-2 NDVI data.

Yang et al. used multispectral remote sensing to monitor CRR infection and the effects of fungicide treatment [8]. Three camera systems were used in this study. A three-camera imaging system collected green (555-565 nm), red (625-635 nm), NIR (845-857 nm) band images. A four-camera imaging system covered blue (430-470 nm), green (530-570 nm), red (630-670 nm), and NIR (810-850 nm) bands. And a two-camera imaging system included blue, green, and red bands with an additional 720nm long-pass filter to obtain a NIR band. All images were collected at 3048 m AGL altitude height with 1.0-1.3m ground resolution. At this resolution, multispectral remote sensing is able to monitor CRR infection as well as fungicide treatment applications. Topguard (flutriafol) fungicide sprayed at 2.34 L/ha (full rate) proved efficient on CRR. Reduced rate to 1.46 L/ha (2/3 full rate) didn't work efficiently as the full rate. Compared to the dryland field, the response of fungicide was more consistent in the irrigated field.

1.2.3. Various imaging and analysis techniques have been used to map CRR

NDVI and the NIR band have been used to produce estimated field maps of plant height, leaf area index and yield, offering a potentially attractive mid-season management tool for site-specific farming in dryland cotton [11]. For yield estimation, Vegetation indices (VIs) based on NIR and red-edge band combinations or NIR and green band combinations have sometimes shown better performance than the traditional red and NIR combination. Normalized difference vegetation index (NDVI) is very commonly used in remote sensing for agricultural applications.

$$NDVI = \frac{(NIR-RED)}{(NIR+RED)} \tag{1}$$

NDVI integrated over time has shown significant correlations with lint yield [13].

Classification is a statistical method to organize data into different classes based on features of the data. In remote sensing, two main classification categories are supervised and unsupervised. In 2005, Yang used an unsupervised 2-zone clustering method to classify aerial images. Yang et al. (2014) applied the Iterative Self-Organizing Data Analysis Technique (ISODATA) as an unsupervised classification method on multispectral images to generate 9-class and 16-class images to detect CRR [8]. In 2016, Yang et al. used the ISODATA unsupervised classification on NDVI maps to generate 2-zone images to detect CRR [23]. In 2015, unsupervised ISODATA was applied on both multispectral images and NDVI maps to generate 2-class CRR infection images. Supervised classification such as Support Vector Machine (SVM), Mahalanobis distance, minimum distance, maximum likelihood, neural network, and Spectral Angle Mapper (SAM) were also compared. The results indicated that all eight classification methods could achieve good results, and unsupervised classification applied to multispectral images was accurate at detecting CRR [22]. In 2017, Song et al. also used the ISODATA unsupervised classification to assess the Sentinel-2A satellite data to detect CRR. And the results turned out that the classification had high overall accuracy. But the coarse spatial resolution of the Sentinel-2A satellite data made some small CRR areas and non-infested areas misclassified [25].

Change detection is a term for common methods of monitoring changes in a specified area over time. Yang et al. (2016) used change detection to assess the progress of CRR between 2001 and 2011 were compared [23]. The results indicated that CRR tends to show up in the same general areas across many years. If one were to take into account the potential expansion of the disease when developing fungicide prescription maps, a buffer area could be applied around the infection area.

1.2.4. Variable-rate application of fungicide has been made based on prescription maps

Variable-rate technology (VRT) can automatically adjust spray rates of agricultural inputs based on crop needs at a particular location. It can reduce labor and cost on spraying by saving unnecessary spraying, but it requires a fairly high precision positioning system such as GPS [28]. Yang (2014) et al. used VRT on CRR treatment [8]. Zero or full rate fungicide was applied when the sprayer drove into non-infested and infested areas, respectively. Considering the possibility of expansion of a CRR infection area, a buffer zone around infested areas needs to be used in creating prescription maps. The distance of the buffer zone is decided based on image resolution and equipment size and precision capability. Buffer zone distances from 0 to 10 m were assessed. A five-meter buffer area was appropriate in relation to the 1m ground resolution of the imagery.

1.2.5. UAVs can provide high-resolution imagery

Low altitude remote sensing (LARS) is able to provide images with higher spatial resolution, which can provide more information for agricultural production. Since unmanned aerial vehicles (UAVs) were introduced into agricultural remote sensing, the spatial resolution is improved along with temporal resolution [29] (Figure 1.3), since UAVs can be flown the weather permits anytime. Piloted aircraft are a conventional way to acquire canopy imagery. They can typically carry large and heavy equipment such as sophisticated sensors and cameras. Piloted aircraft applications need an automatic image triggering system. Compared to manned aircraft, UAVs have a limited payload capacity. However, they can fly lower and slower than manned aircraft. The above-ground height is commonly 20 to 100 meters. As a result, it is able to obtain higher spatial resolution. In addition, UAV flights cost less than traditional manned aircraft remote sensing.

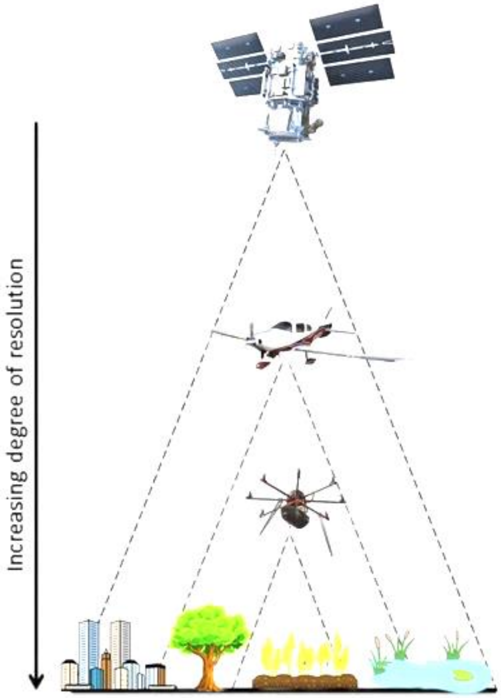

Figure 1.3 The height of sensor will affect the collected imagery resolution

Huang et al. (2016) used UAV remote sensing for crop production management. An X8 octocopter rotary-wing UAV with a GoPro HERO3+ camera was used. The UAV was able to carry an 800 g payload and fly for 15 min. The resolution was 2.7cm/pixel at

45 m AGL. Five hundred fifty images were captured to study soybean injury in response to different doses of dicamba herbicide. Sixty images were selected for mosaicking. NDVI could not be calculated because the camera had no NIR band. Normalized difference photosynthetic vigor ratio (NDPVR) was thus derived and used to estimate soybean yield. The relationship between NDPVR and estimated soybean yield is as high as 0.96 R^2.

Zhou et al. used UAV RS to predict rice yield [30]. A multi-rotor MK-Oktokopter was used. The maximum payload was 2.5 kg. An RGB commercial camera and six-band multispectral camera were used. The multispectral camera was sensitive to 490, 550, 680, 720, 800, and 900 nm bands, which correspond to blue, green, red, red edge, and two NIR bands. The multispectral images were collected at 100m AGL, while the RGB images were captured at 50m AGL. The experiment was conducted between 10:00 A.M. and 2:00 P.M. local time. The VIs, including NDVI and VARI, had a good relationship with LAI, which is useful for yield prediction. The 720nm red edge and the 800 nm NIR bands were more effective in predicting yield for grain. Both the multispectral and RGB images are reliable for rice growth and yield estimation. But the VIs derived from multispectral images had higher correlate with grain yield than VIs derived from RGB images.

Albetis et al. used a fixed-wing UAV based RS to detect grape disease in a vineyard [31]. A MicaSense RedEdge camera was used to capture images at 120 m AGL with 85% forward overlap and 70% side overlap. The resolution was 8cm/pixel. Radial basis function (RBF) SVM classifier was used to differentiate diseased from non-diseased areas. Bare soil, shadow, inter-row vegetation and, grape vegetation was classified. The classification accuracies were achieved from 0.97 to 0.99 in four vineyards. The biophysical parameters (BP), the spectral band (SB), and VIs were compared. VIs worked the best on disease discrimination, and BP came next. SB did the worst on disease separability.

Romero et al. also applied UAV RS in a vineyard [32]. A DJI Phantom 3 rotary-wing UAV carried a SEQUOIA multispectral sensor to capture images at 30m AGL, achieving 4cm/pixel resolution. The images contained green, red, red edge, and NIR bands. Pix4D software was used to calculate VIs, and Qgis software was used for geometric correction. An artificial neural network (ANN) was used for estimating water potential.

UAVs can be categorized as a rotary-wing or fixed-wing. Rotary UAVs are more common because they are usually cheaper and easier to use. They also don’t have strict requirements for longer launching and more open space of landing locations, but the coverage area is limited by flying speed and battery life. They have a more stable in-air flight and slower speed and thus are able to generate higher quality mosaicked images. Rotary wing UAVs are used more commonly in relatively small areas of study, such as vineyards. On the other hand, fixed-wing UAVs can cover a larger area because of their higher flying speeds. They are able to cover 60-100 acres area without switching batteries depending on weather conditions. They are more suitable for larger fields with open space. They usually require more landing space as well.

The use of UAVs leads to higher resolution (cm-level) imagery. High resolution can make plant level image analysis, such as object-based classification possible.

Superpixel is an algorithm that segments images into pieces based on shape, color, texture, etc. Each piece can be called a superpixel. In essence, the Superpixel method converts images from pixel-level to district-level and thus belongs to the image segmentation processing category. Superpixel will keep the main features of aggregated pixels and lead the number of processing nodes to decrease sharply. As a result, it can significantly improve the image processing speed.

Sultani et al. used Superpixel to detect objects in pavement images. Different shaped objects such as patches, manhole covers, and markers could be detected efficiently with the Superpixel algorithm [33]. They used Superpixel first to divide the images into many small segments. The features like the histogram of oriented gradients (HOG), co-occurrence matrix (COOC), intensity histogram (IH), and mean intensity (MI) of each superpixel were calculated. HOG and COOC are the texture and shape characteristics, while IH and MI are the intensity variations of each superpixel. Then, SVM was used to generate classification based on each feature.

Superpixel has also been used to detect disease in Agriculture. Zhang et al. used Superpixel associated with the k-means clustering method to recognized plant disease from diseased leaf [34,35]. In 2017, Zhang et al. developed a new method based on the Superpixel algorithm to detect cucumber diseases. The leaf images were divided into superpixels, then applied expectation maximization (EM) to estimate the maximum likelihood and obtain the lesion image. After feature extraction, SVM was used to detect the disease. The result indicated that the proposed method has the highest recognition rate and fastest processing speed among the comparison. In 2018, Zhang et al. proposed a new leaf recognition method based on Superpixel, K-means, and pyramid of histograms of orientation gradients (PHOG) algorithms. The RGB leaf image was divided into segments first by using the Superpixel algorithm. Then K-means clustering was applied to show the lesion section of leaf. PHOG features were extracted and used to recognize the disease. Three apple and three cucumber leaf diseases were used to assess the method. The result indicated that the proposed method is effective and achieved the highest recognition rate among the comparison most of the time.

1.3. Objectives

According to the literature review, remote sensing for CRR has already been conducted based on satellite and manned aircraft platforms. The prescription map can be generated from a remote sensing image whose ground resolution is as high as 1 m/pixel. However, no study has used UAV as a platform to detect CRR and generate high precision prescription maps based on high-resolution UAV imagery data.

UAV based remote sensing provides high-resolution imagery data for CRR. Successful utilize of UAV remote sensing could potentially move a massive further step on precision agriculture. No research has treated CRR in plant-level.

The objective of this study was to (1) demonstrate that UAV image data can be used to build cotton root rot prescription maps with the conventional classification method, (2) propose new regional classification methods that more suitable to UAV image data for

CRR detection, and (3) proposed plant-by-plant level CRR detection and classification methods to identify CRR in the field.

2. UAV REMOTE SENSING TO DELINEATE COTTON ROOT ROT

Abstract. Cotton root rot (CRR) is a persistent soil-borne fungal disease that is devastating to cotton crops in certain fields, predominantly in Texas (TX). Research has shown that CRR can be prevented or mitigated by applying fungicide during planting, but fungicide application is expensive. The potentially infected area within a field has been shown to be predictable, so it is possible to apply the fungicide only at locations where CRR exists, thus minimizing the amount of fungicide applied across the field. Previous studies have shown that remote sensing from manned aircraft is an effective means of delineating CRR-infected field areas. In 2015, an unmanned aerial vehicle (UAV) was used to collect high-resolution remote-sensing images in Thrall, TX, in a field known to be infected with CRR. In 2017, the fungicide was applied based on a prescription map derived from data of 2015. The results show that the prescription map helped to reduce 89.1% of the fungicide applied in the field and potentially saved a cost of $690 USD on fungicide application.

Acknowledgments: We thank Lantian Shangguan, Xiwei Wang, and Roy Graves for helping in data collection.

2.1. Introduction

Cotton root rot (CRR) is a destructive plant disease in the southwestern U.S. that was observed as early as the 19th century [3,4]. CRR is caused by the soil-borne fungus, *Phymatotrichopsis omnivora*, which is thermophilic and thrives in alkaline soils (pH:

7.2–8.5). The fungus spreads through root contact between plants and the growth of mycelia in the soil [7], usually killing a cotton plant within ten days of infection [27] (Figure 2.1). If the disease occurs at an early stage of growth, the plant will die before bearing fruit. If it occurs after flowering, yield and lint quality will be reduced as the plant ceases fruiting processes. The area of CRR infection in a field can exceed 50% as it expands during the growing season [8]. Early attempts to control CRR were neither economical nor effective [36], but flutriafol fungicide was recently found to protect cotton plants if applied before infection, at either planting or an early growth stage. Uniformly applying fungicide to disease-infested fields has become common practice to prevent CRR [37,38]. However, the disease is not homogeneously distributed in fields [37], but it tends to occur at the same field positions each year, so historical positions of CRR incidence can be used to precisely apply fungicide in subsequent years. Variable-rate technology (VRT) is commonly used in fertilizer and fungicide application[37–41], as it can automatically adjust the application rates of agricultural inputs based on crop needs at a particular location, reducing cost by eliminating the unnecessary application of a product. Yang et al. used VRT on fungicide application during planting to control CRR, applying the full rate in known CRR-infested areas and zero in non-infested areas [8].

Figure 2.1 The CRR-infected cotton plants were killed and became wilt and brown.

Remotely sensed images have proven to be useful in distinguishing CRR-infested from healthy field areas in both dryland and irrigated fields [21], providing a record of CRR field positions. The goal of remote sensing for CRR is basically to map dying and dead plants in an infested field, late in the season when the disease is at its full extent. While both multispectral and hyperspectral images have been used successfully in this task, differentiating dead or dying cotton plants from live ones is readily accomplished with color-infrared (CIR) or even visible (RGB) images, so three-band multispectral imagery is appropriate because RGB and CIR cameras are relatively inexpensive, uncomplicated to use, and widely available [9].

Remote sensing has been studied widely as a means of understanding various crop phenomena. In the past, remote sensing was conducted with cameras or other sensors on either manned aircraft or satellites. Satellite images tend to have lower spatial resolution than aerial images but can be readily acquired, commonly for a reasonable cost, at a known orbital frequency. However, cloudy conditions may obscure the area of interest when the satellite is overhead. Aerial images, on the other hand, tend to have higher resolution and flexibility in the timing of image acquisition, but they may be more difficult or expensive to acquire.

Most research on remote sensing for CRR detection has been conducted with manned aircraft. Taubenhaus et al. were the first to report using remote sensing for the study of cotton root rot, photographing an infested cotton field from an aircraft with a handheld camera [18]. Nixon et al. introduced CIR photography to document the distribution of CRR infection and determine the effect of chemical treatment to mitigate it [19]. Multispectral video imagery of CRR was evaluated as early as 1987 [20]. Yang et al. used remote sensing with global positioning system (GPS) technology to precisely map cotton root rot by 2015 [22]. Late-season remote sensing in cotton has also been used to evaluate the effectiveness of defoliation and regrowth control strategies [24].

While the literature indicates that remotely sensed multispectral images can be used successfully to detect CRR-infested areas in cotton fields, the resolution of those images has not been high enough to support highly precise fungicide applications. Typically, CRR zones have been delineated in the images, and buffer strips have been applied around those zones during prescription map development to ensure that small CRR areas are not missed when the fungicide is applied. The thickness of the buffer strip is determined based on image resolution and equipment size and capability for precision application. Buffer strip thicknesses from 0 to 10 m have been evaluated, and a 5-m buffer area has been shown to be appropriate in relation to 1-m image resolution [8]. As precision agriculture advances, however, delineating CRR at a finer scale, even the plant-by-plant level, becomes desirable in order to prevent fungicide application in areas where it is not needed. Unmanned aerial vehicles (UAVs) have recently become an increasingly viable tool for high-resolution remote sensing that could enable the creation of prescription maps for highly precise fungicide application. While a great deal of research has recently been conducted with UAVs in agriculture, no prior research has shown that UAV-based remote sensing can be used to generate a prescription map for CRR fungicide application.

Using remote sensing to develop a prescription map for fungicide application requires classification of a field into CRR-infested and non-infested areas. A major consideration in classification of remotely sensed images is noisy image data. Vignetting and bidirectional reflectance distribution function (BRDF) can cause certain portions of an image to erroneously appear darker or lighter than other portions [42], complicating the task of image classification. UAV remote sensing compounds these difficulties. To create an overall image of a large field, typical in cotton production, many UAV images must typically be mosaicked together. Mosaicking UAV images with vignetting and BRDF can lead to striping noise. However, image-processing techniques like principal component analysis (PCA) can reduce the effect of noise in an image [43,44].

Remote sensing has proven useful for detecting CRR and enabling the generation of prescription maps for fungicide applications, but the cost needs to be low compared to the economic gains from reducing fungicide applications. UAV remote sensing may provide image data for high-resolution CRR detection and prescription map development at a reasonable cost, but the images' high resolution and the required mosaicking may introduce noise issues that make accurate classification difficult. The goal of this study was to demonstrate that UAV remote sensing data can be used to develop a high-quality fungicide prescription map for CRR. Specific objectives included (1) developing methods for generating prescription maps from UAV remote sensing data, (2) applying a UAV-based prescription map on an actual farm, and (3) evaluating the prescription map in terms of effectiveness and economic benefit.

2.2. Materials and Methods

2.2.1. Study site

This study was conducted on a 33.7-ha (83.3-ac) dryland field (Figure 2.2) near Thrall, Texas, with a history of growing cotton in rotation with corn and a history of CRR. The field was planted with cotton in 2015 and 2017, and the plan was to develop a prescription map from 2015 UAV data and use it to apply fungicide at the 2017 planting.

Figure 2.2 The study field is (a) located in Williams County, Texas, (the Texas county map is from Mapsof.net http://mapsof.net/texas/texas-county-map[45]**), named (b) "West Poncho."**

2.2.2. Multispectral image acquisition and ground truth

On August 22, 2015, a cloud-free day, image data were acquired between 10:00 and 15:00 local time with a multispectral camera (1 J3 model, Nikon Corp., Minato City, Tokyo, Japan; Figure 2.3c) modified from RGB to provide CIR images. The specific spectral bands were green at roughly 500 to 560 nm, red at 570 to 640 nm, and near-infrared (NIR) at 680 to 760 nm. This sensor was carried by a fixed-wing UAV (Lancaster model, PrecisionHawk Corp., Raleigh, NC, USA; Figure 2.3a). The sensor collected 4608 × 3072 pixels per image band, giving 3.67-cm/pixel resolution when flown at 120 m above ground level (AGL). The camera was set to autoexposure for the flight mission, and the overlap was set to 70% in forward and sideward directions in the mission-planning software.

On August 20, 2017, a cloud-free day, image data were again acquired between 10:00 and 15:00 local time with a five-band multispectral camera (RedEdge model, Micasense Corp., Seattle, WA, USA; Figure 2.3d) carried by a different fixed-wing UAV (Mapper model, Tuffwing LLC, Boerne, TX, USA; Figure 2.3b). The camera collected 1280 × 960 pixels per image band, giving 7.64-cm/pixel resolution when flown at 120 m AGL. The specific spectral bands were blue at roughly 475 to 500 nm, green at 550 to 565 nm, red at 665 to 675 nm, red edge at 715 to 725 nm, and NIR at 825 to 860 nm. This camera was also set to autoexposure for the flight mission, and overlap was set to 80% in the forward direction and 70% in the sideward direction in the mission-planning software.

On both flight dates, dead plants in apparent patches of CRR were sampled, and evidence of CRR fungus was found on the roots of the plants. Around twenty infected plants were checked in the field each year. These infected plants all had symptoms of CRR including white fungal growth on the main root (Figure 2.4). The fungus was verified as *Phymatotrichopsis omnivora* in the laboratory.

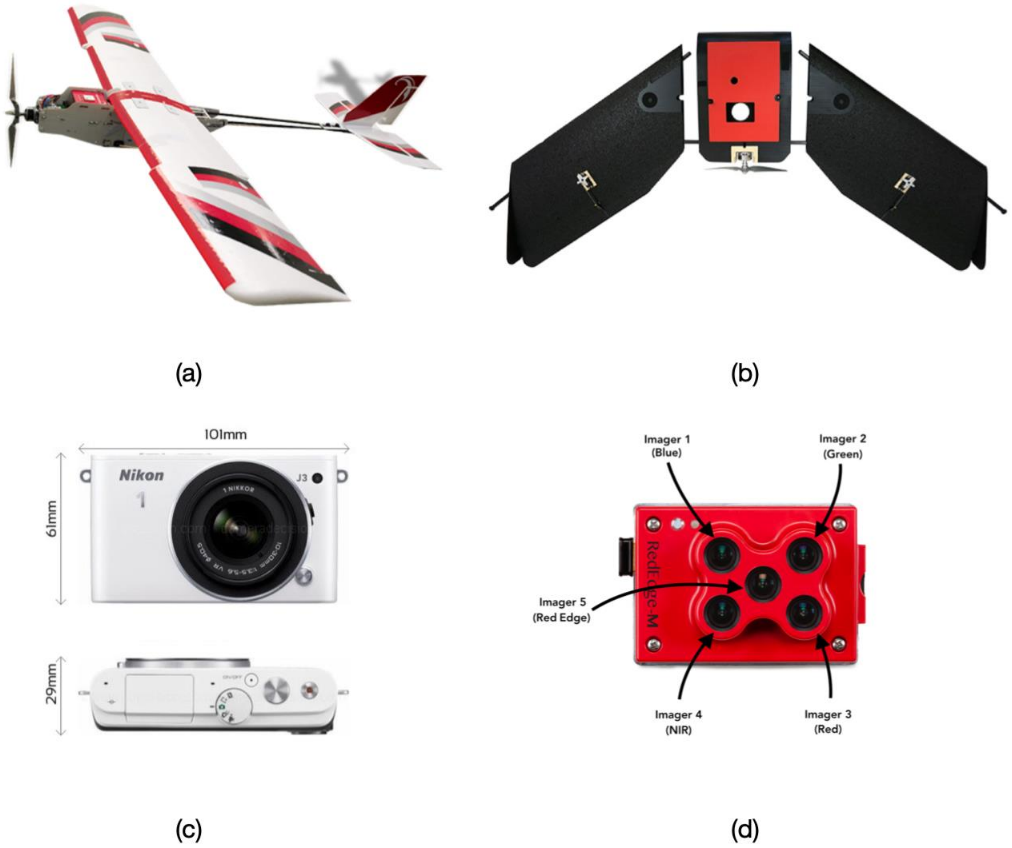

(a) (b) (c) (d)

Figure 2.3 The (a) Precision Hawk unmanned aerial vehicle (UAV) platform with (c) a Nikon 1 J3 sensor was used in 2015, and the (b) Tuffwing Mapper with Micasense sensors were used in the 2017 data collection.

Figure 2.4 *Phymatotrichopsis omnivora* fungal organism (marked with the red circle) was found on a ground-truth dead plant in the field in 2015.

2.2.3. Image Pre-processing and Prescription Map Development

The 2015 images were mosaicked with photogrammetry software (Pix4D Mapper package, Pix4D Corp., Lausanne, Switzerland). The high resolution of the UAV images resulted in some unwanted data classes such as bare ground between planting rows and plant shadows, which made it difficult to directly conduct a two-class classification into healthy and CRR-infested zones. Thus, the image was resampled at 1.0 m/pixel after mosaicking to achieve a resolution similar to that of manned aircraft images. Principal components analysis (PCA) was then applied in image-processing software (ENVI package, Harris Geospatial Solutions Inc., Boulder, CO, USA) to the resampled mosaic to the remove striping noise that was caused mainly by BRDF. To generate a CRR prescription map, the data were processed with the following additional procedures (Figure 2.5).

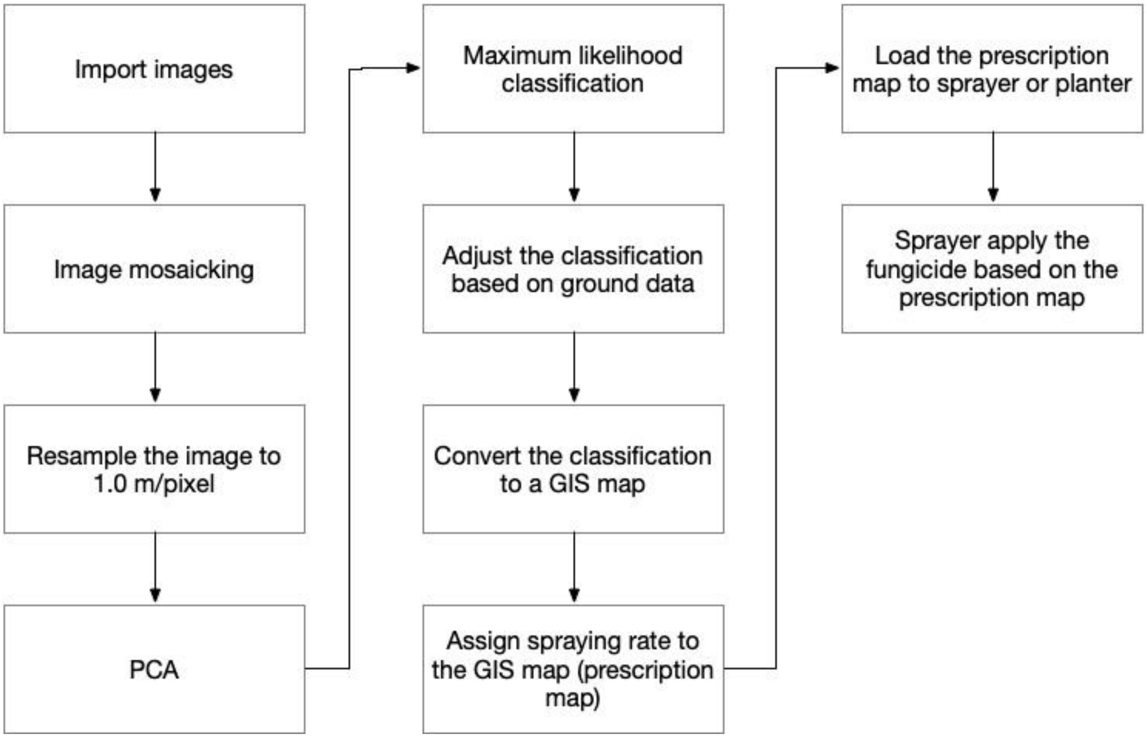

Figure 2.5 The procedure to develop a prescription map in ENVI and ArcMap. GIS, Geographic Information System; PCA, principal component analysis.

The maximum likelihood classifier was applied to the third principal-component image also in ENVI image-processing software. This supervised classifier requires the user to select and label training data [46] to differentiate CRR-infested regions from healthy regions. Ten similar-size regions for both classes, uniformly distributed across the field and approximately 20,000 pixels in total, were manually selected as training data, and the software calculated a classification rule based on these training data. The classification was then executed based on the classification rule. A binary vector map was then generated in geographic information system (GIS) software (ArcMap package, ESRI Corp., Redlands, CA, USA) based on the classification results. Manual manipulation of the size of CRR-infested zones was necessary at a few locations to avoid the influence of known non-CRR causes of bare-soil pixels such as mis-seeding during planting. Such misclassified CRR-infested zones were changed to healthy regions based on ground observations and the spectral and shape features of the zone. For example, CRR zones typically have some amorphous or circular shape, so a long thin rectangular patch of bare soil could be taken as a mis-seeded area and rejected as a CRR zone.

Current spray applicators used in conjunction with cotton planters cannot achieve sub-meter resolution, so very small (< 1.0 × 1.0 m^2) areas classified as CRR-infested were marked as zero-fungicide treatment areas in the prescription map. On the larger infested areas, it is conceivable that they may expand to form an even larger infested area in subsequent years, so a 5.0-m buffer strip, the appropriate buffer thickness indicated by Yang et al.[23], was added around all larger CRR-infested areas. The final classification, generated as a binary raster map, was converted into a shapefile (vector map) in the GIS software, and the CRR application area was roughly 1.9 ha (4.6 ac), about 5.5% of the field. A classification (Figure 2.6a) was generated as a binary raster map and then converted into a vector map (Figure 2.6b).

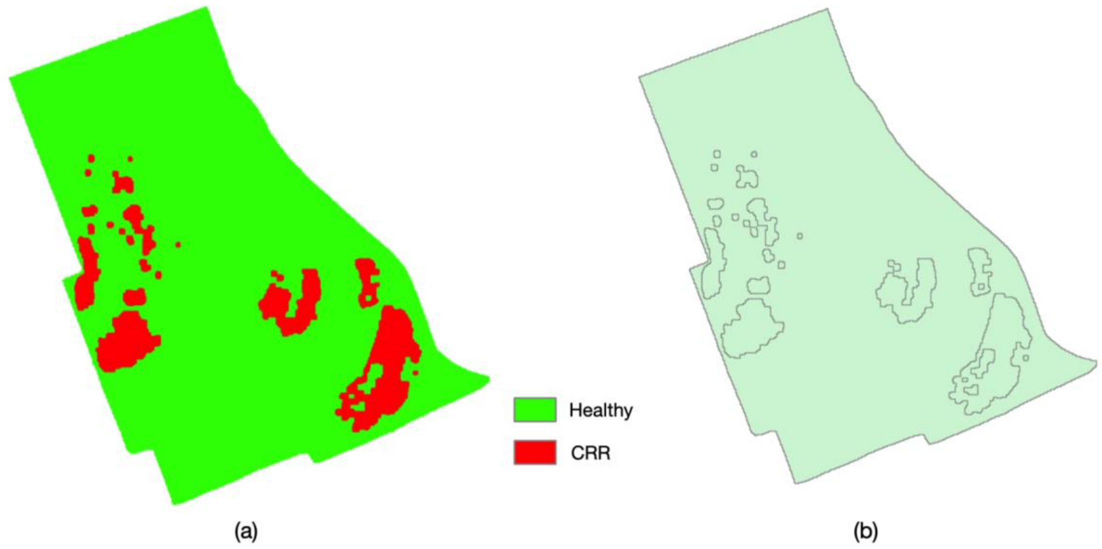

Figure 2.6 (a) A two-class classification raster map was converted to a (b) vector prescription map generated from the data of 2015 and applied to the fungicide spraying of 2017.

2.2.4. Prescription Map Application

The prescription map was loaded into a Trimble Field-IQ spray control system (Trimble, Sunnyvale, CA) on a Case IH Magnum 210 tractor (CNH Industrial Corp., Racine, WI, USA). The tractor pulled a Case IH 1230 Early Riser 12-row planter during planting, and that planter came equipped with a spray system. A customized hydraulic pulse-width modulation (PWM) valve was added to control the spraying (Figure 2.7). The fungicide (Topguard Terra brand, FMC Agricultural Solutions, Philadelphia, PA, USA) was applied in the row along with the seed, and the application was controlled automatically based on the prescription map generated from the 2015 image data. The rate of flutriafol applied to CRR-infested areas was 0.24 L per 0.405 ha (8,0 fl oz/ ac) mixed with water and sprayed at rate of 23 L of liquid solution per 0.405 ha (6.0 gal/ac).

A spray rate of zero was assigned to non-infested areas. The sprayer-control system controlled the sprayer on the planter as two six-row sections. When one planter section moved into a zone classified as CRR-infested, the nozzles on that section began spraying fungicide at the full rate. The nozzles stopped spraying when the planter section exited the CRR-infested zone.

Figure 2.7 CASE IH 1230 12-row Early Riser planter used in the experiment.

2.2.5. Performance evaluation of fungicide application with the UAV-based prescription map

To evaluate the performance of the 2017 fungicide application, which was based on a prescription map generated from UAV image data collected in 2015, image data were collected near the end of the 2017 growing season. The 2017 images were mosaicked in the same way as with the 2015 image data, but two additional quality-control measures were performed on the 2017 data. First, eight ground control points

(GCPs) were used in 2017 to improve the geographical accuracy of the mosaicked image. The GCPs were placed in the field at the four corners and four midpoints of each side. The geographic coordinates of each GCP centroid were collected with a Geoexplorer 6000 (Trimble, Sunnyvale, CA) GNSS receiver and used as references for georectification during mosaicking; the user selected corresponding points on the image mosaic and entered the coordinates into the mosaicking software. Second, a set of three radiometric-calibration reference tiles of light gray (≈45% reflectance), medium gray (≈20% reflectance), and dark gray (≈3% reflectance) were placed next to one of the GCPs. The actual reflectance spectra of the tiles were collected soon after the flight mission with a portable handheld spectroradiometer PSR+ 3500 (Spectral Evolution, Haverhill, MA) and used in mosaicking processing to radiometrically calibrate the mosaicked image. A relationship between the digital number (DN) in the image and reflectance was established with the calibration references, and the image mosaic was converted to a reflectance image with an empirical linear model. To develop ground truth data on the distribution of CRR for the performance evaluation, the CRR-infested areas were delineated manually in the same way as was done with the 2015 data. The locations of infested regions in 2015 were rechecked on the 2017 image to determine whether the CRR showed up again. The locations of the specific infested areas, as well as percent CRR coverage, were compared between 2015 and 2017.

2.2.6. Economic analysis

There are three scenarios for dealing with a CRR-infested field: no treatment, treating the entire field with fungicide, and treating the field with fungicide according to a prescription map. Comparisons need to be made among the costs associated with these three treatment scenarios on a production-size farm: (1) the cost of loss in revenue due to CRR, (2) the cost of fungicide applied to the field, and (3) the cost of developing a prescription map and precisely applying fungicide. These costs were modeled for the three treatment scenarios based on actual data and a few reasonable assumptions. The field under study yielded 243 kg per 0.405 ha (536 lb/ac) in 2017, and the price of cotton fiber is $1.66 USD/kg ($0.755 USD/lb). The cost of the fungicide is $29.65 USD/ha ($12 USD/ac). The control system and hydraulic PWM valve cost approximately $5,000 USD. For image collection, a commercially available rotary-wing UAV with a modified multispectral camera could cost $1,600 USD. Software for image analysis (Pix4D Mapper and ArcMap) costs approximately $3,600 USD, but less expensive software might be available. The cost of labor for an operator to perform image analysis is hard to estimate, but a reasonable assumption for an experienced person of $30 USD/h was made. Roughly 8.0 h were required to generate this 82-ac prescription map, including image mosaicking and classification, as well as prescription map conversion. However, it was estimated that an experienced operator performing these tasks regularly could develop the prescription map for a field in roughly 4.0 h, and this time should be adequate also for a much larger field. The cost of image analysis could potentially be reduced in the future through automation of image classification[47] and other tasks performed with software. The overall cost for the three treatment scenarios was modeled based on these data and plotted to indicate the optimal treatment scenario for production farms of various sizes and numbers of fields and with different yields and proportions of CRR infestation.

2.3. Results and Discussion

2.3.1. Prescription map development

Based on observations of the 2015 image data as validated by the ground-truth data, it was clear that two large CRR-infested areas were located in the southern half of the field. One was on the western side (Spot A) and the other on the eastern side (Spot B) (Figure 2.8a). The removal of striping noise along the UAV flight path in the mosaic by way of PCA can be seen in Figure 2.8b, which shows that the stripes in the original 2015 image mosaic (Figure 2.8a) are not observed in the third principal component image (Figure 2.8b). The original mosaic clearly has erroneous "lines" running in two directions (see red arrows), which resulted from the fact that two flight missions with different flight directions were used to collect the images that made up this mosaic.

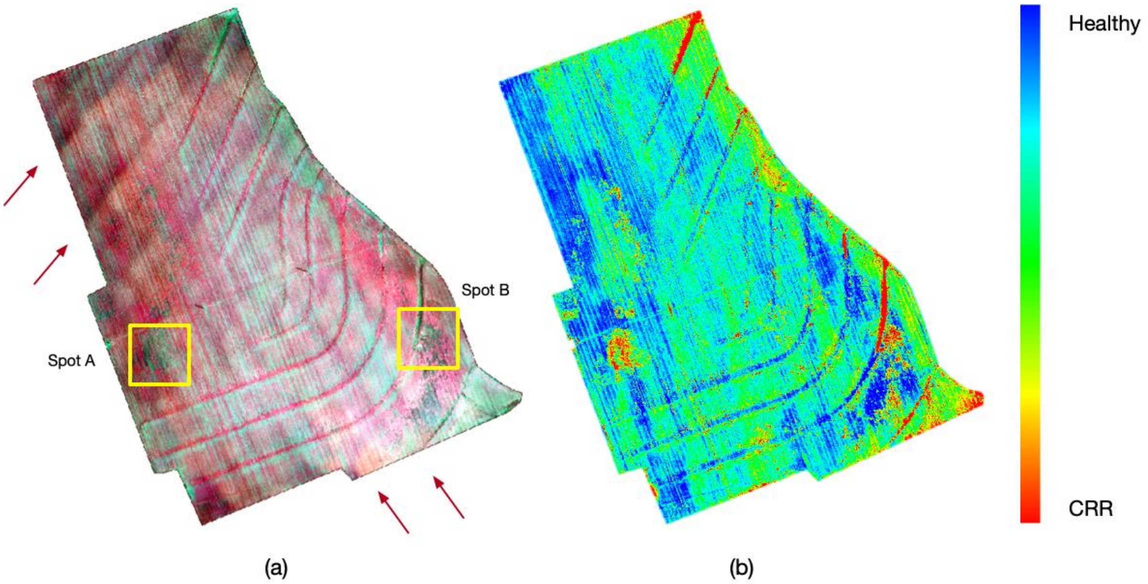

Figure 2.8 (a) Original multispectral image mosaic from 2015, with Spots A and B highlighting the location of CRR-infested areas. The striping noises can be observed from the direction of red arrows. (b) PCA band 3 of the 2015 multispectral image. The striping noises shown in (a) is disappeared.

2.3.2. Prescription map application

When the classified 2015 image of the field was compared to the classified 2017 image of the field, it was clear that a large majority (89%) of the CRR-infested area in 2015 was non-infested in 2017. The overall proportion of CRR-infested area in the field dropped from 5.52% in 2015 to 0.55% in 2017 (Table 2.1). These results suggest that fungicide application, with the UAV-based prescription map as a guide, mitigated the CRR, but the extent of CRR infestation varies from year to year and is commonly less in drier years. The precipitation in the 2017 growing season (May to August) was 495 mm, which was more than the 439 mm of the 2015 growing season. That the weather facilitated CRR development in this area in 2017 was also supported by the CRR levels in two adjacent fields, about 2.14 out of 12.50 ha (17.3%) in one field and 0.34 out of 1.54 ha (23.4%) in the other. However, there are no observations of these other fields in 2015 to compare with the study field.

Table 2.1 Root rot-infected area and occupied percentage of the field in 2015 and 2017.

	2015	**2017**
Field area (acres)	83.32	82.31
Root rot infected area (acres)	4.60	0.45
Infected percentage (%)	5.52	0.55

Figure 2.9 shows in detail how the two main CRR-infestation zones in the study field (spots A and B from Figure 2.8) changed from 2015 to 2017. Almost all of the CRR-infested areas in 2015 did not show symptoms in 2017. Both zones were clearly much smaller overall in 2017. The fungicide apparently protected the cotton plants in those zones from CRR or postponed the infection, giving the plants time to produce some yield. Ideally, a clear-cut demonstration of the benefit of a prescription map would be done within the same year and the same field. One approach to accomplishing this in future work would be placement of a non-treated area within the center of a CRR infestation zone. However, the circumstances of the experiment reported here – moist weather in 2017 which promotes CRR and high infestation levels in adjacent fields –

strongly suggest the precision-applied fungicide was the principal reason for the great reduction in infestation between 2015 and 2017.

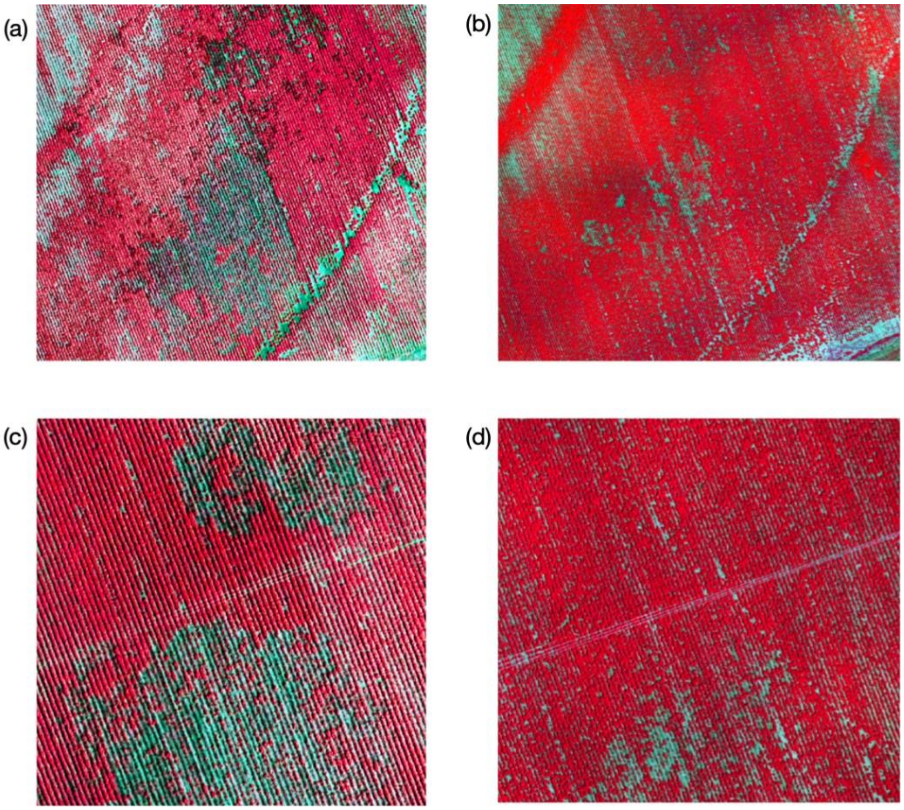

Figure 2.9 Fungicide spaying according to a prescription map reduced the infected area by 2017.

2.3.3. Economic analysis

The 2017 yield of the dryland field under study was approximately 242 kg per 0.405 ha (533 lb/ac). Assuming no CRR, the yield would have been roughly 243 kg per 0.405 ha (536 lb/ac). The average cotton price in 2017 was about $0.755 USD per 0.45 kg (per 1.0 lb). Thus about $402 USD of cotton was produced per 0.405 ha (per 1.0 ac) in the healthy zones. Theoretically, this 33.3 ha (82.3 ac) field could have produced

$33,304 USD (19,899.6 kg) of cotton if there had been no CRR. However, 1.9 ha (4.60 ac) of the field was classified as having CRR infection in 2015, which could have caused a $1,862 USD loss in 2017 if no treatment had taken place, reducing the revenue to $31,433 USD. The full rate of 237 mL per 0.405 ha (8 fl oz/ac) of flutriafol spray would cost about $30 USD per ha ($12 USD per ac) for the product alone; if the fungicide were applied to the entire 33.3 ha, it would cost $987 USD. With adequate fungicide treatment, it could be expected that no yield loss would be caused by CRR; thus, the total revenue from the cotton yield would be $32,318 USD from that field, which is $885 USD higher than with no treatment ($31,433 USD). The actual application area in 2017 was 3.9 ha (9.6 ac) including the 5-m added buffer thickness, so the actual fungicide cost was $115 USD. Therefore, the total revenue would have been $33,007 USD, the highest revenue among all scenarios, not considering the equipment cost of the VRT sprayer (Table 2.2).

Table 2.2 The detailed revenue comparison in 2017 between three scenarios in the studied field without considering the cost of equipment. NT= No treatment (calculated data), EF= Applied the fungicide to the entire field (calculated data), PM= Applied the fungicide based on the prescription map (actual data).

	Treatment area (ac)	Cost of fungicide (USD)	Loss of cotton (USD)	Revenue (USD)
NT	0	0	1,861.53	31,443.33
EF	82.23	986.76	0	32,318.10
PM	9.6	115.2	182.08	33,007.58

When comparing the three scenarios for dealing with a CRR-infested field, the treatment that achieved the highest revenue varied according to CRR-infested proportion of the farm, total field area, the number of fields on the farm, and yield (Figure 2.10). Assuming the farm has five separate cotton fields with a moderate-to-low yield (243 kg per 0.405 ha), when the CRR proportion is less than roughly 3%, applying no fungicide is superior to applying fungicide to the entire field (Figure 2.10a, 2.10b). Otherwise, applying to the entire field is better than no treatment. When the total area of the farm is larger than roughly 400 ha, applying fungicide with a prescription map appears to be preferable. In general terms, applying fungicide with a prescription map becomes more preferable as total field area increases (Figure 2.10a). For a farm with 25 smaller fields, the prescription map becomes more preferable when the overall farm is larger than roughly 560 ha, because the smaller individual field sizes mean more cost associated with image analysis. The larger the size of the individual fields on a cotton farm, the more preferable a prescription map.

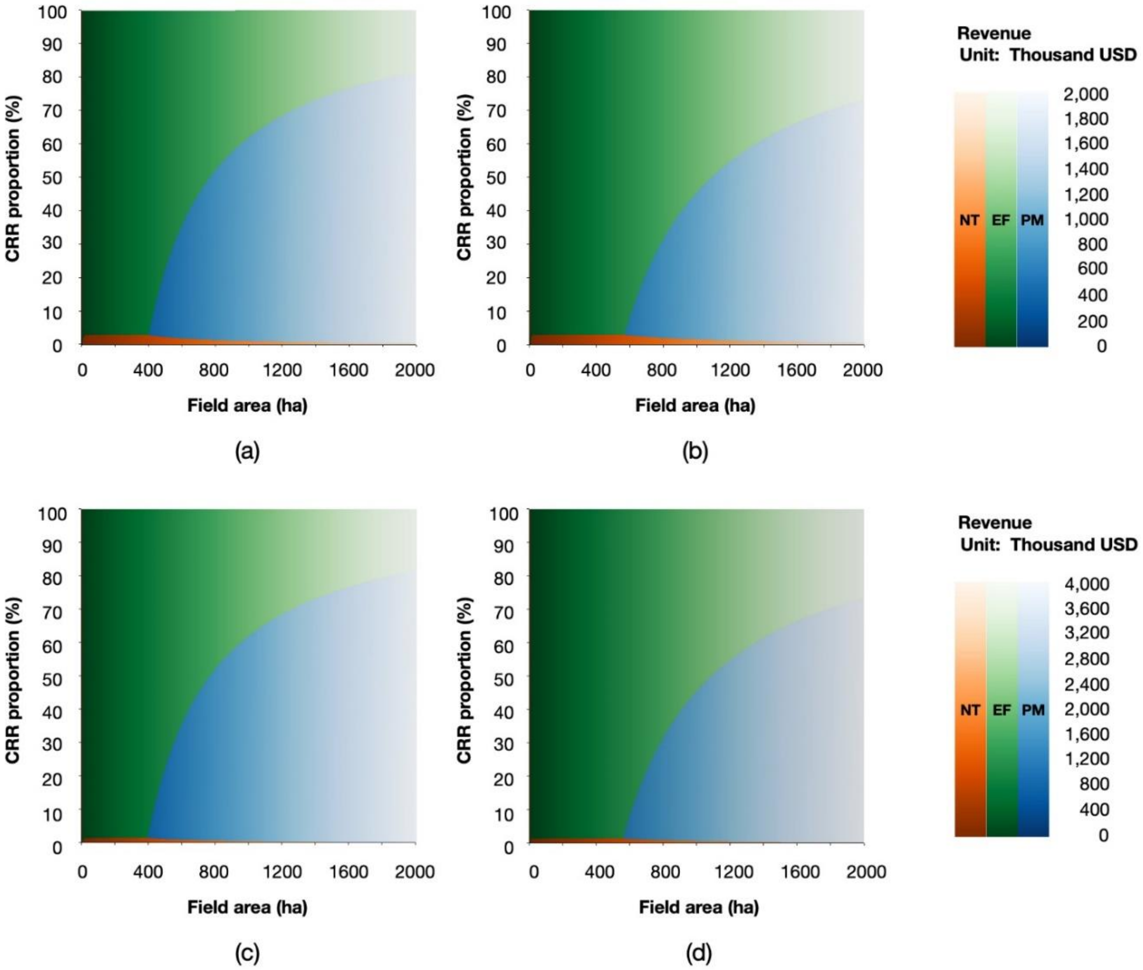

Figure 2.10 The treatments achieved the highest revenue (USD in thousands) based on the combination of CRR proportion of the field (%) and the field area (ha). (a) Five separated fields summed 2,000 ha area with moderate-to-low yield (243 kg per 0.405 ha); (b) Twenty-five separated fields summed 2,000 ha area with moderate-to-low yield (243 kg per 0.405 ha); (c) Five separated fields summed 2,000 ha area with moderate-to-high yield (486 kg per 0.405 ha); (d) Twenty-five separated fields summed 2,000 ha area with moderate-to-high yield (486 kg per 0.405 ha). NT, no treatment; EF, apply the fungicide to the entire field; PM, apply the fungicide with a prescription map.

Assuming the farm has moderate-to-high yield (486 kg per 0.405 ha) on five separate cotton fields, applying fungicide to the entire field is superior to applying no fungicide when the CRR proportion is greater than roughly 1.5%, (Figure 2.10c, 2.10d).

Once the total area of the farm is larger than roughly 390 ha, applying fungicide with a prescription map is the preferred option. For a farm that has 25 fields, the prescription map is preferred when the overall field area is larger than roughly 550 ha. Increased yield means that no fungicide treatment is less likely to be an acceptable option for a CRR-infested field. This is true because it would be better to apply fungicide instead of accepting cotton loss when the yield is high.

Considering a similarly yielding farm of roughly 800-ha (2,000-ac) with 5% CRR-infested area in 2017, if no treatment were applied, the total revenue would have been roughly $769,000 USD. If the entire field were treated with fungicide, the revenue would have increased to about $785,000 USD. If the field were treated with a prescription map, the revenue would have increased to about $797,000 USD, about $12,000 USD (1.5%) greater than for treating the entire field and about $28,000 USD (3.6%) greater than for no treatment.

As noted previously, in addition to UAVs, manned aircraft have proven useful for generating prescription maps for CRR treatment[27]. This type of imagery could be provided by companies who collect aerial images and charge by the hour or by the area covered. However, the cost of image acquisition would likely be high compared to UAV imagery. This option was not considered here partly because the focus was on UAVs but also because modeling the cost would have been complicated by the small size of the market and the variation in offerings. High-resolution satellite images have also been used to detect CRR, but free satellite imagery such as Landsat has too coarse resolution to generate a useful prescription map, and 1-m resolution imagery may be too costly because of mandatory minimum areas needed for purchase. In addition, the image quality and even availability of satellite data is easily affected by cloudiness, making its utility uncertain. Thus, UAV imagery appears to be an excellent choice for developing prescription maps for fungicide application in CRR-infested cotton fields.

2.4. Conclusion

In this study, remote sensing with UAV-based multispectral imagery was shown to be able to detect CRR. A method for using UAV images to develop a fungicide prescription map for CRR was successfully developed. An actual UAV-based prescription map was tested and found to be effective at mitigating CRR, reducing by 89% the amount of fungicide sprayed in the field under study, while the CRR area was reduced from 5.52 to 0.55% of the field. VRT application adds cost to the operation of applying fungicide, but the relatively small one-time investment could be overcome fairly easily in one season on an 800-ha (2000-ac) farm with 5% CRR infestation. In the 33.3-ha cotton field under study in this research, the UAV-based prescription map with VRT fungicide application resulted in a savings of $690 USD. For further economic analysis, a model was developed to estimate the marginal benefits of treating CRR-infested fields on a farm with a history of CRR. The model considered the CRR-infested proportion of the farm, the overall farm size, the number of fields, and the yield. The model indicated that it is generally better to treat a CRR-infested field rather than leaving it without treatment, and application based on a prescription map is more preferable as the size of the farm goes up, the number of fields in the farm goes down, and the yield goes up.

3. AUTOMATIC CLASSIFICATION OF COTTON ROOT ROT DISEASE BASED ON UAV REMOTE SENSING*

Abstract: Cotton root rot (CRR) is a persistent soilborne fungal disease that is devastating to cotton in the southwestern U.S. and Mexico. Research has shown that CRR can be prevented or at least mitigated by applying a fungicide at planting, but the fungicide should be applied precisely to minimize the quantity of product used and the treatment cost. The CRR-infested areas within a field are consistent from year to year, so it is possible to apply the fungicide only at locations where CRR is manifest, thus minimizing the amount of fungicide applied across the field. Previous studies have shown that remote sensing (RS) from manned aircraft is an effective means of delineating CRR-infested field areas. Applying various classification methods to moderate-resolution (1.0 m/pixel) RS images has recently become the conventional way to delineate CRR-infested areas. In this research, an unmanned aerial vehicle (UAV) was used to collect high-resolution RS images in three Texas fields known to be infested with CRR. Supervised, unsupervised, and combined unsupervised classification methods were evaluated for differentiating CRR from healthy zones of cotton plants. Two new automated classification methods that take advantage of the high resolution inherent in UAV RS images were also evaluated. The results indicated that the new automated methods were up to 8.89% better than

---

*Wang, T., Thomasson, J.A., Yang, C., Isakeit, T. and Nichols, R.L., 2020. Automatic Classification of Cotton Root Rot Disease Based on UAV Remote Sensing. Remote Sensing, 12(8), p.1310.

conventional classification methods in overall accuracy. One of these new methods, an automated method combining k-means segmentation and morphological opening and closing, provided the best results, with overall accuracy of 88.5% and the lowest errors of omission (11.44%) and commission (16.13%) of all methods considered.

Acknowledgments: We thank Cody Bagnall, Lantian Shangguan, Xiongzhe Han, Xiwei Wang, and Roy Graves for helping in data collection. We thank Ryan M. Collett for helping in selection of survey fields.

3.1. Introduction

Cotton root rot (CRR), caused by the fungus *Phymatotrichopsis omnivora*, is a major disease problem for cotton production in Texas and the southwestern U.S. It was first observed in the 19th century, and it kills cotton and other dicots by preventing water and nutrients from being transported from roots to the rest of the plant [3]. An infected plant dies so quickly that the death of the plant is often the first observable symptom. The fungus tends to occur in specific portions of fields and thrives in warm, moist, and alkaline (7.2–8.5) soil environments. The fungus spreads, commonly in circular patterns, through root contact between plants and the growth of mycelia in the soil [7]. Once infected, a plant usually dies within ten days [8]. If the disease occurs in the early stage of growth, the plant will die before bearing any fruit. If it occurs late enough to allow plants to flower, the disease will reduce the yield and lint quality.

CRR-infested areas in a field can expand to more than 50% of an entire field area during the season [8]. Until recently, control practices were neither economical nor effective [36]. However, a fungicide, flutriafol, known commercially as Topguard Terra (FMC Agricultural Solutions, Philadelphia, PA), was proven effective for CRR [22,48–50]. To apply the fungicide most efficiently, the CRR-infested areas must be identified. Because the CRR fungus is long-lived and colonizes specific areas of a field, the disease typically occurs at the same locations over many years, so future infested locations can be assumed to be consistent with historical position data. Multispectral and hyperspectral remote sensing (RS) have been used to accurately distinguish infested areas from non-infested areas. Three-band multispectral is widely available and thus a good candidate for practical application [9].

RS is appropriate for identifying CRR zones because of its efficiency over large areas [51]. Taubenhaus et al. used RS for this purpose as early as the 1920s [18], photographing an infested cotton field from an airplane with a handheld camera. Nixon et al. introduced color-infrared (CIR) photography as early as the 1970s, documenting the distribution of CRR infection and detecting the effect of chemical treatment for CRR [19]. Multispectral video imagery of CRR was evaluated as early as 1987 [20]. Yang et al. later used this technique along with a high-precision global positioning system (GPS) receiver to map CRR [21]. Their research indicated that this method could be used to delineate the CRR-infested areas in both dryland and irrigated fields. Song et al. (2018) proved that Sentinel-2A satellite images, which have a multispectral spatial resolution of 10 m, could be used to detect CRR [25]. Unmanned aerial vehicles (UAVs) can fly at a lower above-ground level (AGL) than manned aircraft and satellites, so UAVs can supply imagery with higher resolution. However, there is scant literature about research on UAV-based RS for CRR delineation.

On the other hand, RS with UAVs has increased in agricultural research in recent years and has been considered for yield prediction, production management, disease detection, etc. [24,30–32,52–58]. For example, Huang et al. used a rotary-wing UAV with an RGB camera to derive the normalized difference photosynthetic vigor ratio (NDPVR) index to estimate soybean yield [53]. Zhou et al. used a rotary-wing UAV with RGB and other multispectral cameras to generate normalized difference vegetation index (NDVI) and visible atmospherically resistant index (VARI) in an effort aimed at yield prediction in grain [30]. This research also indicated that the red edge and near-infrared (NIR) bands were effective in predicting yield. Albetis et al. used a fixed-wing UAV with a multispectral camera to detect grape disease in a vineyard [31]. Images were captured at 120 m AGL with 85% forward overlap and 70% side overlap. A radial basis function (RBF) support vector machine (SVM) classifier was used to differentiate diseased from non-diseased areas. The overall classification accuracy ranged from 97% to 99%. Su et al. found that wheat yellow rust disease could be detected with UAV-based spectral data and vegetation indices. The red and NIR bands performed best at separating infected from non-infected plants [59]. Mattupalli et al. used a fixed-wing UAV at 120 m AGL to carry an RGB camera to detect *Phymatotrichopsis* root rot (PRR) in alfalfa [54]. The images were downgraded to a resolution of 0.10 m prior to supervised classification with a maximum likelihood classifier, which achieved an overall accuracy of 90% to 96%.

It is clear that UAVs are useful as RS platforms for various agronomic uses including disease detection. Furthermore, application equipment for crop protection inputs is undergoing continuous advances in the level of precision. It is thus desirable to exploit the extremely high resolution (e.g., 2-cm) afforded by UAV RS by classifying the images to produce prescription maps for (e.g.,) fungicides to mitigate CRR, possibly even at the level of single plants. However, this type of map creation commonly requires two-class image classification, and conventional classifications use lower-resolution image data to achieve this. In lower-resolution images, aggregated pixels do not represent reflectance information from unique objects on the ground. Pixels in a live plant zone will likely include live plants and shadows and soil, whereas pixels in a dead plant zone will include dead plants and shadows and a greater amount of soil. These aggregated pixels give a general response that enables two-class classification between live plant zones and dead plant zones. The high resolution of UAV images means many of the pixels consist of one unique object type. These differences in detailed information content between image resolutions were quantified by Matese et al., who compared NDVI values among satellite data, manned-aircraft data, and UAV data. They reported NDVI ranges of 0.02, 0.04, and 0.08, respectively, making clear the higher variability and thus information content in the UAV data[60]. The increase in non-aggregated pixels leads to a larger number of data categories, presenting difficulties in classifying images directly into two classes like CRR and healthy. It must also be noted that CRR in cotton presents particular challenges for high-resolution imagery that are not present in some other crops like alfalfa. For example, alfalfa tends to be planted in closely spaced (e.g., 19 to 20 cm) rows and thus presents a full canopy in early growth stages, so issues related to more than two classes (e.g., including healthy plants, diseased plants, sunlit soil between rows, and shaded soil between rows) may not be evident in alfalfa when they are evident in cotton, which is commonly planted with 76 to 102 cm row spacings. Images from UAVs can be resampled to a lower resolution to give an aggregated-pixel response (e.g., Mattupalli et al. resampled UAV data to 0.1 m [54]), but doing so can defeat the purpose of creating a highly detailed prescription map that can take full advantage of the utility of extremely high-resolution UAV data. Thus, classification methods need to be developed to accurately classify the larger number of pixel categories in high-resolution CRR images.

Various classification methods [61–69] have been widely used in RS image analysis [46,70–73]. Huang et al. noted that supervised classification is commonly used but is time-consuming and costly because of human involvement in training data selection [74]. They proposed an automatic selection method to classify land cover, but thresholds between classes still had to be determined manually. Yang et al. evaluated several conventional classification methods for mapping CRR from manned-aircraft images having been resampled to a 1.0-m resolution. Two of the classifications were unsupervised: ISODATA on four-band (blue, green, red, and NIR) multispectral data, and ISODATA on NDVI. Six additional classifications of multispectral data were supervised: minimum distance, Mahalanobis distance, maximum likelihood, SVM, spectral angle mapper, and neural network. They found that both supervised and unsupervised classification methods were effective, but the supervised methods were generally more accurate [22]. The unsupervised classifications involved from two to twenty classes, and those with higher numbers of classes were more accurate, the optimal numbers of classes being 17 and 19 for two different fields. Even though the two-class unsupervised methods did not require manual selection of training data, the more accurate unsupervised methods with more than two classes did require an extra procedure involving class combination based on human expertise. Ideally, accurate unsupervised methods requiring no human intervention could be used. However, in differentiating CRR-infected plants from healthy plants in multispectral RS images, the CRR and healthy datapoints (pixels) have varying degrees of two-class separability in multi-dimensional (e.g., green, red, and NIR) space. Ideally, a clear margin (i.e., defined pixel value) between the two classes would exist, but this is generally not the case. On the other hand, with the SVM classifier, a “soft margin” (i.e., a permissible range for the pixel value) can be constructed by establishing a tolerance level for misclassification, a so-called penalty factor, which can be adjusted to improve the overall classification. The soft margin exemplifies the advantages of supervised methods in classifying data strictly based on spectral responses. It is desirable to find a way to combine the automated nature of unsupervised methods with the more accurate nature of supervised methods.

Furthermore, non-seeded areas of the field caused by planter malfunctions are difficult to differentiate from CRR areas by classifications based simply on spectral responses, because the bare soil in those areas gives a similar spectral response to that of CRR areas where dead plants and soil make up a combined response, with soil commonly being predominant. The fact that these non-seeded areas have a known rectangular shape is helpful, however. It is conceivable to automate procedures in conjunction with classification that takes local shape into account.

Considering the advantages of high-resolution UAV images and the attendant difficulties of classifying CRR in cotton as well as the need for simple and rapid data processing, it is desirable to (a) incorporate the additional information available in high-resolution UAV images into improved classification methods, and (b) develop automated methods of image classification. The specific objectives were thus to (1) develop automated classification methods to detect CRR at high resolution from UAV imagery, and (2) compare the proposed automated classification methods to conventional unsupervised and supervised classification methods for CRR detection that require resampling of UAV RS imagery to a lower resolution.

3.2. Materials and Methods

3.2.1. Study sites

This study was conducted on three dryland fields (Figure 3.1) near Thrall, Texas, with a history of cotton in rotation with corn and a history of CRR: Chase field (“CH”; 30°35'28.46"N, 97°17'33.03"W, 12.5 ha), West Poncho field (“WP”; 30°35'47.07"N, 97°17'45.77"W, 32.9 ha), and School House field (“SH”; 30°35'38.88"N, 97°17'30.16"W, 12.7 ha).

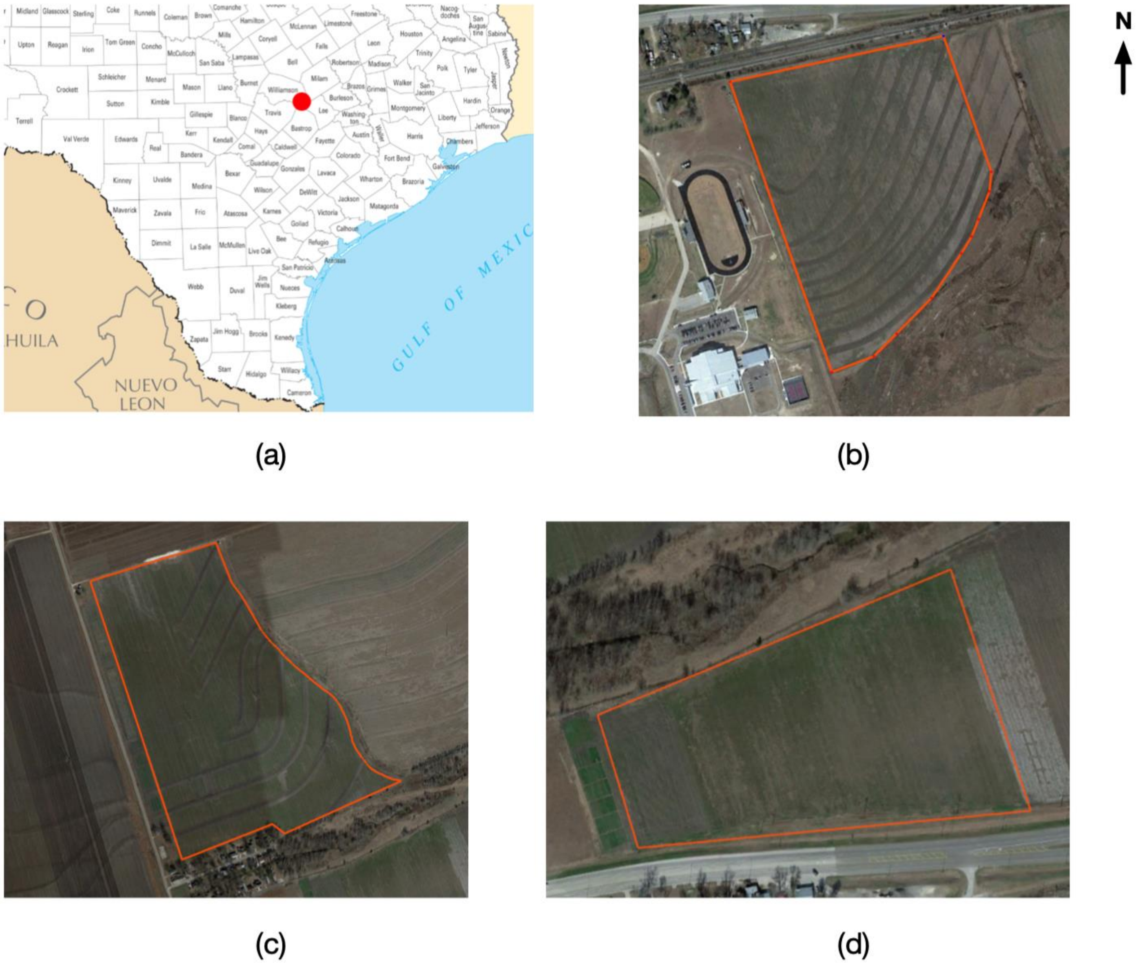

Figure 3.1The study was conducted at (a) a farm in Williamson County, Texas [45]**; (b) The 'Chase' field (CH for short) (Scale 1:10000); (c) The 'West Poncho' field (WP for short) (Scale 1:15000); and (d) The School House field (SH for short) (Scale 1:6000)**

3.2.2. Data collection

On Aug. 20, 2017, image data were acquired with a RedEdge camera (Micasense, Seattle, WA, USA) (Figure 3.2) carried by a Tuffwing Mapper fixed-wing UAV platform (Tuffwing LLC, Boerne, TX, USA) (Figure 3.3) flying at 120 m AGL. The camera collected images with 1280 x 960 pixels at 7.64 cm/pixel resolution in five bands: blue (475-500 nm), green (550-565 nm), red (665-675 nm), red edge (715-725 nm), and NIR (825-860 nm). The images were taken between 11:00 and 13:00 local time on a cloud-free day, with fixed exposure settings that had been experimentally determined to be optimal for the crop, location, date, and time of day. The manual exposure settings were 0.44, 0.44, 0.44, 1.00, and 0.44 milliseconds, and gain settings were 1x, 1x, 2x, 2x, 2x, respectively for Blue, Green, Red, NIR and Rededge bands.

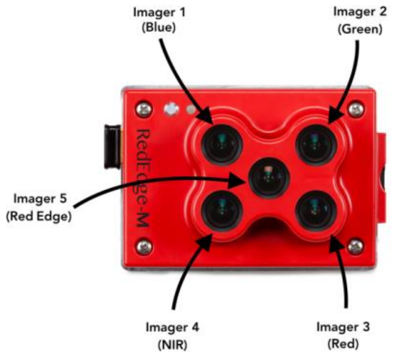

Figure 3.2 MicaSense RedEdge camera. It has five separate imaging sensors with specific optical filters to provide five spectral bands. The weight is 150g and the size is 12.1 cm x 6.6 cm x 4.6 cm (4.8” x 2.6” x 1.8”), so it is designed well for use on small UAVs.

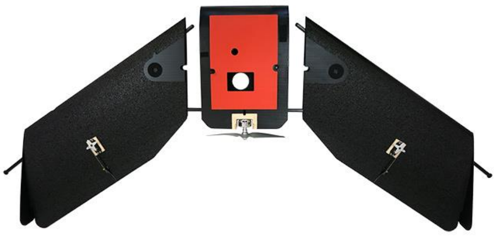

Figure 3.3 Fixed-wing UAV “TuffWing UAV Mapper.” The aircraft body is made of expanded polypropylene (EPP) foam with reinforcing carbon fiber spars, so it is strong with low mass to maximize flight time. Including the Micasense RedEdge camera, the weight is about 2kg, and the wingspan is 1218cm. At the manufacturer-reported flying endurance of 40 min, the Tuffwing can cover 275 acres at 100 m AGL.

3.2.3. Data processing

With the AGL and camera used, a 0.95-ha area was covered with each image. The overlap percentages used for UAV surveys were 80% forward-lap and 70% side-lap. Raw images were saved in tiff format with GPS and inertial measurement unit (IMU) data stored in metadata. Image mosaicking was performed in Pix4D software (Lausanne, Switzerland). When the ground control point (GCP) information was used in processing the mosaic, three to six overlapping images per location were tied, which is varied on the distance between GCPs and the edge of the mosaic. All these procedures were conducted in Pix4D. The point cloud density is in the “High” option with the minimum number of matches of 3. The 3D textured mesh was generated with the default option “Medium Resolution”.

A Trimble Geoexplorer 6000 (Trimble, Sunnyvale, CA) GPS receiver was used to measure the coordinates at the center of ground control points (GCPs) in order to geo-reference the images. Geo-referencing was also performed in Pix4D, and the centers of the GCPs in each raw image were manually identified and linked to the corresponding ground truth GPS coordinates.

Three radiometric calibration references were used: light gray (≈ 45% reflectance), medium gray (≈ 20% reflectance), and dark gray (≈ 3% reflectance). The reflectance spectra of the calibration references were collected on the day of flight with a portable spectroradiometer (PSR+ 3500 High-Resolution Full Range Portable Spectroradiometer, Spectral Evolution, Haverhill, MA). On each calibration reference, the reflectance spectra of five points (one close to each corner and one at the center) were collected and averaged. A linear relationship between digital number (DN) values and reflectance was derived for each image band (Figure 3.4). Based on these relationships, each image mosaic was converted to reflectance in ENVI software (Harris Geospatial Solutions, Boulder, CO). Then the UAV mosaics were resampled at 1.0-m resolution for use by the conventional classifiers.

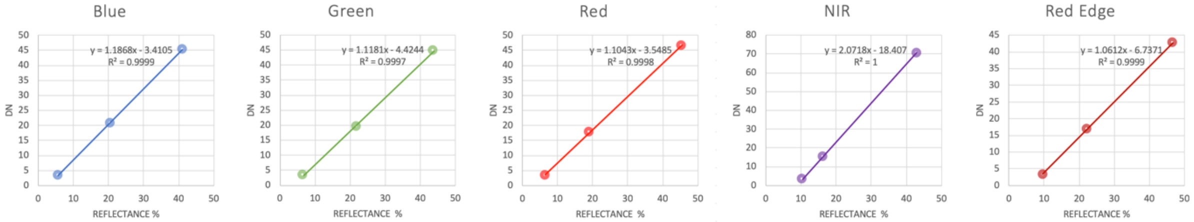

Figure 3.4 The linear relationships between DN value and reflectance of the calibration tiles in the MicaSense camera's five spectral bands.

3.2.4. Classifications

Unsupervised and supervised methods were used to classify image data into two classes that indicated healthy and CRR-infested areas. The data used by each classifier in generating a classification result were only the green, red, and NIR bands from the MicaSense camera. This selection was based on three reasons. First of all, Yang et al. compared 3-band multispectral data (green, red, NIR) to hyperspectral data (475 to 845nm) for CRR detection [9]. The spectral range of the hyperspectral data included the bandwidth range of the red edge. The results indicated both multispectral and hyperspectral images could similarly accurately distinguish the CRR-infested area, giving convincing evidence that CIR data (green, red, NIR) are sufficient to detect CRR. Second, in work preliminary to the research discussed herein, two performance comparisons based on the SVM classifier with different sets of training data were made among groups of all five bands (B, G, R, NIR, red edge), four bands (G, R, NIR, red edge), CIR (G, R, NIR), and RGB. Results indicated that CIR performed the best of all the groupings. Accuracies averaged 82.0 % for five bands, 83.0% for four bands, 84.2% for CIR, and 77.2% for RGB. Finally, CIR cameras are in fairly common use, while five-band multispectral cameras are not, and a commonly applicable solution was desired. All the conventional classifications thus were generated based on CIR data, and the images were resampled to 1.0-m resolution.

3.2.4.1. Conventional classification

The green, red, and NIR bands from the MicaSense camera were used as input to the classifiers, and the associated CIR images were used for visual evaluation of the classification methods. These images covered 5.68-ha, 0.42-ha, and 0.34-ha portions of the CH, SH, and WP fields, respectively (Figure 3.5). The 1.0-m resampled data were used with all the conventional classification methods, because standard operating procedure for this type of remote-sensing analysis involves resampled data.

All the conventional classifications were conducted in ENVI. Each image was processed individually with corresponding classification methods. One unsupervised classification method was used to classify the image data directly into two classes, and three unsupervised methods were used to classify the image data into three, five, or ten classes that were then combined into two classes based on user judgment.

K-means clustering is an unsupervised classification method that does not require labeled training data. It can classify the data based on the similarity of data in multidimensional space. The user specifies the number of clusters to be generated based on knowledge of the application; e.g., if only CRR and healthy regions were evident, only two clusters would be specified. Initially, “seeds” are generated in the data space randomly to serve as initial cluster centroids. Individual data are classified into the category associated with the closest cluster centroid. Then the centroids are recalculated based on the data in the new classes. The data are relabeled into a new class based on the updated centroid position. Iteration of these steps continues until the centroids no longer move significantly according to specified stopping criteria. In this way, most of the healthy and CRR-infected cotton can be differentiated because of the big difference between their spectral responses.

The k-means clustering method was applied to each image to generate two-class, three-class, five-class, and ten-class classification. The two-class classification was regarded as unsupervised classification, while the others were regarded as semi-supervised because class combinations were based on human expertise. In the three-class classification, Classes 1 and 2 were combined as the healthy class, and Class 3 was assigned as the CRR class. In the five-class classification, Classes 1 through 3 were combined as the healthy class, and Classes 4 and 5 were combined as the CRR class. In the ten-class classifications, Classes 1 through 6 were combined as the healthy class, and Classes 7 through 10 were combined as the CRR class.

Additionally, four supervised classification methods were used to classify the image data directly into two classes, and all used the same training regions of interest (ROIs). In each field, about 20,000 to 40,000 pixels (about 0.5% to 1.0% of an entire field) were selected for each class. The training data were uniformly distributed across the fields. Different classification rules were calculated from the training data for each supervised classification method. The classifications were then generated based on these rules. The unsupervised methods were all based on k-means classification, while the supervised methods included support vector machine (SVM), minimum distance, maximum likelihood, and Mahalanobis distance.

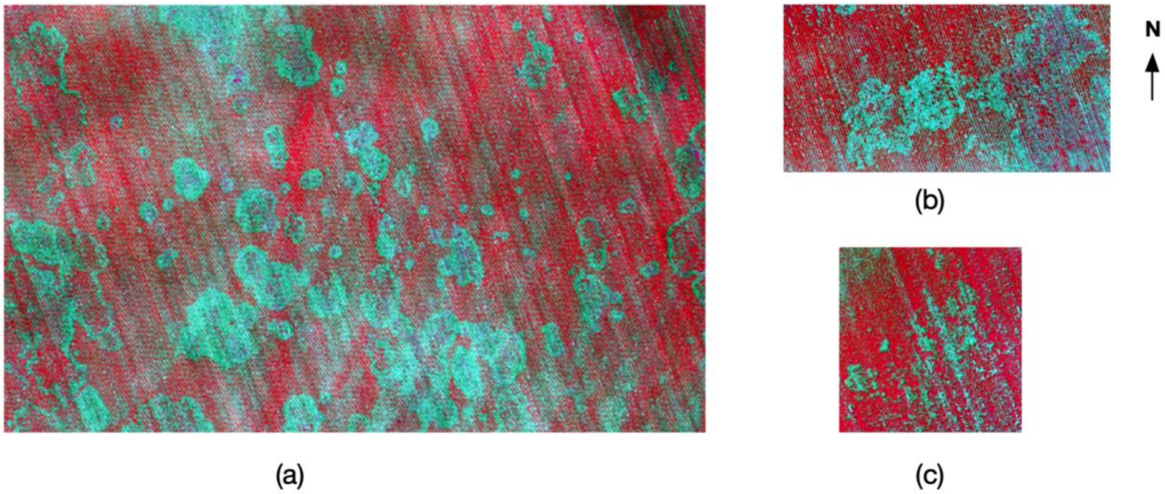

Figure 3.5 Multispectral CIR images for (a) 'Chase' field (Scale 1:3000), (b) 'School house' field (Scale 1:1550), and (c) 'West poncho' field (Scale 1:2110).

3.2.4.2. An improved semi-supervised classifier based on k-means and SVM

Unsupervised clustering methods such as the k-means method can classify data without human intervention but tend to compromise on accuracy. On the other hand, supervised classification methods like SVM, do not classify the data automatically but tend to be more accurate. It was noted previously that SVM was used to differentiate disease in RS images [20]. SVM has proven capable of classifying CRR accurately with 1.0-m resolution images [22], but it requires training data typically selected by a human operator. It was proposed to use k-means to automatically select training data that would subsequently be used by SVM for complete image classification.

The idea behind combining k-means clustering with SVM was to classify pixels into CRR and healthy classes automatically while maintaining relatively high accuracy. Figure 3.6

makes it clear that CRR and healthy cotton generally have strong differences in reflectance. However, large numbers of pixels on the boundaries are not easily separable. Once clusters are generated, many pixels are located between the two cluster centroids, and there is overlap among the pixels. Visualization of sampled data of CRR and healthy cotton plants indicates that the data are not linearly separable either in two dimensions or three dimensions (green, red, and NIR). Unsupervised clustering such as k-means separates the data with a flat plane equidistant from cluster centroids and can cause large amounts of misclassification. Unlike k-means, which is a so-called hard classifier in that it has no tunable parameters, SVM with the RBF kernel trick can generally classify image data based on labeled training data and a flexible classification rule involving the influence distance of training data and the aforementioned penalty factor. The RBF kernel trick can map the raw dataset into a higher dimensional space for separating the data more easily, and thus make the SVM classification more accurate.

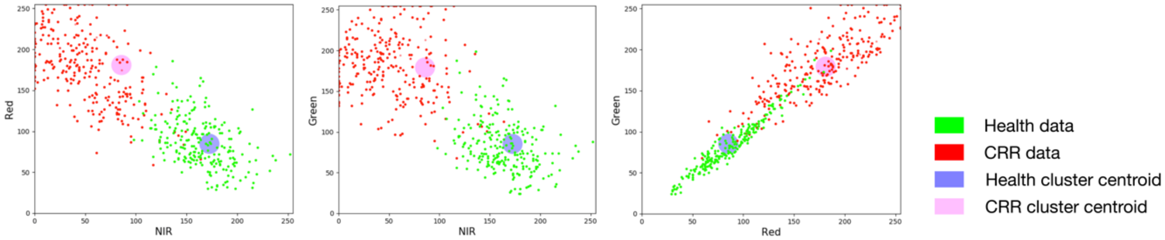

Figure 3.6 The relationships between bands in a sampled dataset along with k-means cluster centroids.

The method of combining k-means and SVM processes (KMSVM) is able to label clusters of data points automatically based on the human experience built into the code that

CRR pixels have lower reflectance overall. The workflow of KMSVM is shown in Figure 3.7. The k-means algorithm was used to automatically select initial training data from the original high-resolution image mosaics, because the high-resolution data should have many more non-mixed pixels, enabling more precise placement of the plane between the cluster centroids. Two-class k-means clustering was thus applied to the raw ortho-mosaicked image as the first step of pre-processing to locate the distribution of CRR and healthy plants. The CRR-infected plants were assigned a digital number (DN) of 0, and the healthy plants were assigned a DN of 255. Another step was required to optimize the training data, because the ideal training data selected by the k-means algorithm must contain as much as possible of the unique features of the corresponding class and must avoid the features of the other classes. Therefore, simple linear iterative clustering (SLIC) Superpixel segmentation was then applied to optimize the training data based on probability associated with the size and shape of small zones (superpixels) in the images corresponding to the expectations for individual cotton plants (Figure 3.8). The SLIC Superpixel segmentation method was applied with a minimum superpixel compactness of 300 to the binary k-means classification data. The seeding rate for the SLIC Superpixel algorithm was based on the expected size of an individual cotton plant based on row width and spacing of cotton seeds. The SLIC Superpixel segmentation algorithm divided the binary image into hundreds of superpixels, calculated the mean value of DN in each superpixel, and reassigned the mean value as the new DN of each superpixel. A new DN value larger than 243 meant the segment contained more than 95% pixels labeled as healthy in the training dataset. On the other hand, DN values smaller than 12 meant 95% of the classified infested area in the segment was labeled as CRR in the training dataset. After this step, superpixels were assigned as either CRR or healthy in order to train the SVM classifier. The RBF SVM algorithm was then used on the resampled 1.0-m data to execute the final classification.

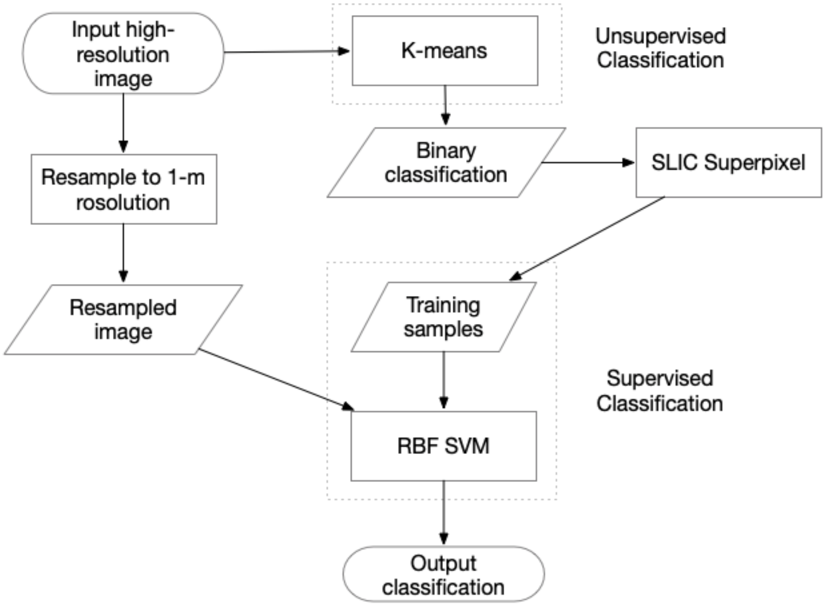

Figure 3.7 The workflow of the proposed k-means support vector machine (KMSVM) method. KMSVM makes use of unsupervised clustering and the superpixel algorithm to select training data for SVM classification

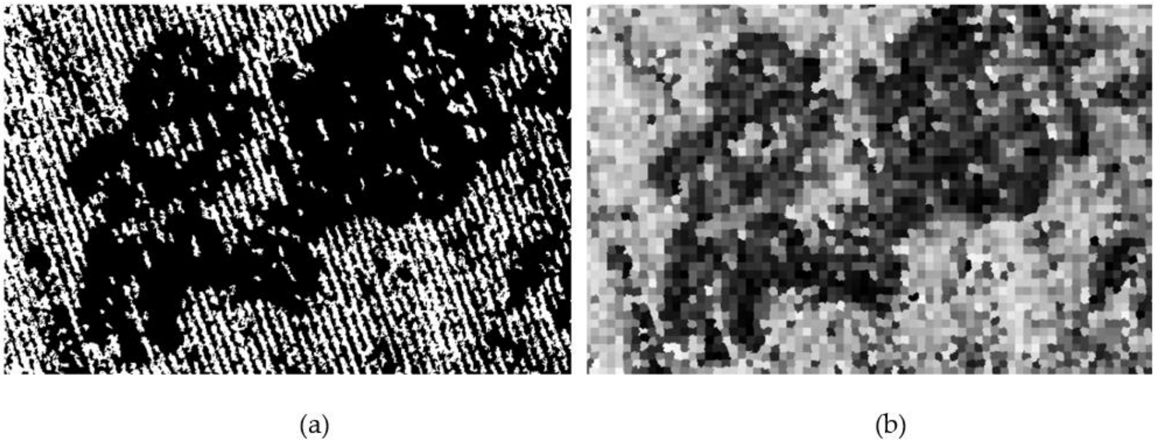
(a) (b)

Figure 3.8 A k-means classification (a) was converted to a super-pixel image (b) by using the simple linear iterative clustering segmentation method (Scale 1:700).

3.2.4.3. An improved classification based on k-means segmentation

The k-means segmentation (KMSEG) algorithm was based on k-means clustering and morphological processes. The addition of morphological processes was expected to mitigate misclassifications associated with non-seeded areas resulting from a planter malfunction. These areas are commonly misclassified as CRR zones, but their rectangular shape can be exploited to better classify them. The workflow of KMSVM is shown in Figure 3.9. The images were first classified with k-means, and then dilation and erosion were applied to the k-means classification result in order to segment larger CRR zones. UAV RS provides high-resolution image data, but more irrelevant data like pixels of bare soil between planting rows are introduced (Figure 3.10). Once the two-class k-means classification was generated based on a UAV high-resolution image mosaic, the bare soil between planting rows was classified as

CRR. In conventional classification approaches, to avoid the effects of bare soil between planting rows, the image resolution is downgraded so that the pixels of plants and gaps between rows are aggregated. A shortcoming of this process is that a large amount of information is lost with the decreasing image resolution, especially at the boundaries between infected and uninfected regions. The KMSEG method generates the classification directly on the original high-resolution image mosaics and then smooths the classification result through a morphological closing process. A 3x3 filter was used for dilation in the healthy cotton class to fill the gaps between rows. Then erosion of the healthy cotton class was conducted with the same size filter to shrink the class and neutralize the influence of dilation at the boundaries between CRR and healthy cotton regions. This morphological closing procedure aims to remove small or narrow bare soil areas. Five iterations each of dilation and erosion were used to ensure boundaries between classes were not affected. Finally, a morphological opening, erosion followed by dilation, was conducted in the same number of iterations, which cleaned the small healthy areas inside of infected areas.

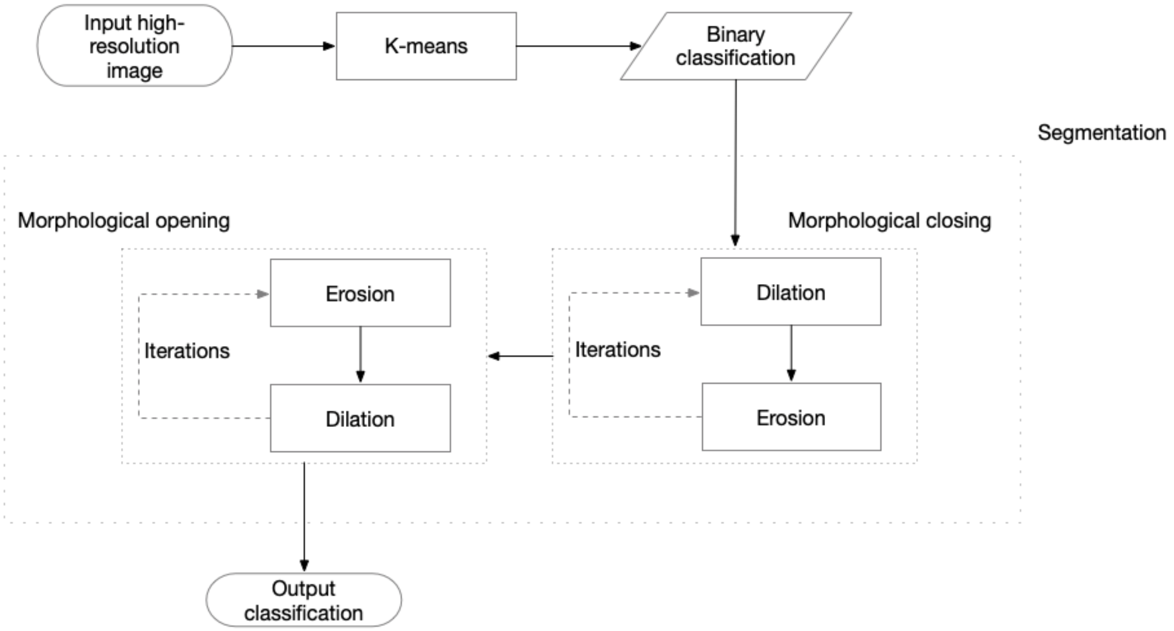

Figure 3.9 The workflow of the proposed k-means segmentation (KMSEG) method. KMSEG makes use of unsupervised clustering and morphological image processing methods to classify the image.

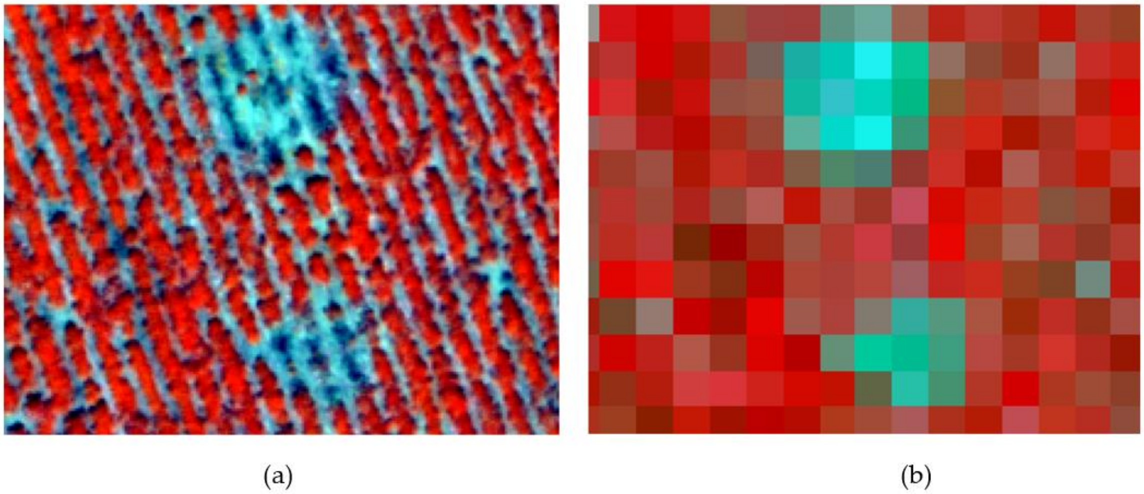

Figure 3.10 The cotton root rot (CRR) infested cotton shown in color-infrared composites with different resolutions: (a) 0.076 m/pixel; and (b) 1 m/pixel (Scale 1:200).

3.2.5. Accuracy assessment

Accuracy assessment is an indispensable procedure of image classification [75,76]. A ground-truth map was used to assess the accuracy of classifications. The ground-truth map was drawn manually according to collected GPS coordinates and the following protocols:

a) A region with more than 10 adjacent cotton plants infected with CRR was marked as a CRR-infested region.

b) In a CRR-infested area, a region with more than 10 adjacent healthy cotton plants was regarded as a non-infested area.

A digitizer and graphic pad were used in this procedure. An expert in RS and plant pathology used experience and judgment to delineate infested areas. The generated map was classified into two values, ‘0’ (healthy) and ‘1’ (CRR) (Figure 3.11).

The classifications derived from the various classifiers were also converted to a binary map to test their accuracy against the human expert classification. As in the ground-truth map, the healthy area is represented by ‘0’ and the infested area is represented by ‘1’. When the two maps were overlaid, the intersecting (i.e., correctly classified) parts were assigned a value of ‘1’are, while the non-intersecting (i.e., misclassified) parts were assigned a value of ‘0’.

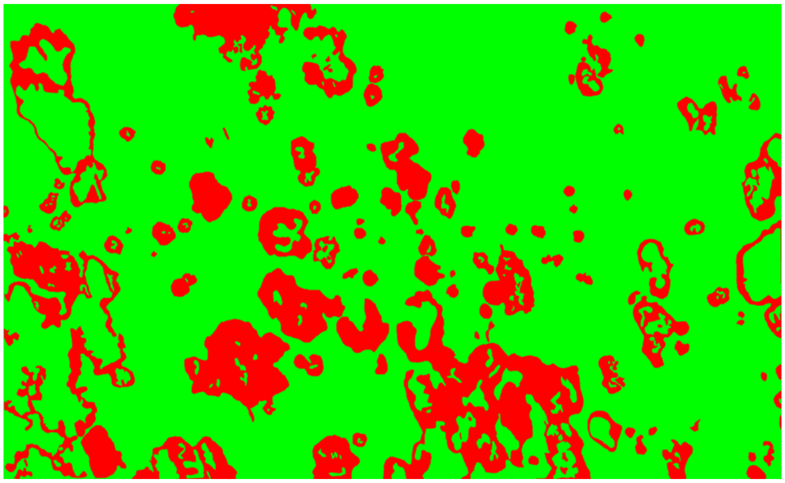

Figure 3.11 The ground-truth map of Chase field was used for accuracy assessment (Scale 1:2800)

To assess the accuracy of classifications, the confusion matrix including agreement, omission error, commission error, and overall accuracy was generated. An error of omission represents pixels that belong to a class but are not classified into that class. For instance, the omission of CRR means CRR infested areas fail to be classified as CRR. This error is termed producer's accuracy. Error of commission represents pixels which belong to one class but are classified into another class. For example, the commission error of CRR means healthy cotton plants are classified as CRR. This error is termed user's accuracy.

For an accurate classification, both omission and commission errors should be at a low level. A high omission error of the CRR-infested class means that a large number of CRR-infested areas are classified healthy. Contrarily, a high commission error of the infested class means many healthy plants are misclassified as CRR-infected plants. Compared with the omission of the CRR-infested class, the commission of the CRR-infested class is more tolerable, because the CRR-infested area may extend or shrink year by year, and slight over-application of fungicide is more likely to guarantee an effective treatment result.

3.3. Results

3.3.1. The newly proposed classification methods

Thirty confusion matrices corresponding to the ten classifiers and the three cotton fields (CH, WP, and SH) were developed and compared. Tables 3.1 and 3.2 are detailed examples of the confusion matrix for KMSVM and KMSEG in the CH field. The results from all 30 confusion matrices are summarized in Table 3.3. KMSVM had consistent performance in all three fields. The overall accuracies for KMSVM in the CH, WP, and SH fields were 90.69%, 84.47%, and 88.15%, respectively. Table 3.1 shows that 12,528,215 pixels in CH were evaluated in the accuracy assessment. Exactly 684,758 pixels (24.09%) of healthy plants were overclassified into the CRR-infested class. Additionally, 481,191 pixels (18.24%) of CRR-infected plants failed to be detected. Finally, 9,205,114 pixels of healthy plants and 2,157,162 pixels of infected plants were correctly classified with an overall accuracy of 90.69% and a kappa coefficient of 0.7277, indicating substantial agreement (0.61-0.80) with the true data[77,78]. The KMSVM classification results are at about the same accuracy level as the supervised classifications (Table 3.3).

Table 3.1 A confusion matrix of k-means SVM regional classification for Chase field

Overall accuracy		90.69%				
Kappa Coefficient		0.7277				
	Class types determined from the reference source (Ground-truth)				Commission	Omission
Class types determined from classified map		Infested plants	Healthy plants	Totals		
	Infested plants	2157162	684748	2841910	24.09%	18.24%
	Healthy plants	481191	9205114	9686305	4.97%	6.92%
	Totals	2638353	9889862	12528215		

The same dataset was used to evaluate the KMSEG method (Table 3.2). KMSEG had better performance than KMSVM in overall accuracy, kappa coefficient, error of commission and error of omission. For the CH field, the overall accuracy (92.63%) was as good as those for the supervised classifications (Tables 3.1 and 3.3), and the commission error (17.65%) and omission error (17.29%) were relatively low.

Table 3.2 Confusion matrix of k-means segmentation regional classification for Chase field

Overall accuracy		92.63%				
Kappa Coefficient		0.7786				
	Class types determined from reference source (Ground-truth)				Commission	Omission
Class types determined from classified map		Infested plants	Healthy plants	Totals		
	Infested plants	2182161	467623	2649784	17.65%	17.29%
	Healthy plants	456192	9422239	9878431	4.62%	4.73%
	Totals	2638353	9889862	12528215		

Table 3.3 The summarized results of accuracy comparison between unsupervised, combined-unsupervised, supervised classifications, and proposed automatic regional classifications. Three cotton fields were used to evaluate the methods of classification between healthy and cotton root rot (CRR) infested field areas.

		Overall Accuracy					Kappa Coefficient				
		CH	WP	SH	Mean	Std. Dev.	CH	WP	SH	Mean	Std. Dev.
U	2-class k-means	78.60%	78.76%	81.44%	**79.60%** ^{a}	1.60%	0.5106	0.4527	0.6162	**0.5265** ^{A}	0.0829
C-U	3 to 2-class k-means	88.89%	87.26%	79.45%	**85.20%** ^{ab}	5.05%	0.6868	0.5751	0.5392	**0.6004** ^{A}	0.0770
	5 to 2-class k-means	88.67%	88.81%	83.49%	**86.99%** ^{ab}	3.03%	0.6085	0.5293	0.6452	**0.5943** ^{A}	0.0592
	10 to 2-class k-means	90.97%	88.01%	81.14%	**86.71%** ^{ab}	5.04%	0.6986	0.5885	0.5911	**0.6261** ^{A}	0.0628
S	SVM	92.02%	78.66%	87.48%	**86.05%**^{ab}	6.79%	0.7587	0.4481	0.7345	**0.6471** ^{A}	0.1728
	Minimum distance	88.12%	86.14%	82.79%	**85.68%**^{ab}	2.69%	0.6753	0.5604	0.6346	**0.6234** ^{A}	0.0583
	Maximum likelihood	91.71%	77.92%	87.65%	**85.76%**^{ab}	7.09%	0.7498	0.4419	0.7422	**0.6446** ^{A}	0.1756
	Mahalanobis distance	89.60%	87.13%	86.27%	**87.67%**^{ab}	1.73%	0.7076	0.5764	0.7144	**0.6661** ^{A}	0.0778
PA	KMSVM	90.69%	84.47%	88.15%	**87.77%**^{ab}	3.13%	0.7277	0.6048	0.7494	**0.6940** ^{A}	0.0780
	KMSEG	92.62%	85.80%	87.06%	**88.49%**^{b}	3.63%	0.7786	0.6428	0.7379	**0.7198** ^{A}	0.0697

		Error of Commission (CRR class)					Error of Omission (CRR class)				
		CH	WP	SH	Mean	Std. Dev.	CH	WP	SH	Mean	Std. Dev.
U	2-class k-means	50.43%	56.88%	27.16%	**44.82%**^{a}	15.63%	7.84%	14.10%	18.00%	**13.31%** ^{A}	5.13%
C-U	3 to 2-class k-means	30.04%	40.17%	17.43%	**29.21%**^{ab}	11.39%	17.22%	28.28%	41.43%	**28.98%** ^{BCD}	12.12%
	5 to 2-class k-means	14.26%	24.23%	19.36%	**19.28%**^{ab}	4.99%	44.58%	51.63%	25.30%	**40.50%** ^{D}	13.63%
	10 to 2-class k-means	10.85%	37.51%	21.20%	**23.19%**^{ab}	13.44%	34.95%	29.83%	30.73%	**31.84%** ^{CD}	2.73%
S	SVM	18.50%	57.07%	16.18%	**30.58%**^{ab}	22.97%	19.66%	15.04%	16.69%	**17.13%** ^{AB}	2.34%
	Minimum distance	32.90%	43.70%	22.15%	**32.92%**^{ab}	10.78%	14.48%	24.71%	23.19%	**20.79%** ^{ABC}	5.52%
	Maximum likelihood	19.38%	57.88%	18.53%	**31.93%**^{ab}	22.48%	20.17%	13.23%	12.39%	**15.26%** ^{AB}	4.27%
	Mahalanobis distance	28.74%	40.79%	20.73%	**30.09%**^{ab}	10.10%	15.18%	26.86%	13.25%	**18.43%** ^{ABC}	7.36%
PA	KMSVM	24.09%	32.34%	9.26%	**21.90%**^{ab}	11.70%	18.24%	25.17%	9.97%	**17.79%** ^{ABC}	7.61%
	KMSEG	17.64%	7.46%	23.30%	**16.13%**^{b}	8.03%	17.29%	11.95%	5.09%	**11.44%** ^{A}	6.12%

Note: U stands for unsupervised, C-U stands for combined-supervised, S stands for supervised, PA stands for proposed automatic. (α=0.05, Duncan test)

3.3.2. Comparison between newly proposed and conventional classification methods

The conventional unsupervised and supervised classification methods were compared with the newly proposed methods (Table 3.3). The two-class k-means clustering method was able to generate CRR distribution maps automatically, similar to KMSVM and KMSEG from an automation perspective. However, the average accuracy of 79.60% and the average kappa coefficient of 0.5265 were lower than those for KMSVM (87.77% and 0.6940) and KMSEG (88.49% and 0. 7198). The error of omission of 13.31% was acceptable, but the error of commission was 44.82%, indicating that nearly half of the estimated CRR area was over-classified. The two proposed methods performed significantly better than two-class k-means ($\alpha = 0.05$) in terms of commission error. However, the omission errors were similar between two-class k-means and the two proposed methods.

The combined three-class, five-class, and 10-class k-means clustering methods achieved accuracies of 85.20%, 86.99%, and 86.71%, respectively, indicating that generating more classes for k-means clustering improved classification results and reduced the error of commission to the level of the proposed methods. However, the procedure of combining classes required human input and knowledge of relevant classes, making these methods less desirable than the proposed methods from the perspective of automation. Compared with the two-class k-means classification, the combined multi-class k-means classifications had better results in overall accuracy, kappa coefficient, and error of commission, but the differences were not significant ($\alpha = 0.05$). For the error of omission, the two-class k-means classification performed significantly better than the combined multi-class k-means classifications.

The performance of the four supervised classifications was generally good. The overall accuracies for SVM, minimum distance, maximum likelihood, and Mahalanobis distance were 86.05%, 85.68%, 85.76%, and 87.67%, respectively. The respective errors of commission were 30.58%, 32.92%, 31,93%, and 30.09%, and the respective errors of omission were 17.13%, 20.79%, 15.26%, and 18.43%. Compared with KMSVM and KMSEG, the supervised classification methods had similar performance in terms of accuracy and kappa coefficient. However, the errors of commission of the supervised classifications were almost twice those of the proposed methods. And the errors of omission were also higher than those of the proposed methods. Figure 3.12 shows the classification results of eight conventional and two proposed classifiers for the CH field. The CRR-infested zone is in dark gray, and the healthy zone is in light gray. Each classification in Figure 3.12 has a corresponding error map that shows the difference between the classification and the ground truth map. The omission error of CRR is in cyan and represents misdetection of CRR, while the commission error of CRR is in pink and represents overclassified CRR. The classification results of the CH field indicated that all the supervised classifications, especially SVM (Figure 3.12e), maximum likelihood (Figure 3.12g), and Mahalanobis distance (Figure 3.12h), had large commission errors (see stripes) at the northwest corner of the CH field where non-seeded areas were wrongly classified into CRR.

KMSVM (Figure 3.12i) also had a similar misclassification at the northwest corner of the CH field.

A scatterplot of errors of commission versus errors of omission is shown in Figure 3.13. The shorter the distance from the classifier to the origin, the less overall error the classifier had. The error data points of the conventional classifiers fell roughly along a common curve, while the two proposed classification methods, which took advantage of the higher resolution of the UAV image mosaics, were much closer to the origin.

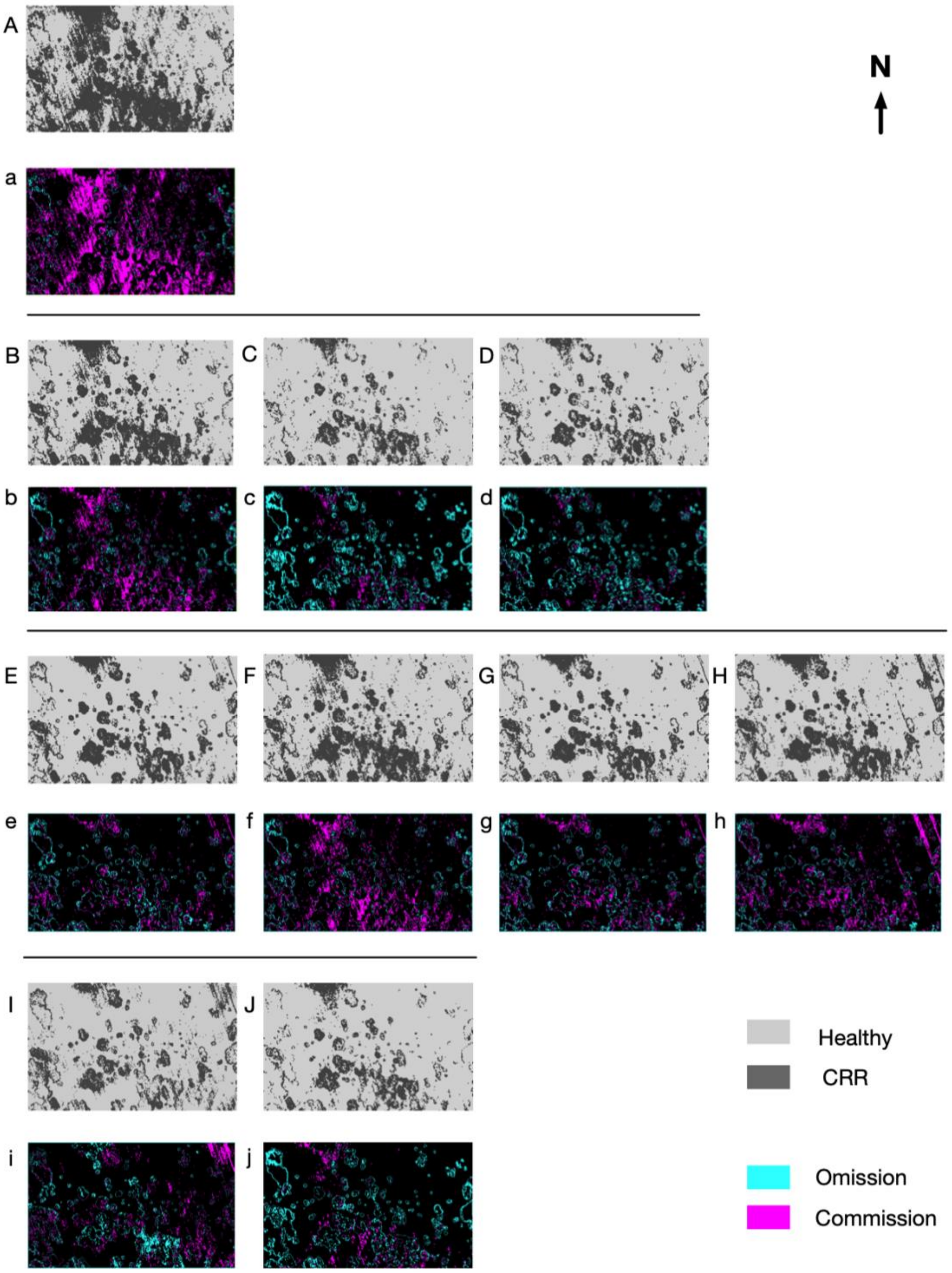

Figure 3.12 Classification results of (A) 2-class k-means, (B) combined 3-class k-means, (C) combined 5-class K-means, (D) combined 10-class k-means, (E) SVM, (F) Minimum distance, (G) Maximum likelihood, (H) Mahalanobis distance, (I) KMSVM, and (J) KMSEG. And corresponding error maps of (a) 2-class k-means, (b) combined 3-class k-means, (c) combined 5-class k-means, (d) combined 10-class k-means, (e) SVM, (f) Minimum distance, (g) Maximum likelihood, (h) Mahalanobis distance, (i) KMSVM, and (j) KMSEG. (Scale 1:9000)

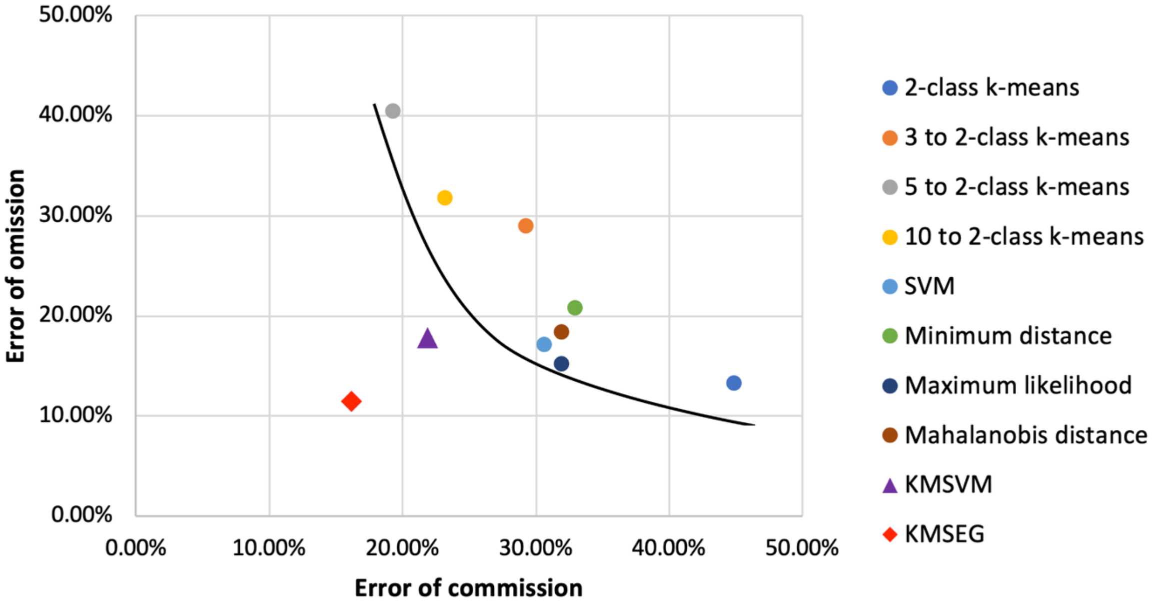

Figure 3.13 Error of commission versus error of omission for 10 classification methods. The errors of conventional classifications were distributed as a curved trend. The proposed methods KMSVM and KMSEG are superior and lie off the trend line

3.4. Discussion

An idealized goal of developing CRR detection methods is to enable the uploading of raw UAV images to a cloud server or farm computer for automatic image mosaicking and processing and then to convert the classified map to a prescription map as the final product. The prescription map would be loaded to the control system for the planter to apply fungicide automatically at planting. The entire process including image classification would ideally be automatic or at least semi-automatic. Although supervised classification and combined unsupervised classification have good classification results, they all require human expertise, making it impossible to process the data automatically. On the other hand, unsupervised classification with the two proposed methods, KMSVM and KMSEG, meets the requirement of automation.

A dataset containing roughly 584,000 pixels of data sampled from two different fields was used to analyze the features of CRR data. Statistical analysis of CRR and healthy sample data indicates that the DN values of both CRR and healthy cotton follow a bell-shaped distribution in green, red, and NIR bands (Figure 3.14). Assuming the distance between two cluster centroids is normalized to 100%, the data closer than 50, 33, and 25% to the closer centroid were considered in groups with respect to classification accuracy. The 50% group was correctly classified in the range of 42 to 58%. The 33% group was correctly classified in the range of 77 to 96%. Finally, the 25% group was correctly classified in the range of 85 to 100%. Selecting training data by using k-means classification directly may cause overfitting in classification. Selecting training data around the cluster centroid within 33% of the distance between two cluster centers could be a strategy to automatically select training data, but this may lead to underfitting. Therefore, SLIC Superpixel segmentation was introduced to improve the fit associated with the training data. The non-linear separable feature of the data is one of the reasons that the conventional unsupervised classifier was not able to directly achieve a good classification result.

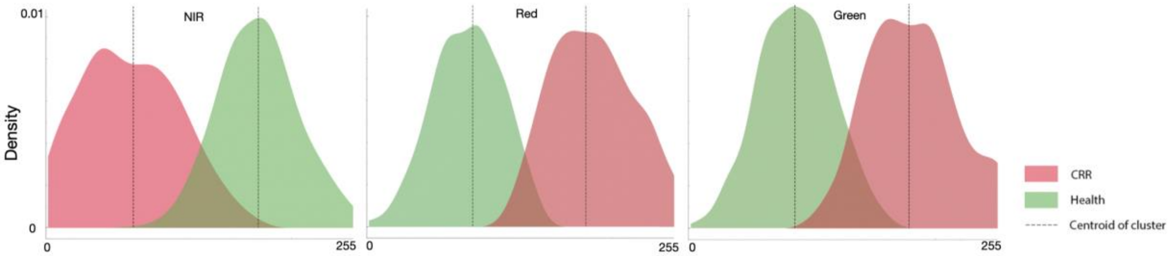

Figure 3.14 Spectral value distribution of CRR-infested and healthy plants.

Combined multi-class k-means methods were able to improve the accuracy of the classification compared to the two-class k-means methods. More classes could lead to higher accuracy theoretically, because the boundary effects could be reduced with the increasing number of classes. However, the decision criterion for class combination was subjective. Considering the combined five-class k-means classification as an example, combining Classes 1 and 2 to the CRR class and Classes 3, 4 and 5 to the healthy class led to very similar accuracy as compared to combining Classes 1, 2 and 3 to CRR and Classes 4 and 5 to healthy. The first combination had high omission error, while the second combination had high commission error, indicating that Class 3 included both CRR and healthy areas. Rigid separation of classes caused inaccurate and subjective results.

The conventional supervised classifications and KMSVM had difficulty distinguishing CRR-infected plants from non-seeded areas. The unsupervised methods also had a similar issue, but it was not as severe as with the supervised methods. This issue occurred because the spectral features of CRR plants and bare soil were similar. Using only spectral information led to misclassification. However, KMSEG avoided this issue by making use of the morphology of how CRR presents itself in the field. CRR-infested areas are generally in circular or ring shapes [8], but non-seeded areas caused by planter mechanical failure are normally in strips with bare soil. Taking the CH field as an example, there is a seeding error at the northeast corner (Figure 3.12). The bare soil area caused by mis-seeding is long and narrow. The morphological closing transformation procedure in KMSEG tended to aggregate the strip-shaped bare soil pixels (Figure 3.15). This is one reason why KMSEG achieved the lowest error of commission among all methods.

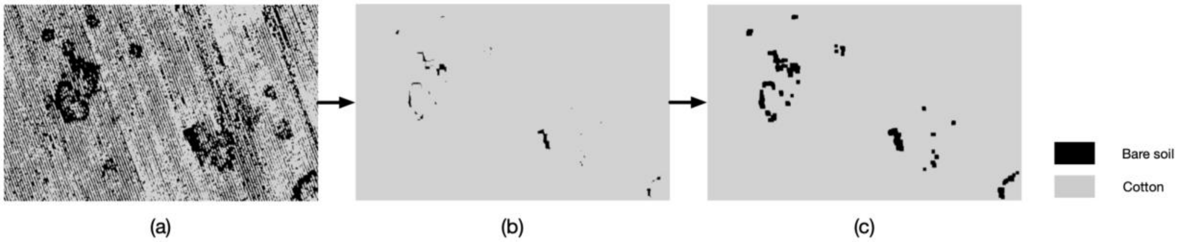

Figure 3.15 The strip-shaped bare soil pixels were effectively removed using morphological closing transformation at northeast of CH field. The (a) k-means classification was applied (Scale 1:2000) (b) dilation of healthy cotton class followed by (c) erosion of healthy cotton class.

An ideal classifier for detecting CRR should have not only good overall accuracy but should also keep the omission and commission errors of the CRR class as low as possible. Commission error indicates over-classification; i.e., larger commission error means more fungicide treatment area, which wastes fungicide and increases environmental risk. On the contrary, a large omission error causes the under-application of fungicide to infested areas, thus reducing cotton yield and quality. In future studies, image classification should be optimized to minimize misclassified areas while reducing application costs.

A principal benefit of using the high-resolution imagery of UAVs is that it may ultimately enable highly precise application of fungicide to protect cotton plants from CRR, but for this research it also enabled highly precise ground truth maps to be used for accuracy assessment. The classifications were evaluated based on all image pixels in a specific zone instead of randomly sampled points, making the result more robust. However, the pixels at a boundary of two classes could decrease the overall accuracy more easily in some scenarios (Figure 3.16). This phenomenon is known as the boundary effect, and while it could influence the absolute accuracy somewhat, it was not expected to affect the comparisons between classifiers. The results (Table 3.3) basically agreed with Yang's research [22] in that the combined unsupervised classification methods were as good as the supervised classification methods. The maximum likelihood classifier was slightly better than Minimum distance in overall accuracy. The SVM had the best overall accuracy among all the supervised classifiers. But overall, the supervised classifiers all performed well and showed no major differences.

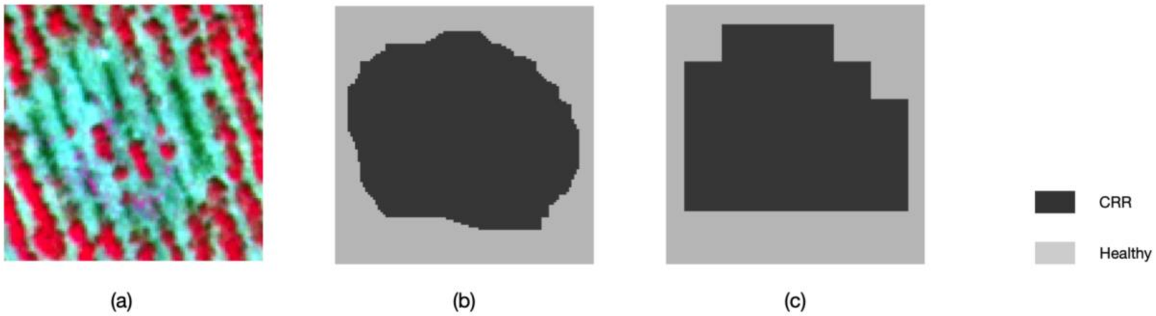

Figure 3.16 The pixels at the boundary of two classes could impact the accuracy. (a) The raw CIR image derived (Scale 1:200) (b) ground-truth image which could have boundary effect when compared to (c) real classification.

Two morphological operations were used with the high-resolution data to account for shape in the proposed classification methods: opening and closing was used in KMSEG to eliminate non-seeded areas, and superpixel analysis was used in KMSVM to enable specific focus on cotton plants. While these spatially focused operations can potentially account for the different look of other causes of plant death and wilt, the image analysis done here assumes CRR to be the major cause of wilted and dead plants, based on historical knowledge that CRR is in the field, and sampling of individual plants verifies it, along with the commonly round patterns in the field.

The particular innovations were fully automated classifiers, classifiers that perform well with high-resolution UAV data, and the inclusion of spatial information in the classifiers. We believe the proposed classification methods can be useful in other disease and pest detection contexts. However, it must be noted that the proposed methods were designed specifically for use in CRR, in which in-season mitigation is not possible. The goal with CRR is to allow the disease to take its course so the full-scale of the disease pattern can be measured. Once the disease pattern is clearly delineated at high resolution, fungicide can be applied during planting with extreme precision to minimize cost and environmental risk.

While a fixed-wing UAV was used in this work, rotary-wing UAVs are more common today, particularly in research applications. We used a fixed-wing aircraft because we desire to develop a data-collection and classification system that may be potentially practical on-farm, and thus covering large fields quickly is critical. Because fixed-wing aircraft generate lift from forward speed, they are more efficient at staying in the air over large areas and can cover a 100-acre field in a typical 20-minute flight, including adequate overlap for the orthomosaicking process.

3.5. Conclusions

This study compared multiple conventional classifiers and proposed two improved automatic classifiers, KMSVM and KMSEG, to classify CRR-infected and healthy plants in cotton fields. KMSVM is a self-labeling machine learning classifier, while KMSEG emphasizes morphological processes, and both of these were used in a way that took advantage of the high resolution inherent in UAV images. All the classifiers were evaluated based on two criteria, automation and accuracy. The two proposed methods performed better in terms of accuracy than the conventional classifiers and could be implemented automatically. In particular, the KMSEG classifier had the best performance in terms of overall accuracy (88.39%), Kappa coefficient (0.7198), error of commission (16.13%), and error of omission (11.44%). The two-class unsupervised classification had the lowest overall accuracy (79.60%) and the highest error of commission (44.82%), but it had the advantage in automation over the supervised classifications. The combined multi-class unsupervised classifications and supervised classifications had relatively good accuracy (85.2 to 87.67%) but required human intervention. Overall, the proposed methods proved superior in classifying high-resolution UAV images into healthy and diseased areas at roughly the level of a single plant.

4. A PLANT-BY-PLANT COTTON ROOT ROT IDENTIFICATION METHOD BASED ON UAV REMOTE SENSING

Abstract: Cotton root rot (CRR), caused by the fungus *Phymatotrichopsis omnivora,* is a destructive cotton disease that mainly affects the crop in Texas. Flutriafol fungicide applied at or soon after planting has been proven effective at protecting cotton plants from being infected by CRR. Previous research has indicated that CRR will reoccur in the same regions of a field as in past years. CRR-infected plants can be detected with aerial remote sensing (RS). As unmanned aerial vehicles (UAVs) have been introduced into agricultural RS, the spatial resolution of farm images has increased significantly, making plant-by-plant (PBP) CRR classification possible. An unsupervised classification algorithm, PBP, based on the Superpixel concept, was developed to delineate CRR-infested areas at roughly the single-plant level. Five-band multispectral data were collected with a UAV to test these methods. The results indicated that the single-plant level classification achieved overall accuracy as high as 95.94%. Compared to regional classifications, PBP classification performed better in overall accuracy, Kappa coefficient, errors of commission, and errors of omission. The single-plant fungicide application was also effective in preventing CRR.

Acknowledgments: We thank Cody Bagnall, Lantian Shangguan, Xiongzhe Han, Xiwei Wang, and Roy Graves for helping in data collection. We thank Ryan M. Collett for helping in selection of survey fields.

4.1. Introduction

The United States (U.S.) produced 20.9 million 218-kg (480-lb) bales of cotton in the 2017-2018 season with a production value of $7.2 billion (USD), ranking 3rd after India and China, and it is the largest cotton-exporting country in the world [1]. The state of Texas produced 9.5 million bales, approximately 44 % of U.S. cotton production, ranking 1st in the U.S. [1]. While Texas is by far the largest producing state, a major obstacle to cotton production in Texas is a disease called cotton root rot (CRR) or Texas root rot. The disease is caused by the soilborne fungus, *Phymatotrichopsis omnivora*, a destructive plant disease throughout the southwestern U.S. The first documented study of CRR was in the 19th century by Pammel [3]. The disease rots the root, disrupting the vascular system and preventing water and nutrients from being transported from the roots to the rest of the plant, eventually killing the plant. An infected cotton plant usually dies within ten days. If the disease develops in an early stage of growth, the plants will die before bearing fruit. If it develops after flowering, the disease will reduce yield and lower the quality of the cotton lint by stopping transport of nutrients to the maturing bolls.

The fungus spreads within a field by direct root contact between plants and the growth of its mycelia through the soil [79]. Infested field areas are commonly circular in shape [8], providing an indication of the cause of plant death. One study reported that the overall area of plants infected with CRR in a particular field increased from 10 to 50% from August to September [8], during a later growth stage of the crop. Until the recent advent of soil-applied flutriafol fungicide, several control practices (e.g. crop rotation, soil fumigation, host resistance) were tested but found to be either not economical or not effective [8]. Because CRR generally occurs at the same place in a field from year to year, its position can be mapped, allowing for targeted spot treatments of flutriafol fungicide. Both multispectral and hyperspectral imagery can distinguish infected areas accurately, but three-band multispectral is a preferred technique, being effective, less expensive, more widely available, and simpler to use than hyperspectral [9].

The large sizes of typical cotton fields make it impractical to map CRR position from ground-based platforms. Remote sensing, on the other hand, can provide such data quickly and relatively inexpensively, and it is thus an important technology for practical CRR sensing [9]. Visible, near-infrared (NIR), and thermal remote sensing data have been studied widely with aerial and satellite platforms to understand many crop phenomena [80]. Biotic and abiotic stresses, including insects, pathogens, weeds, drought, and nutrition deficiencies have been widely studied with remote sensing [81–86], in addition to applications such as yield prediction and general crop management [17,60,87,88]. In cotton, remote sensing has been used to evaluate the effectiveness of defoliation and regrowth control strategies [24] as well as in other applications.

Remote sensing has also been used to map CRR in cotton fields dating back to 1929 [18]. Nixon et al. later introduced color-infrared (CIR) technology to document the distribution of CRR infestation and to detect the effect of chemical treatment for CRR [19]. Multispectral video imagery of CRR was evaluated and reported as early as 1987 [20], and Yang et al. reported using manned-aircraft based remote sensing and high precision global positioning system (GPS) technology to map CRR in 2015 [22].

Satellite images typically have relatively low resolution but can be acquired periodically at a reasonable cost. However, there is a risk that clouds may cover the view when the images are taken. Aerial images commonly have higher spatial resolution that may be advantageous as well as some flexibility in timing, but the cost of acquisition is relatively high [10]. Previous research indicates that airborne and satellite multispectral imagery data can be used to successfully detect the CRR-infested area in both dryland and irrigated fields [21,25,89,90]. The resolution of such imagery limits CRR mapping to field zones, but unmanned aerial vehicles (UAVs) have recently emerged as remote-sensing tools that provide resolution high enough to potentially enable even single-plant level prescription map creation. Compared to manned aircraft, UAVs have a limited payload capacity, but they can fly lower and slower than manned aircraft. The above-ground level (AGL) with UAVs is commonly 20 to 120 m, providing for spatial resolution at the cm level. The temporal resolution of UAVs is commonly improved as well [29] because UAVs can be flown anytime the weather permits. In addition, UAV flights generally cost less than traditional manned aircraft remote sensing.

Rotary-wing UAVs are much more common than fixed-wing UAVs for agricultural remote sensing. Rotary-wing UAVs are slower and more stable in flight and thus are able to generate higher-quality mosaicked images. However, the slower flying speed also generally leads to smaller coverage area. On the other hand, fixed-wing UAVs flying at the legally allowable limit of 120 m AGL are commonly able to cover a 24 to 40 ha (60 to 100 acre) area on one battery charge (about 20 minutes), depending on the weather conditions. Therefore, fixed-wing UAVs appear to be well-suited to the large-area farming that is commonly seen in cotton production.

UAV remote sensing has been increasingly used in agricultural research in recent years and has been considered for general production management, yield prediction, , and disease detection. [24,30–32,53,54,60]. RGB (red, green, and blue) and other multispectral sensors are commonly used, but the frequently used normalized difference vegetation index (NDVI) requires the NIR band. Without the NIR band, the normalized difference photosynthetic vigor ratio (NDPVR) and the visible atmospherically resistant index (VARI) can be calculated, and they have been used to estimate crop yield [30,53]. Both RGB and other multispectral images have been used for rice growth and yield estimation. However, the vegetation indices (VIs) derived from multispectral images including NIR correlate better with grain yield than VIs derived from RGB images [30]. Albetis et al. used the support vector machine (SVM) classifier on UAV images to differentiate diseased from non-diseased areas of vineyards. Because of the high spatial resolution, they could distinguish grapevine vegetation from bare soil, shadow, and inter-row vegetation. A high classification accuracy of 97 to 99% was achieved in four vineyards [31]. Furthermore, artificial neural networks (ANNs) have been used to estimate water potential in vineyards based on UAV data [32]. While a great deal of recent agricultural research has involved UAV-based remote sensing, there is scant research about UAV-based remote sensing for the delineation of CRR.

In general, classification procedures are a way to categorize data according to various characteristics. Classification in RS means categorizing or mapping an image into different classes depending on the features of the data such as tone, texture, pattern, etc. Unsupervised and supervised classification are common and differ according to whether human-guided training is involved in classifying the data.

The Superpixel algorithm segments images into many multi-pixel pieces (superpixels) based on shape, color, texture, etc. In essence, the Superpixel method converts images from pixel-level to district-level, and thus belongs to the image segmentation category in image processing. The Superpixel algorithm keeps the main features of the aggregated pixels, resulting in a sharp reduction in the number of data-containing units. As a result, it improves the image processing speed significantly. Sultani et al. used the Superpixel algorithm to detect objects in pavement images [33]. Different shaped objects such as patches, maintenance hole covers, and markers could be detected efficiently. After dividing the images into many small segments, features like histogram of oriented gradients (HOG), co-occurrence matrix (COOC), intensity histogram (IH), and mean intensity (MI) of each superpixel were calculated. HOG and COOC are texture and shape characteristics, while IH and MI are spectral intensity variations. Then, SVM was used to generate classifications based on each feature. The Superpixel algorithm has also been used to detect disease in agricultural crops. Zhang et al. developed a new method based on the Superpixel algorithm to detect cucumber diseases [34,35]. Leaf images were divided into superpixels, and then the expectation maximization (EM) method was applied to obtain lesion images. After feature extraction, SVM was used to detect the disease. The result indicated that the proposed method had the highest recognition rate and fastest processing speed compared to four other methods that have been used for cucumber disease recognition. Zhang et al. later proposed a new leaf recognition method based on the Superpixel algorithm, k-means, and pyramid of histograms of orientation gradients (PHOG) algorithms [34,35]. First, the RGB leaf image was divided into segments with the Superpixel algorithm. Then, k-means clustering was applied to segment the lesion section of the leaf. PHOG features were extracted and used to recognize the disease. Three apple and three cucumber leaf diseases were used to assess the method. The result indicated that the proposed method was effective and usually achieved the highest recognition rate compared to other methods that had been used for cucumber disease recognition.

Conventional CRR identification methods developed for 1-m resolution aerial images can only detect the CRR-infested area at the regional level, leading to the application of a large amount of fungicide to field areas that do not need it. UAV remote sensing makes high-resolution data collection possible, meaning that fungicide treatments could conceivably be applied at the level of individual plants. To take advantage of these high-resolution data, a novel high-precision CRR identification method is proposed to enable high-precision CRR detection and treatment. The objectives of this research were thus to (1) develop and evaluate a plant-by-plant (PBP) CRR detection and classification method; (2) compare the PBP classification method to common regional classification methods; and (3) examine the effectiveness of PBP fungicide treatment to validate the necessity for the method.

4.2. Materials and Methods

4.2.1. Study sites

This study involved five selected regions in four dryland cotton fields (Figure 4.1) in central Texas, USA, near the town of Thrall: Chase section 1 (CH1), Chase section 2 (CH2), West Poncho (WP), School House (SH), and a field for a plot test (PL) to examine the effectiveness of various fungicide treatments. All of these fields and regions have a history of CRR infestation.

Figure 4.1 The study was conducted on Stiles farm located in Williamson County, central Texas. The five areas of field experiments were marked on the map.

4.2.2. Data collection

A fixed-wing UAV (Tuffwing Mapper, Tuffwing LLC, Boerne, TX, USA; Figure 4.2a) was used to acquire image data of all the fields and regions on a cloud-free day, August 20, 2017. This UAV is equipped by the manufacturer with a global navigation satellite system (GNSS) receiver and an inertial measurement unit (IMU). A multispectral camera (RedEdge, Micasense, Seattle, WA, USA; Figure 4.2b) mounted on the UAV collected images at 120-m above ground level (AGL). The images had a pixel resolution of 7.64 cm and contained five spectral bands: blue (≈475 to 500 nm), green (≈550 to 565 nm), red (≈665 to 675 nm), red edge (≈715 to 725 nm), and NIR (≈825 to 860 nm). The images were taken between 11:00 and 13:00 local time with an optimized fixed-exposure. Eight ground control points (GCPs) were used during each flight to improve the geographical accuracy of the mosaicked image of each field area. The GCPs were placed in each field at the four corners and four midpoints of each side. Ground-truth data were collected on August 25, 2017, and involved using a GPS receiver to record boundary locations of some CRR zones (Figure 4.3). A total of about 20 plants from these zones were removed and evaluated for the presence of the fungus on the roots in order to validate the presence of CRR in the zone.

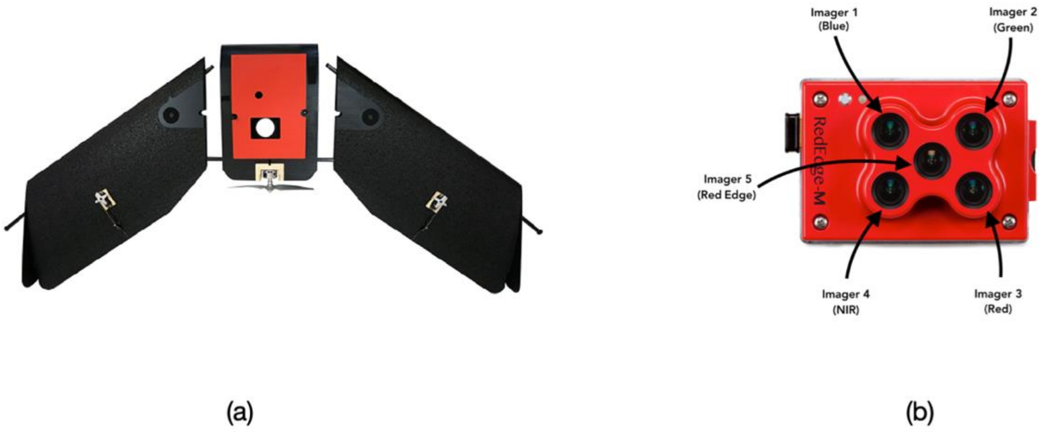

Figure 4.2 The images were captured from (a) a fixed-wing UAV “TuffWing UAV Mapper” with (b) MicaSense RedEdge camera.

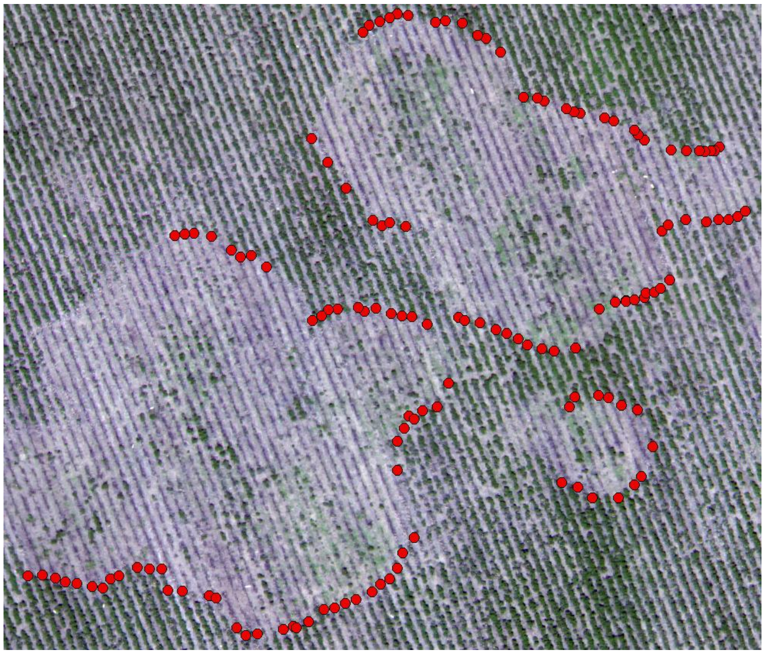

Figure 4.3 A portion of ground-truth data collected on Aug 25, 2017. Totally 627 ground-truth data points (in red) were recorded to delineate the boundary of some CRR-infested zones.

4.2.3. Data preprocessing

A 0.95-ha area was covered in each image with the AGL and camera used. An 80% forward overlap and 70% side overlap flight plan was used for image acquisition. The raw images were collected in tiff format with data from the GNSS receiver and IMU stored as image metadata. Image mosaicking was conducted with Pix4D software (Pix4D S.A, Lausanne, Switzerland). A Geoexplorer 6000 (Trimble, Sunnyvale, CA) GNSS receiver was used in the fields to collect the coordinates of the GCP centroids for geo-referencing of the images, also conducted in Pix4D. The centers of the GCPs in each raw image were manually linked to the corresponding ground-truth GNSS coordinates during the geo-referencing process.

Figure 4.4 PSR+ 3500 Spectroradiometer was used to collect reflectance information.

Three spectrally flat reference tiles were used for radiometric calibration: dark gray (≈3% reflectance) medium gray (≈20% reflectance), and light gray (≈45% reflectance). The actual reflectance spectra of the calibration tiles were collected with a portable spectroradiometer (Figure 4.4) (PSR+ 3500, Spectral Evolution, Haverhill, MA). A linear relationship between known reflectance and image-pixel digital numbers (DNs) was established for each band. All DN images were converted to reflectance images in ENVI software (Harris geospatial solution, Boulder, CO) based on these relationships.

4.2.4. Regional classification

Previous studies have used regional classification for CRR detection [8,9,22,23,25,91]. In a related prior study involving UAV remote sensing of CRR [92], each CRR-infested zone was identified as a region of plants rather than individual plants. The image data were classified into healthy and CRR-infested regions with unsupervised, semi-supervised, and supervised classification methods. The unsupervised and semi-supervised methods were based on k-means clustering and included one two-class method (unsupervised) and three multi-class (3, 5, and 10 classes) methods that combined more classes to form two classes based on user knowledge and judgment (semi-supervised). The supervised methods, which required selection of training data by a human operator, were two-class methods and included support vector machine (SVM), minimum distance (MD), maximum likelihood (ML), and Mahalanobis distance (MHD) classifiers. The CIR images of four of the five regions described above (the other region in the current study was used for a fungicide application test as described below) were used to evaluate the classification methods by comparing their overall accuracies, errors of omission and commission, and kappa coefficients. These images covered 5.68-ha, 0.15-ha, 0.42-ha, and 0.34-ha of field regions CH1, CH2, SH, and WP, respectively (Figure 4.5). In the current study, the regional classification results from the related prior study were used for comparison with plant-by-plant classification.

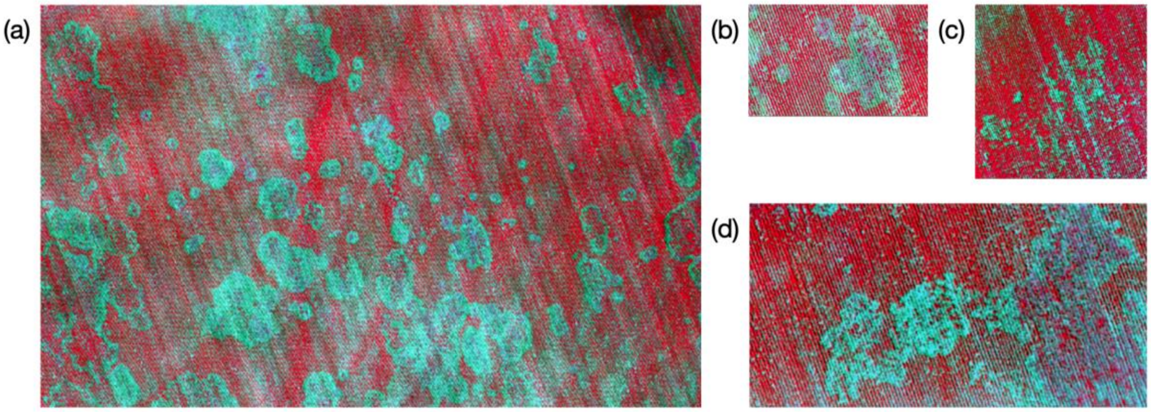

Figure 4.5 Multispectral color-infrared (CIR) images for (a) Region 'CH1' (Scale 1:3000), (b) Region 'CH2' (Scale 1:2000), (c) Region 'WP' (Scale 1:2400), and (d) Region 'SH' (Scale 1:3800). The regions were shown in different scales for a better visualization of details.

4.2.5. Plant-by-plant classification

The high spatial resolution of UAV RS images makes it possible to detect CRR infection at a plant-by-plant (PBP) level of precision. The 7.64-cm resolution in the current study provides for roughly 120 pixels per plant zone at full canopy cover, assuming 76-cm (30-in.) row spacing and average seeding distance of 12 cm (4.6 in.) at 45,000 seed per 0.405 ha (1.0 ac.). This number of pixels per plant should be adequate for identifying specific features to enable discrimination of plants based on spectral and spatial information. A new PBP classification method was thus proposed and based on Superpixel and k-means algorithms. This combination of algorithms was selected because the Superpixel algorithm, used appropriately, should have the capability to identify single plant zones, and k-means has been demonstrated to distinguish CRR-infected from healthy plants.

The simple linear iterative clustering (SLIC) Superpixel algorithm [93,94] is based on visual color converted to the three-dimensional (3D) spherical CIE-Lab color space. CIE-Lab expresses colors in numeric terms and deals with the issue that colorimetric distance in measurements does not correspond with the color difference perceived by humans. In this study, CIR images were used based on the fact that healthy plants are more easily visually differentiated from unhealthy plants with CIR instead of visual color images. In CIR images, the image spectral bands are converted from green to blue, red to green, and NIR to red for visual display. Other researchers have used NIR to enhance the SLIC Superpixel algorithm results based on RGB [95], but in this study the SLIC Superpixel algorithm was used on the RGB-channel outputs of the CIR images, so CIR was directly converted to an artificial CIE-Lab by way of a CIR-based XYZ color space.

Figure 4.6 is the flowchart of the PBP classification algorithm. The SLIC Superpixel algorithm was first applied to a CIR image, and a number (k) of superpixel “seeds” were then generated and distributed uniformly across the image. The imported image was then divided into superpixels (small, rather homogenous, areas in the image) based on spectral and shape information around each “seed.” The mean of the DN values within each superpixel was calculated and assigned to the superpixel so that it had a single DN value. The number (k) of superpixels was user-determined and provided to the algorithm based on the field planting rate; i.e., the number of superpixels was expected to be similar to the number of cotton plants in the image, multiplied by a scaling factor to account for bare soil areas in the image. K-means clustering was applied to the superpixel image to achieve a two-class regional classification, with “1” and “0” to represent CRR and healthy zones, respectively. At the same time, planting rows were detected by calculating the gradient of the raw image. A binary plant row image was generated, with “0” and “1” representing plant rows and the gaps between them, respectively. The centroids of each superpixel were identified and marked as potential cotton plant centroids, with “1” and “0” representing cotton plant and bare soil, respectively. The centroids of superpixels located in the CRR zone (as determined by k-means) and the planting row were regarded as locations of CRR-infected plants. The centroids of superpixels located in healthy zones and within the planting row were regarded as locations of healthy plants.

The classifier logic was applied to all image pixels and can be expressed with the following equation:

$$C = \begin{cases} 0 | \, S_n \cap P_n = 1, \ \mathrm{Z}_n = 0 \\ 1 | \, S_n \cap P_n = 1, \ \mathrm{Z}_n = 1 \\ 2 | \, other\ pixels \end{cases} \tag{1}$$

where Z_n is the regional classification based on k-means, in which value “0” = healthy zone, and value “1” = CRR zone; S_n is the status of superpixel centroid location or not superpixel centroid location, in which value “0” = not superpixel centroid location, and value

“1” = superpixel centroid location; P_n is the status of planting row or gap between rows, in which value “0” = gap, and value “1” = row; and $C = \{\psi | \psi: \mathbb{R} \rightarrow \{0,1,2\}\}$ is an overall class containing all pixel classes.

While C = 0, the superpixel centroid location is marked as an individual healthy cotton plant. While C = 1, the superpixel centroid location is marked as a CRR-infected plant. C = 2 represents no superpixel centroid at this location, no matter whether the pixel is classified as healthy or infested.

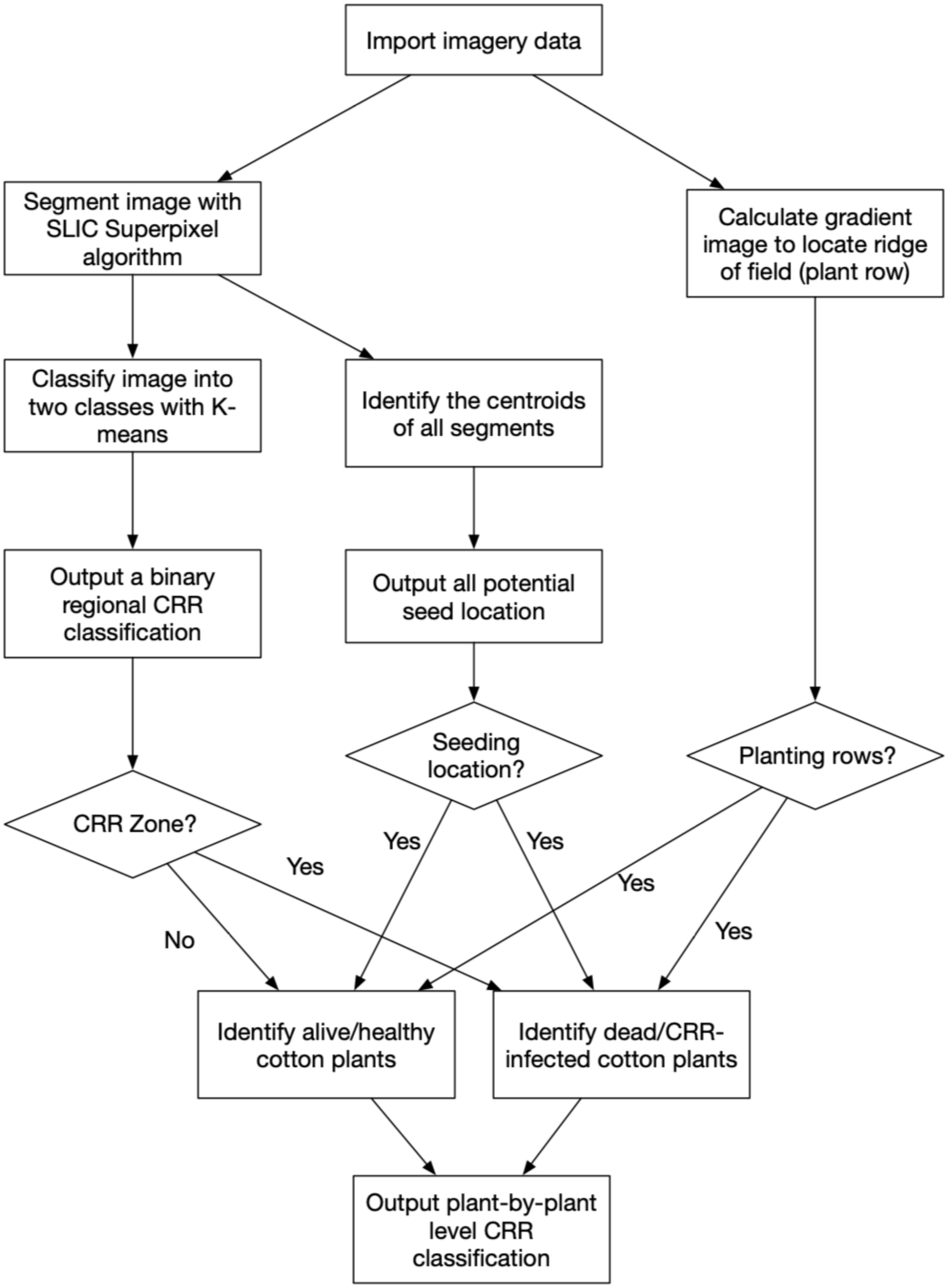

Figure 4.6 Flow chart of unsupervised plant-by-plant (PBP) classification algorithm. CRR= cotton root rot; SLIC= simple linear iterative clustering.

4.2.6. Accuracy assessment

Accuracy assessment involves specific means of evaluating the performance of classifications [75,76]. A ground-truth map was drawn manually on the original high-resolution UAV images. In this process, the ground-truth data collected on Aug 25, 2017, were used as a visual reference when applying the following protocol. Zones in the field with more than approximately ten immediately adjacent infected plants were categorized as CRR-infested zones. In larger CRR-infested zones, more than ten immediately adjacent healthy plants were categorized as healthy zones. The regional classification maps were resampled to the higher resolution of the ground-truth map and compared to it on a pixel-by-pixel basis. This method is common for accuracy assessment of raster-based classification maps. On the other hand, the PBP classification maps, which were vector point maps, were compared to the ground-truth map at only the locations of the superpixel centroids; i.e., the classification of a superpixel was compared to the pixel at its centroid location on the ground-truth map. This method was selected to enable comparison to the ground-truth map at the plant level instead of the pixel level. It should be noted that the number of comparisons between a regional classification and the ground-truth map was much higher than the number for PBP classification. However, the methods used are considered reasonable for the type of data being evaluated; e.g., the regional classification maps did not have adequate resolution for plant-level comparison. Confusion matrices were developed based on the individual comparisons within these zones (Table 4.1).

Table 4.1 Confusion matrix to evaluate classification methods.

		Class types determined from reference source (Ground-truth)		
Class types determined from classified map		Healthy plant	Infested plant	Totals
	Healthy plant	A	B	A+B
	Infested plant	C	D	C+D
	Totals	A+C	B+D	A+B+C+D

The kappa coefficient, which indicates the agreement between the "predicted" and "true" values, was calculated from the derived confusion matrices and the following formula

$$k = \frac{N\sum_{i=1}^{n} t_{i,i} - \sum_{i=1}^{n}(G_i P_i)}{N^2 - \sum_{i=1}^{n}(G_i P_i)} \tag{2}$$

where N is the total number of pixels; i is the class number; $t_{i,i}$ is the correctly classified number of pixels in Class i; G_i is the total number of pixels classified as Class i in ground-truth data; and P_i is the total number of pixels classified as Class i in the predicted data.

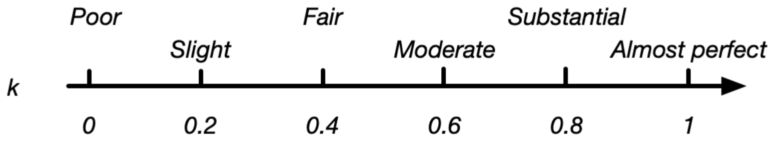

Figure 4.7 The interpretation of the Kappa coefficient

A kappa value of 1 indicates that the classification has perfect agreement with the true value, and a value of 0 indicates no agreement between the classification and ground truth (Figure 4.7). The errors of commission, representing a measure of false-positives, and errors of omission, representing a measure of false-negatives, were also calculated to evaluate the classifiers. Regional classification methods including k-means, SVM, MD, ML, and MHD were compared to the PBP classification method based on overall classification accuracy, the kappa coefficient, and errors of commission and omission.

4.2.7. Test of PBP fungicide treatment in field

An in-furrow, at-planting spray application is the most common way to apply the Topguard Terra (FMC Agricultural Solutions, Philadelphia, PA) fungicide (flutriafol) that is licensed for treatment of CRR. The continuous application of the fungicide over the top of seeds as they are planted treats not only soil close to the seed, but also a length of soil between seeds that may not need treatment. This process may result in applying more product than necessary, so it is important to determine whether applying the fungicide to individual seeds or plants is effective. To test whether PBP fungicide treatment is effective in protecting cotton plants from CRR infection, a stem-drench treatment – also proven in research trials to be an effective application method – was used in place of the at-planting application method. Specifically, the fungicide spray solution was applied to the stem of the cotton plant and a small amount of soil surrounding the stem. An 18.3-m × 30.5-m (60-ft × 100-ft) test plot in field region PL was used to conduct this experiment.

Four treatments were applied: (1) a conventional at-planting treatment of in-furrow continuous spray over the top of planted seeds, applied with a tractor-pulled planter; (2) a stem-drench continuous spray, applied manually with a backpack sprayer; (3) a stem-drench pulsed spray on individual plants, applied manually with a backpack sprayer; and (4) a no-fungicide control. The experiment had 24 rows (Figure 4.8) of 100 ft (30.48 m) in length, with an adjacent pair of rows receiving a treatment, and three replications per treatment, arranged in a randomized complete block design. For the two continuous-spray treatments, Topguard Terra was applied at 0.675 g active ingredient in 216 mL per 30.5 m (100 ft) of row length. This rate is equivalent to the labeled application rate of 237 mL (8 fluid oz.) formulation in 37.9 L (10 gal.) of water applied to 0.405 ha (1.0 ac.).

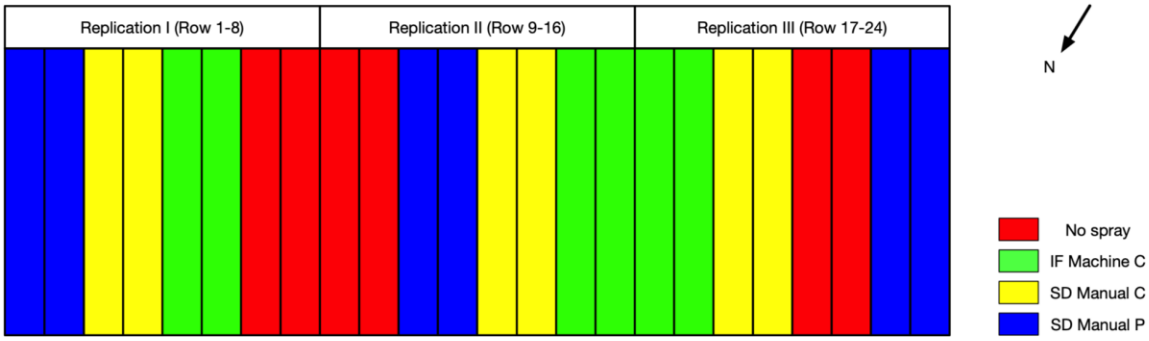

Figure 4.8 Plot design for testing the effectiveness of fungicide on plant-by-plant treatment. Note: IF Machine C = in-furrow machinery continuous spray, SD manual C = stem-drench manual continuous spray, and SD Manual P = stem-drench manual pulsed spray.

(a)

(b)

Figure 4.9 (a) A Case IH 1230 planter was used for in-furrow application; and (b) a CO2 –pressurized backpack sprayer was used for manual treatments.

A CASE IH 1230 12-row Early Riser planter (Case Corp., Wisconsin, USA) with 76.2 cm (30-inch) row spacing was used for seeding of all treatments and the application of the in-furrow fungicide treatment (Figure 4.9a). The seeding rate of Phytogen 490 cotton seed was roughly 45,000 per 0.405 ha (1.0 ac.). For the manual continuous-spray and pulsed stem-drench treatments, a pressurized CO_2 backpack sprayer was used (Figure 4.9b) with a pressure of 241 kPa (35.0 psi). Plots were planted and the in-furrow treatment was applied at planting on May 10, 2018. The soil temperature was 34 ℃（94 ℉).

The manual continuous and pulsed stem-drench spray treatments were applied when the cotton plants were at the four true leaf growth stage, on June 6, 2018. Spray was applied close to the stems at a height of 2 to 3 cm above the ground. With the pulse treatment, the volume of water containing the fungicide applied to the rows varied depending upon plant stand and spacing, with an average of 268 mL per 30.5 m (100 ft) of row; the application range was 160 to 450 mL. In other words, 1.67 mL of flutriafol (active ingredient) was used on average per 30.5-m-length of cotton plant row, and the actual flutriafol application range was 1.00 to 2.80 mL. For comparison, in-furrow planting consumed 1.68 mL flutriafol per 30.5-length of row. The experiment was repeated in 2019 with a reduction in fungicide application rate. An average of 122 mL of fungicide (0.67 mL flutriafol) was used per row for stem drench pulse spray treatment in 2019 (range: 60 mL to 130mL).

4.3. Results

4.3.1. Plant-by-plant classification

One example (Region CH2) of the progression of the image processing results from each step in the PBP classification method is shown in Figure 4.10. The raw image (Figure 4.10a) gradient was calculated to identify the planting rows (Figure 4.10b). SLIC Superpixel segmentation was applied to the gradient map to determine possible locations of individual plants (Figure 4.10c). The original pixels of the raw image were aggregated into larger superpixels (Figure 4.10d) to identify individual plant locations. The k-means algorithm was applied to the superpixels to generate a two-class regional classification (Figure 4.10e). The final result of PBP classification is shown in Figure 4.10f, in which each individual healthy plant is marked with a yellow point, and each CRR-infected plant is marked with a blue point.

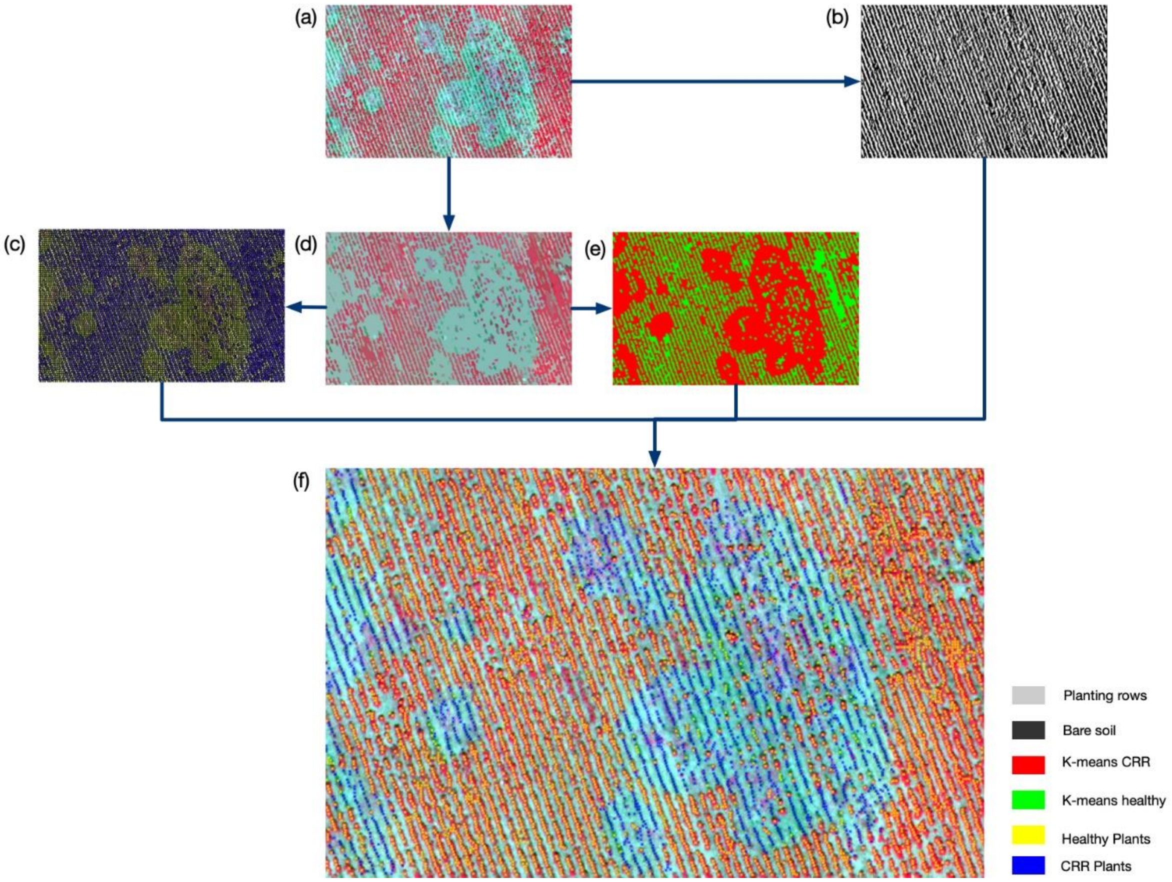

Figure 4.10 The imagery results getting from each step of unsupervised PBP classification algorithm. each image indicated: (a) CIR raw image, (b) the location of planting row, (c) the position of each individual plant, (d) the result of Superpixel segmentation, (e) the regional distribution of CRR-infested areas, and (f) the final result of PBP classification. In (b), planting rows are shown in light grey, and bare soil is shown in black. In (e), healthy regions are shown in green, and CRR-infested regions are shown in red. In (f), each yellow dot represents a healthy cotton plant, and each blue dot represents and CRR-infected plant.

The accuracy assessment of PBP classification showed that it is a highly accurate method of differentiating between healthy and CRR-infected plants at the individual-plant level. In Region CH2, the PBP classification had the highest overall accuracy of 95.94%, as well as the highest Kappa coefficient of 0.8617, which indicated very strong agreement between classification and ground-truth data (Table 4.2). Table 4.2 is the confusion matrix for PBP classification applied to Region CH2. Over 11,000 plants identified by the PBP algorithm in CH2 were evaluated, and about 82% of those were identified as healthy according to ground-truth data. About 13.1% of the healthy plants were misclassified as CRR-infected (overclassification), while about 9.5% of the actually CRR-infected plants were misclassified as healthy (underclassification).

Table 4.2 Confusion matrix of PBP classification for Region CH1.

		Class types determined from reference source (Ground-truth)			**Commission**	**Omission**
Class types determined from classified map		Healthy plant	Infected plant	Totals		
	Healthy plant	8,963	186	9,149	186/9149 2.03%	268/9231 2.9%
	Infected plant	268	1,771	2,039	268/2039 13.14%	186/1957 9.5%
	Totals	9,231	1,957	11,188		

The PBP classifications were also generated for CH1, WP, and SH. In CH1, the PBP algorithm achieved an overall accuracy of 93.5%, a kappa coefficient of 0.7848, an error of commission of 16.1%, and an error of omission of 18.6%. In SH, the PBP algorithm also had a high accuracy of 90.6% with a kappa coefficient of 0.7494. The errors of commission and omission were 12.2% and 8.5%, respectively. Compared to the other regions, WP had the lowest accuracy of 88.4%, but even this level would typically be acceptable for field application. The kappa coefficient, error of commission, and error of omission for WP were 0.6048, 20.9%, and 26.8%, respectively.

4.3.2. Comparison to regional classifications

Thirty-six confusion matrices were generated from the results of the nine overall classification methods as applied to the four field regions. These confusion matrices are summarized in Table 4.3. The two-class k-means classifier identified CRR-infected cotton plants in the image automatically, but the overall accuracy averaged only 77.5%. The kappa coefficient of 0.491 also indicated relatively weak agreement between the classification and ground-truth data. The error of commission of 46% indicated that almost half the plants classified as CRR-infected were overclassified. Manually combining three-class, five-class, and ten-class k-means classifications improved the overall accuracy to 83.5%, 84.4%, and 84.1%, respectively. The kappa coefficients also increased to 0.547, 0.552, and 0.576, respectively, indicating moderate agreement between classification and ground truth. However, it must be noted that combining classes required expertise from and implementation by the user, meaning that the ideal of automated processing was not realized.

Using supervised classifiers including SVM, MD, ML, and MHD increased the overall accuracy to 86.3%, 85.7%, 86.5%, and 87.7%, respectively. All of these classifiers performed significantly better ($\alpha = 0.05$) than two-class k-means in overall accuracy. The kappa coefficients for these classifiers were 0.659, 0.636, 0.667, and 0.786, respectively. While supervised classifiers performed better than the unsupervised and semi-supervised classifiers, they did not perform as well as the PBP classifier, and it must be noted that these also need human intervention, specifically for selection of training data based on subjective judgment.

The PBP classification method averaged 92.1% overall accuracy, by far the best among all classifiers considered. This accuracy level was significantly higher ($\alpha = 0.05$) than that of the unsupervised and combined unsupervised classifiers. The average kappa coefficient was 0.786, indicating strong agreement between the classifications and ground truth, and this value was significantly better ($\alpha = 0.05$) than that of all the other classifiers considered. The average errors of commission and omission, 15.56% and 15.85%, were also the lowest in the overall comparison group.

Table 4.3 The accuracy comparison between unsupervised, combined-unsupervised, supervised classifications, and proposed automatic regional classifications.

		Overall Accuracy (%)						Kappa Coefficient					
		CH1	CH2	WP	SH	Mean	Std. Dev.	CH1	CH2	WP	SH	Mean	Std. Dev.
U	2-class KM	78.60	71.11	78.76	81.44	77.48 ^{a}	4.42	0.5106	0.3826	0.4527	0.6162	0.4905 ^{a}	0.0988
S-S	3 to 2-class KM	88.89	78.28	87.26	79.45	83.47 ^{ab}	5.38	0.6868	0.3875	0.5751	0.5392	0.5471 ^{ab}	0.1236
	5 to 2-class KM	88.67	76.50	88.81	83.49	84.37 ^{ab}	5.80	0.6085	0.4232	0.5293	0.6452	0.5516 ^{ab}	0.0983
	10 to 2-class KM	90.97	76.36	88.01	81.14	84.12 ^{ab}	6.61	0.6986	0.4264	0.5885	0.5911	0.5762 ^{ab}	0.1122
S	SVM	92.02	87.04	78.66	87.48	86.30 ^{bc}	5.57	0.7587	0.6962	0.4481	0.7345	0.6594 ^{ab}	0.1432
	MD	88.12	85.65	86.14	82.79	85.68 ^{bc}	2.20	0.6753	0.6721	0.5604	0.6346	0.6356 ^{ab}	0.0534
	ML	91.71	88.55	77.92	87.65	86.46 ^{bc}	5.95	0.7498	0.7342	0.4419	0.7422	0.6670 ^{ab}	0.1502
	MHD	89.60	87.89	87.13	86.27	87.72 ^{bc}	1.42	0.7076	0.7238	0.5764	0.7144	0.6806 ^{bc}	0.0698
P	PBP	95.94	93.52	88.43	90.64	92.13 ^{c}	3.28	0.8617	0.7848	0.6048	0.7494	0.7855 ^{c}	0.0746

		Errors of Commission (%)						Errors of Omission (%)					
		CH1	CH2	WP	SH	Mean	Std. Dev.	CH1	CH2	WP	SH	Mean	Std. Dev.
U	2-class KM	50.43	49.89	56.88	27.16	46.09 ^{a}	13.01	7.84	26.72	14.10	18.00	16.67 ^{a}	7.90
S-S	3 to 2-class KM	30.04	26.46	40.17	17.43	28.53 ^{ab}	9.40	17.22	60.87	28.28	41.43	36.95 ^{b}	18.77
	5 to 2-class KM	14.26	40.18	24.23	19.36	24.51 ^{ab}	11.21	44.58	42.32	51.63	25.30	40.96 ^{b}	11.17
	10 to 2-class KM	10.85	40.83	37.51	21.20	27.60 ^{ab}	14.08	34.95	40.57	29.83	30.73	34.02 ^{b}	4.90
S	SVM	18.50	25.38	57.07	16.18	29.28 ^{ab}	18.93	19.66	16.21	15.04	16.69	16.90 ^{a}	1.97
	MD	32.90	29.17	43.70	22.15	31.98 ^{ab}	9.00	14.48	14.13	24.71	23.19	19.13 ^{a}	5.60
	ML	19.38	23.85	57.88	18.53	29.91 ^{ab}	18.79	20.17	11.92	13.23	12.39	14.43 ^{a}	3.87
	MHD	28.74	26.13	40.79	20.73	29.10 ^{ab}	8.48	15.18	9.91	26.86	13.25	16.30 ^{a}	7.37
P	PBP	13.14	16.06	20.88	12.16	15.56 ^{b}	3.91	9.5	18.59	26.80	8.51	15.85 ^{a}	8.60

Note: U = unsupervised, S-S = semi-supervised, S = supervised, P = proposed method, KM = k-means, MD = minimum distance, ML = maximum likelihood, MHD = Mahalanobis distance, PBP = plant-by-plant. Letters a, b, and c in Column Mean indicate statistical different groups ($\alpha = 0.05$, Duncan test).

A comparison chart of the errors of commission and omission is shown in Figure 4.11. Theoretically, the ideal classifier, which has 100% accuracy and thus no errors of commission or omission, should be located at the origin of this coordinate system. The PBP classifier is the one closest to the origin by far, indicating that it clearly performed the best in terms of overall accuracy. It is worth noting here that in the aforementioned related prior study [92], two methods proposed to take advantage of the high resolution of UAV images, k-means plus support vector machine (KMSVM) and k-means segmentation (KMSEG), were evaluated with only regions CH1, WP and SH. The two methods had approximately 22% and 16% error of commission and 18% and 11% of error of omission, respectively. The KMSEG classifier, which is a fully automated regional classifier, generated similar results to the PBP classifier on a somewhat different data set. Both KMSEG and KMSVM are regional classifiers that were designed to take advantage of the morphological information available in high-resolution UAV images. Thus, like the PBP classifier, they were meant as improvements over traditional regional classifiers. The added advantage of the PBP classifier is that it is designed to classify individual plants, a tremendous advantage when subsequently applying fungicide on a PBP basis.

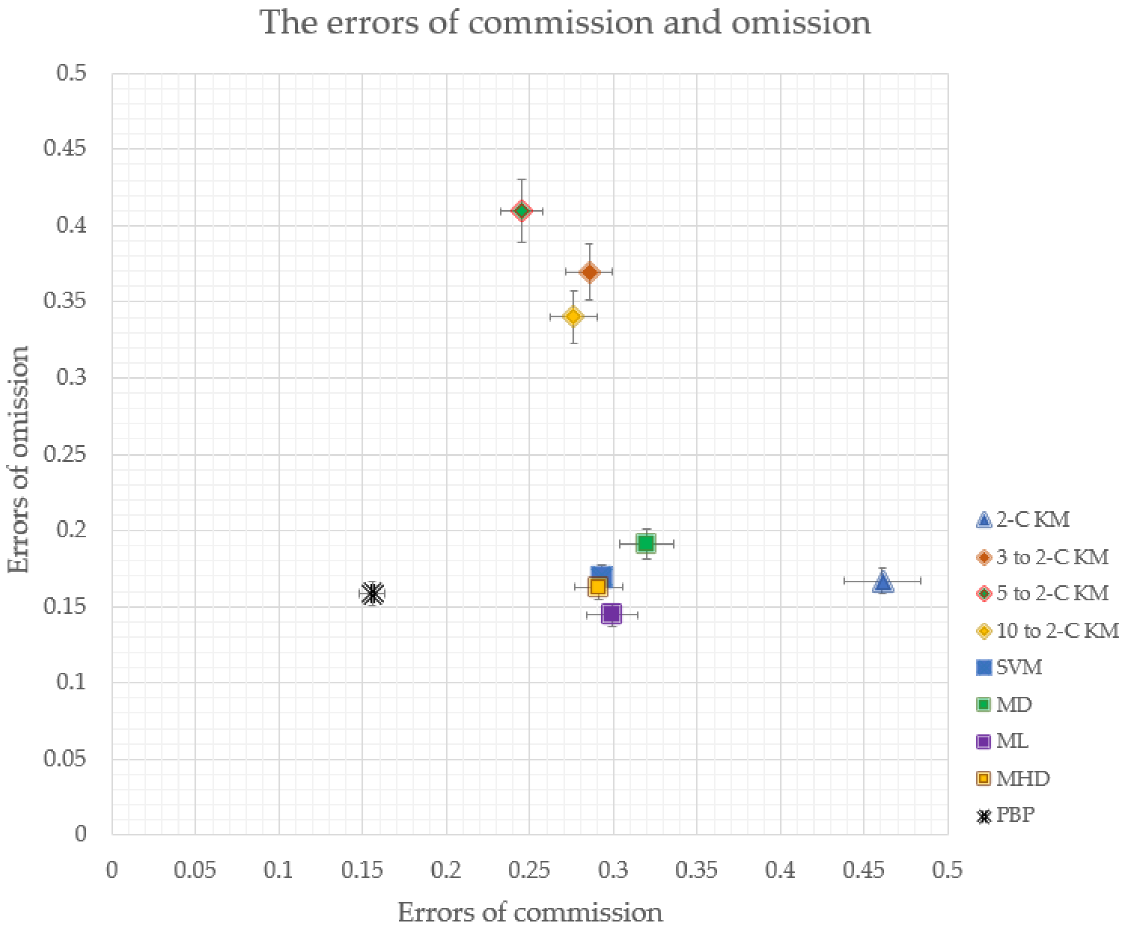

Figure 4.11 Comparison of the errors of commission and omission among classifiers.

4.3.3. Test of method of fungicide application for CRR control

In the study on fungicide application methods, the application of Topguard Terra generally reduced the incidence of CRR compared to the control (Table 4.4), as expected. The manually pulsed stem-drench treatment had the lowest plant mortality among the treatments, but the difference from the other two fungicide treatments was not significant. While in most years, the portion of the field (PL) used in this experiment eventually approaches 100% mortality from CRR, the dry weather in 2018, the first year this study was conducted, resulted in low severity of CRR. Assuming a 5% significance level, there was no statistically significant difference among all the treatments. However, the pulsed stem-drench (i.e., PBP) treatment would be considered significantly better than the no-spray control treatment if a 15% level of significance were assumed. While this is an uncommonly weak significance level, it is reasonable to believe that all three methods of applying fungicide, including the PBP method, offered some protection against CRR. Because of even drier conditions in 2019 than 2018, no CRR development was observed during the experiment, so efficacy could not be assessed in 2019.

Table 4.4 Effect of Topguard Terra application method on CRR (% mortality) in the 2018 experiment.

Method*	Replication 1	Replication 2	Replication 3	Mean**
No spray	4.79	0.32	7.69	4.27 ^{a}
In-furrow	3.92	0.57	0.98	1.83 ^{ab}
Stem Drench C	0.00	2.45	2.17	1.54 ^{ab}
Stem Drench P	0.62	1.42	1.05	1.03 ^{b}

* C= continuous application, P= pulse application **The different letters indicate statistically different groups (α = 0.15, Duncan test).

4.4. Discussion

In this study, the errors of commission represent the percentage of plants over-classified into the CRR category. The errors of omission represent the percentage of CRR-infected plants misclassified as healthy plants. From an economics perspective, omission plays a more important role than commission for CRR detection, because over-spraying of fungicide caused by over-classification would likely cost less than the loss of CRR-infected plants that could have been protected. The zones with weeds growing on bare soil, very possibly next to a dead cotton plant, contributed to the errors of omission.

While not necessarily as critical, it should be noted that the errors of commission were commonly observed at zones where bare soil was evident where there was no CRR-infected plant. The mixed pixels of soil, plant leaves, and shadow of plants, which were commonly present at the boundaries between healthy and infested zones, also caused a large number of errors of commission and omission with the regional classifiers, because the mixed pixels do not represent the reflectance information from a single object.

The homogenieity of the field could also affect the classification accuracy. Regions CH1 and CH2 were from the same cotton field, and the images of them were from the same flight mission. The patterns of planting and disease as well as the reflectance information were similar, and the lighting conditions were the same. The main difference between the regions was that CH2 was smaller than CH1. The results of classification in CH2 were better than in CH1 in most cases, especially for unsupervised classification. One reason is that unsupervised classification clusters data into different classes based on the "otherness" of data. Once the sample size becomes larger, more diverse data besides healthy and infected cotton are introduced into the field of view, such as a concrete road, power line, pond, or other objects. All of this "noise" can reduce the accuracy of classifiers. A prerequisite for an accurate automated classification is to have images consisting of only rows of cotton plants. All the classifiers had relatively low accuracies on Region WP compared to the other three regions. It is possible this was because the planter experienced mis-seeding during planting, causing a narrow and long "dead zone" consisting mainly of bare soil. Manual manipulation can be used as postprocessing to correct the misclassification from mis-seeding, but it violates the intent of automation in classification. Morphological image processing tools such as erosion and dilation could be introduced in the future to improve the performance of differentiating mis-seeding from cotton root rot while maintaining the automation of classification [92].

Comparing regional and PBP classifications is challenging because regional classification is based on pixels while PBP classification is based on individual plants. To make the comparison even more convincing, the classifications should ideally be evaluated with the same protocols. Comparing pixel differences between all classifications (PBP and regional classifications) and the same ground-truth map is a fair way to evaluate and compare classifications, but it is not readily done when the classifiers produce different types of maps as results. The PBP classifier output a vector point map, whereas the regional classifiers output raster maps, so the comparisons to the ground-truth map had to be done with different methods appropriate to each form of data.

In the comparison of fungicide application methods, the results should be validated by further study, as the disease pressure was low in both years due to dry weather conditions. However, the experiment did substantially support the concept of pulse application to reduce fungicide use. In 2018, the manual application of the pulse spray method was inefficient and actually resulted in the application of a greater amount of fungicide than the continuous spray, but in 2019, an average of 43% less fungicide was used because of improvements in the application technique. If efficacy of the fungicide holds up with that method and application rate, the overall concept of PBP detection, mapping, and fungicide application will be validated.

Considering computational requirements, the PBP algorithm required more computing time than the regional classification methods, because segmenting and locating seed positions is computationally intensive. For the 0.15-ha CH2 image, about 30 seconds. was required to generate the classification on a 2016 Macbook Pro computer with an Intel i7-6920HQ central processing unit (CPU) and Radeon Pro 460 graphic processing unit (GPU). The PBP classification algorithm is slower than other conventional regional classification methods, but it is still acceptably fast. While a larger field might require a few hours to complete the classification, these classifications do not need to be done in real time. Rather, they can be performed between growing seasons.

As discussed previously, UAVs provide much higher resolution (decimeter level to centimeter-level) remote sensing data than manned aircraft or satellites (meter level). This study was intended to explore how to make use of the high-resolution data in CRR detection in the creation of PBP prescription maps. The application of fungicide at the PBP level is clearly possible from a technological standpoint. Wilkerson et al. tested a seed-specific in-furrow fungicide application system and found that the system could achieve as high as 95% accuracy for seed-specific treatment in cotton [96]. However, identifying, predicting, locating, and treating the disease at the PBP level are the obstacles to high-precision treatment of CRR, as well as other plant diseases. This study shows that CRR-infected plants in the current season can be individually identified with high accuracy, and PBP fungicide treatment appears to be effective in controlling CRR.

The remaining challenges to be investigated are (1) whether the precise location of individual CRR-infected plants is predictive for the following year, and (2) whether previously developed precision-spray technology [44] enables fungicide to be practically applied at these locations on a seed-by-seed basis.

There is no evidence to suggest that CRR can be cured once a plant is infected; the fungicide must be applied prior to disease development. Thus PBP application of fungicide requires previous years' data to predict CRR-infested areas in future years. The entire PBP classification process can be conducted automatically if an appropriate seeding rate is known beforehand. Management of other crop diseases that can be treated during the growing season could potentially benefit from this type of high-resolution classifier.

4.5. Conclusion

This study involved development and evaluation of a plant-by-plant (PBP) classifier that is able to detect CRR-infected plants at the single-plant level automatically. The PBP classifier is mainly based on the Superpixel segmentation and k-means clustering algorithms. Compared to conventional regional classification methods, PBP achieved the highest overall accuracy of 92.1%, the highest kappa coefficient of 0.786, the lowest errors of commission of 15.6%, and the second-lowest errors of omission of 15.9%. The PBP fungicide treatment in the field was also apparently effective in controlling CRR infection. These results generally validate the idea of plant-level CRR treatment and suggest the likelihood of major advances in high-resolution precision agriculture practices in the future.

5. CONCLUSIONS

A motivation for this dissertation is that it is expected that a UAV can be flown, remote-sensing images collected, and data uploaded to a cloud service platform fairly easily and quickly. An automated algorithm could then identify the CRR location in the field of interest precisely and accurately. The fungicide could then be precisely and economically applied in subsequent years to avoid losses from CRR disease.

UAV remote sensing bears great potential to collect high-resolution information on cotton fields. Diseases like CRR can be efficiently identified, monitored, and controlled with the help of UAV remote sensing. In this dissertation, it was first demonstrated that practical CRR fungicide prescription maps could be generated from UAV based remote sensing data. In 2017 the fungicide was applied based on the CRR-infested locations identified in 2015. The CRR was effectively controlled by the fungicide prescription, and the precision application saved on the cost of fungicide as well as the yield loss caused by CRR.

This dissertation also proposed new automatic regional CRR classification methods that make use of the high-resolution of UAV remote sensing data. It has become known that conventional classification methods often do not perform well on UAV remote sensing data, because the high-resolution of UAV remote sensing data introduces new classes of information that can reduce the classification accuracy. A proposed method called KMSVM (k-means and support vector machine) uses the concept of semi-supervised classification to identify the CRR-infested area automatically with a machine learning approach. Another proposed method, KMSEG (k-means and morphology-based segmentation), uses morphological image processing to fulfill the task of CRR detection accurately and automatically. Both methods performed better than conventional regional techniques in a comprehensive comparison with ground-truth data.

An additional novel classification method was proposed to take further advantage of high-resolution UAV data, such that fungicide could be applied at the plant-by-plant (PBP) level. This method was developed based on Superpixel segmentation and k-means clustering algorithms and can identify individual cotton plants and whether they are CRR-infected or not. A field test demonstrated that treating individual plants maintains the effectiveness of fungicide for protecting the cotton plant.

Based on the results of this dissertation, two remaining research questions to be addressed are as follows. (1) Can precision application technology be improved to apply fungicide at the PBP level to take advantage of the advanced image-processing methods? (2) Is the geographic stability of CRR zones in the field strong enough to allow for predicting CRR in future years and applying fungicide at the PBP level? While these questions remain, it is clear that UAV remote sensing can be used to (a) delineate CRR (and possibly other diseases) at high resolution, even to the level of individual plants, and (b) generate effective prescription maps for at-planting fungicide application to control CRR.

REFERENCES

1. USDA-NASS Agricultural Statistics 2017 Available online: https://quickstats.nass.usda.gov/results/224011AB-C0EF-3937-BBA5-A2774B7C7ECD.
2. United States Department of Agriculture *Cotton: world markets and trade*; 2018;
3. Pammel, L.H. Root rot of cotton or “cotton blight.” *Texas Agric. Exp. Stn. Bull.* **1888**, *4*, 50–65.
4. Neal, D.C. The Occurrence of Viable Cotton Root-Rot Sclerotia in Nature. *Science.* **1929**, *70*, 409–410.
5. Isakeit, T. *Cotton root rot (phymatotrichopsis root rot) and its management*; 2016;
6. Neal, D.C.; Wester, R.E.; Gunn, K.C. Treatment of cotton root-rot with ammonia. *Science.* **1935**, *75*, 139–140.
7. Smith, H. E.; Elliott, F. C.; Bird, L.S. Root rot losses of cotton can be reduced. *Misc. Publ. Agric. Exp. Stn.* **1962**.
8. Yang, C.; Odvody, G.N.; Fernandez, C.J.; Landivar, J.A.; Minzenmayer, R.R.; Nichols, R.L.; Thomasson, J.A. Monitoring cotton root rot progression within a growing season using airborne multispectral imagery. *J. Cotton Sci.* **2014**, *93*, 85–93.
9. Yang, C.; Everitt, J.H.; Fernandez, C.J. Comparison of airborne multispectral and hyperspectral imagery for mapping cotton root rot. *Biosyst. Eng.* **2010**, *107*, 131–139.

10. Gogineni, S.; Thomasson, J.A.; Iqbal, J.; Wooten, J.R.; Kolla, B.M.; Sui, R. Remote sensing input to GIS-integrated cotton growth model: preliminary results. **2004**, *5544*, 186.

11. Read, J.J.; Iqbal, J.; Thomasson, J.A.; Willers, J.L.; Jenkins, J.N. Remote sensing in dryland cotton: Relation to yield potential and soil properties. *Ecosyst. Dyn. Agric. Remote Sens. Model. Site-Specific Agric.* **2003**, *5153*, 61–72.

12. Yang, C.; Everitt, J.H. Using spectral distance, spectral angle and plant abundance derived from hyperspectral imagery to characterize crop yield variation. *Precis. Agric.* **2012**, *13*, 62–75.

13. Sui, R.; Thomasson, J.A.; Hanks, J.; Wooten, J. Ground-based sensing system for weed mapping in cotton. *Comput. Electron. Agric.* **2008**, *60*, 31–38.

14. Calderón, R.; Navas-Cortés, J.A.; Lucena, C.; Zarco-Tejada, P.J. High-resolution airborne hyperspectral and thermal imagery for early detection of Verticillium wilt of olive using fluorescence, temperature and narrow-band spectral indices. *Remote Sens. Environ.* **2013**, *139*, 231–245.

15. Apan, A.; Held, A.; Phinn, S.; Markley, J. Detecting sugarcane "orange rust" disease using EO-1 Hyperion hyperspectral imagery. *Int. J. Remote Sens.* **2004**.

16. Fletcher, R.S.; Escobar, D.E.; Everitt, J.H. Field Spectra and Airborne Digital Imagery for Detecting Phytophthora Foot Rot Infections in Citrus Trees. **2001**, *36*, 94–97.

17. Cook, C.G.; Escobar, D.E.; Everitt, J.H.; Cavazos, I.; Robinson, A.F.; Davis, M.R. Utilizing airborne video imagery in kenaf management and production. *Ind.*

Crops Prod. **1999**, *9*, 205–210.

18. Taubenhaus, J.J.; Ezekiel, W.N.; Neblette, C.B. Airplane photography in the study of cotton root rot. *Phytopathology* **1929**, *19*, 1025–1029.
19. Nixon, P. R., Lyda, S.D., Heilman, M.D., & Bowen, R.L. (1975). Incidence and control of cotton root rot observed with color infrared photography. *MP Tex Agric Exp Stn* **1975**.
20. Nixon, P.R.; Escobar, D.E.; Bowen, R.L. A multispectral false-color video imaging system for remote sensing applications. *Proc. 11th Bienn. Work. Color Aer. Photogr. Videogr. Plant Sci. Relat. Fields* 1987, 295–305.
21. Yang, C.; Fernandez, C.J.; Everitt, J.H. Mapping phymatotrichum root rot of cotton using airborne three-band digital imagery. *Trans. ASAE* **2005**, *48*, 1619–1626.
22. Yang, C.; Odvody, G.N.; Fernandez, C.J.; Landivar, J.A.; Minzenmayer, R.R.; Nichols, R.L. Evaluating unsupervised and supervised image classification methods for mapping cotton root rot. *Precis. Agric.* **2015**, *16*, 201–215.
23. Yang, C.; Odvody, G.N.; Thomasson, J.A.; Isakeit, T.; Nichols, R.L. Change detection of cotton root rot infection over 10-year intervals using airborne multispectral imagery. *Comput. Electron. Agric.* **2016**, *123*, 154–162.
24. Yang, C.; Greenberg, S.M.; Everitt, J.H.; Fernandez, C.J. Assessing cotton defoliation, regrowth control and root rot infection using remote sensing technology. *Int. J. Agric. Biol. Eng.* **2011**, *4*, 1–11.
25. Song, X.; Yang, C.; Wu, M.; Zhao, C.; Yang, G.; Hoffmann, W.C.; Huang, W.

Evaluation of Sentinel-2A satellite imagery for mapping cotton root rot. *Remote Sens.* **2017**, *9*, 1–18.

26. Wu, M.; Yang, C.; Song, X.; Hoffmann, W.C.; Huang, W.; Niu, Z.; Wang, C.; Li, W.; Yu, B. Monitoring cotton root rot by synthetic Sentinel-2 NDVI time series using improved spatial and temporal data fusion. *Sci. Rep.* **2018**, *8*, 1–12.
27. Yang, C.; Westbrook, J.K.; Suh, C.P.C.; Martin, D.E.; Hoffmann, W.C.; Lan, Y.; Fritz, B.K.; Goolsby, J.A. An airborne multispectral imaging system based on two consumer-grade cameras for agricultural remote sensing. *Remote Sens.* **2014**, *6*, 5257–5278.
28. Khanal, S.; Fulton, J.; Shearer, S. An overview of current and potential applications of thermal remote sensing in precision agriculture. *Comput. Electron. Agric.* **2017**, *139*, 22–32.
29. Bagheri, N. Development of a high-resolution aerial remote-sensing system for precision agriculture. *Int. J. Remote Sens.* **2017**, *38*, 2053–2065.
30. Zhou, X.; Zheng, H.B.; Xu, X.Q.; He, J.Y.; Ge, X.K.; Yao, X.; Cheng, T.; Zhu, Y.; Cao, W.X.; Tian, Y.C. Predicting grain yield in rice using multi-temporal vegetation indices from UAV-based multispectral and digital imagery. *ISPRS J. Photogramm. Remote Sens.* **2017**, *130*, 246–255.
31. Albetis, J.; Duthoit, S.; Guttler, F.; Jacquin, A.; Goulard, M.; Poilvé, H.; Féret, J.B.; Dedieu, G. Detection of Flavescence dorée grapevine disease using unmanned aerial vehicle (UAV) multispectral imagery. *Remote Sens.* **2017**, *9*, 1–21.

32. Romero, M.; Luo, Y.; Su, B.; Fuentes, S. Vineyard water status estimation using multispectral imagery from an UAV platform and machine learning algorithms for irrigation scheduling management. *Comput. Electron. Agric.* **2018**, *147*, 109–117.

33. Sultani, W.; Mokhtari, S.; Yun, H.B. Automatic pavement object detection using Superpixel segmentation combined with conditional random field. *IEEE Trans. Intell. Transp. Syst.* **2017**, *19*, 2076–2085.

34. Zhang, S.; Zhu, Y.; You, Z.; Wu, X. Fusion of superpixel, expectation maximization and PHOG for recognizing cucumber diseases. *Comput. Electron. Agric.* **2017**, *140*, 338–347.

35. Zhang, S.; Wang, H.; Huang, W.; You, Z. Plant diseased leaf segmentation and recognition by fusion of superpixel, K-means and PHOG. *Optik (Stuttg).* **2018**, *157*, 866–872.

36. Smith, R. South Texas cotton root rot draws study Available online: https://www.farmprogress.com/south-texas-cotton-root-rot-draws-study (accessed on Sep 23, 2019).

37. Tackenberg, M.; Volkmar, C.; Dammer, K.H. Sensor-based variable-rate fungicide application in winter wheat. *Pest Manag. Sci.* **2016**, *72*, 1888–1896.

38. Tackenberg, M.; Volkmar, C.; Schirrmann, M.; Giebel, A.; Dammer, K.H. Impact of sensor-controlled variable-rate fungicide application on yield, senescence and disease occurrence in winter wheat fields. *Pest Manag. Sci.* **2018**, *74*, 1251–1258.

39. Dammer, K.H.; Ehlert, D. Variable-rate fungicide spraying in cereals using a

plant cover sensor. *Precis. Agric.* **2006**, *7*, 137–148.

40. Xiuyun, X.; Xufeng, X.; Zelong, Z.; Bin, Z.; Shuran, S.; Zhen, L.; Tiansheng, H.; Huixian, H. Variable Rate Liquid Fertilizer Applicator for Deep-fertilization in Precision Farming Based on ZigBee Technology. *IFAC-PapersOnLine* **2019**, *52*, 43–50.
41. Takács, S.; Bíró, T.; Helyes, L.; Pék, Z. Variable Rate Precision Irrigation Technology for Deficit Irrigation of Processing Tomato. *Irrig. Drain.* **2019**, *68*, 234–244.
42. Zheng, Y.; Lin, S.; Kambhamettu, C.; Yu, J.; Kang, S.B. Single-image vignetting correction. *IEEE Trans. Pattern Anal. Mach. Intell.* **2009**, *31*, 2243–2256.
43. Fei, X.; Yu, R.; Li, L.; Wang, G. Adaptive PCA transforms with geometric morphological grouping for image noise removal. *Multimed. Tools Appl.* **2018**, *77*, 23353–23369.
44. Cocianu, C.; State, L.; Vlamos, P. A new adaptive PCA scheme for noise removal in image processing. *Proc. Elmar - Int. Symp. Electron. Mar.* **2008**, *1*, 129–132.
45. Texas County Map - texas maps Available online: http://mapsof.net/texas/texas-county-map.
46. Pal, M.; Mather, P.M. Support vector machines for classification in remote sensing. *Int. J. Remote Sens.* **2005**, *26*, 1007–1011.
47. Wang, T.; Alex Thomasson, J.; Yang, C.; Isakeit, T.; Nichols, R.L. Automatic Classification of Cotton Root Rot Disease Based on UAV Remote Sensing. *Remote Sens.* **2020**, *12*, 1310.

48. Isakeit, T.; Minzenmayer, R.R.; Drake, D.R.; Morgan, G.D.; Mott, D.A.; Fromme, D.D.; Multer, W.L.; Jungman, M.; Abrameit, A. Fungicide management of cotton root rot (Phymatotrichopsis omnivora): 2011 results. In Proceedings of the Proc. of the Beltwide Cotton Conf.; 2012; pp. 235–238.

49. Isakeit, T.; Minzenmayer, R.; Abrameit, A.; Moore, G.; Scasta, J.D. Control of phymatotrichopsis root rot of cotton with flutriafol. In Proceedings of the Proc. of the Beltwide Cotton Conf.; 2013; pp. 200–203.

50. Isakeit, T. Management of cotton root rot. In Proceedings of the Proc. of the Beltwide Cotton Conf.; 2018; p. 43.

51. Yang, C.; Odvody, G.N.; Fernandez, C.J.; Landivar, J.A.; Minzenmayer, R.R.; Nichols, R.L.; Thomasson, J.A. Monitoring cotton root rot progression within a growing season using airborne multispectral imagery. *J. Cotton Sci.* **2014**.

52. Easterday, K.; Kislik, C.; Dawson, T.E.; Hogan, S.; Kelly, M. Remotely sensed water limitation in vegetation: Insights from an experiment with unmanned aerial vehicles (UAVs). *Remote Sens.* **2019**, *11*, 1–19.

53. Huang, Y.; Thomson, S.J.; Brand, H.J.; Reddy, K.N. Development and evaluation of low-altitude remote sensing systems for crop production management. *Int. J. Agric. Biol. Eng.* **2016**, *9*, 1–11.

54. Mattupalli, C.; Moffet, C.A.; Shah, K.N.; Young, C.A. Supervised classification of RGB Aerial imagery to evaluate the impact of a root rot disease. *Remote Sens.* **2018**, *10*.

55. Duan, B.; Fang, S.; Zhu, R.; Wu, X.; Wang, S.; Gong, Y.; Peng, Y. Remote

estimation of rice yield with unmanned aerial vehicle (uav) data and spectral mixture analysis. *Front. Plant Sci.* **2019**, *10*, 1–14.

56. Herrmann, I.; Bdolach, E.; Montekyo, Y.; Rachmilevitch, S.; Townsend, P.A.; Karnieli, A. Assessment of maize yield and phenology by drone-mounted superspectral camera. *Precis. Agric.* **2020**, *21*, 51–76.
57. Cai, Y.; Guan, K.; Nafziger, E.; Chowdhary, G.; Peng, B.; Jin, Z.; Wang, S.; Wang, S. Detecting In-Season Crop Nitrogen Stress of Corn for Field Trials Using UAV-and CubeSat-Based Multispectral Sensing. *IEEE J. Sel. Top. Appl. Earth Obs. Remote Sens.* **2019**, *12*, 5153–5166.
58. Zhang, L.; Zhang, H.; Niu, Y.; Han, W. Mapping maizewater stress based on UAV multispectral remote sensing. *Remote Sens.* **2019**, *11*.
59. Su, J.; Liu, C.; Coombes, M.; Hu, X.; Wang, C.; Xu, X.; Li, Q.; Guo, L.; Chen, W. Wheat yellow rust monitoring by learning from multispectral UAV aerial imagery. *Comput. Electron. Agric.* **2018**, *155*, 157–166.
60. Matese, A.; Toscano, P.; Di Gennaro, S.F.; Genesio, L.; Vaccari, F.P.; Primicerio, J.; Belli, C.; Zaldei, A.; Bianconi, R.; Gioli, B. Intercomparison of UAV, aircraft and satellite remote sensing platforms for precision viticulture. *Remote Sens.* **2015**, *7*, 2971–2990.
61. Ball, G.H.; Hall, D.J. ISODATA, a novel method of data analysis and pattern classification. *Stanford Res. inst Menlo Park CA.* **1965**.
62. Hartigan, J.A.; Wong, M.A. Algorithm AS 136: A K-Means Clustering Algorithm. *J. R. Stat. Soc. Ser. C (Applied Stat.* **1979**, *28*, 100–108.

63. Breiman, L. Random forests. *Mach. Learn.* **2001**, *45*, 5–32.

64. Aha, D.W.; Kibler, D.; Albert, M.K. Instance-Based Learning Algorithms. *Mach. Learn.* **1991**, *6*, 37–66.

65. Burges, C.J.C. A tutorial on support vector machines for pattern recognition. *Data Min. Knowl. Discov.* **1998**, *2*, 121–167.

66. Chang, C.C.; Lin, C.J. LIBSVM: A Library for support vector machines. *ACM Trans. Intell. Syst. Technol.* **2011**, *2*, 27.

67. Dempster, A.P.; Laird, N.M.; Rubin, D.B. Maximum Likelihood from Incomplete Data Via the EM Algorithm. *J. R. Stat. Soc. Ser. B* **1977**, *39*, 1–22.

68. MacQueen, J. Some methods for classification and analysis of multivariate observations. *Proc. fifth Berkeley Symp. Math. Stat. Probab.* **1967**, *1*, 281–297.

69. De Maesschalck, R.; Jouan-Rimbaud, D.; Massart, D.L. The Mahalanobis distance. *Chemom. Intell. Lab. Syst.* **2000**, *50*, 1–18.

70. Mountrakis, G.; Im, J.; Ogole, C. Support vector machines in remote sensing: A review. *ISPRS J. Photogramm. Remote Sens.* **2011**, *66*, 247–259.

71. Gong, P.; Howarth, P.J. Land-use classification of SPOT HRV data using a cover-frequency method. *Int. J. Remote Sens.* **1992**, *13*, 1459–1471.

72. Lu, D.; Weng, Q. A survey of image classification methods and techniques for improving classification performance. *Int. J. Remote Sens.* **2007**, *28*, 823–870.

73. Fauvel, M.; Benediktsson, J.A.; Chanussot, J.; Sveinsson, J.R. Spectral and spatial classification of hyperspectral data using SVMs and morphological profiles. *IEEE Trans. Geosci. Remote Sens.* **2008**, *46*, 3804–3814.

74. Huang, X.; Weng, C.; Lu, Q.; Feng, T.; Zhang, L. Automatic labelling and selection of training samples for high-resolution remote sensing image classification over urban areas. *Remote Sens.* **2015**, *7*, 16024–16044.

75. Congalton, R.G. A review of assessing the accuracy of classifications of remotely sensed data. *Remote Sens. Environ.* **1991**, *37*, 35–46.

76. Huang, C.; Davis, L.S.; Townshend, J.R.G. An assessment of support vector machines for land cover classification. *Int. J. Remote Sens.* **2002**, *23*, 725–749.

77. Landis, J.R.; Koch, G.G. The Measurement of Observer Agreement for Categorical Data. *Biometrics* **1977**.

78. Effect of Cultural Distance on Translation of Culture-Bound Texts. *Int. J. Educ. Lit. Stud.* **2016**.

79. Streets, R.B.; Bloss, H.E. Phymatotrichum root rot. *Phytopathol. Monogr. 8* **1973**.

80. Mahlein, A.K.; Oerke, E.C.; Steiner, U.; Dehne, H.W. Recent advances in sensing plant diseases for precision crop protection. *Eur. J. Plant Pathol.* **2012**, *133*, 197–209.

81. Gogoi, N.K.; Deka, B.; Bora, L.C. Remote sensing and its use in detection and monitoring plant diseases: A review. *Agric. Rev.* **2018**, *39*, 307–313.

82. Qin, Z.; Zhang, M. Detection of rice sheath blight for in-season disease management using multispectral remote sensing. *Int. J. Appl. Earth Obs. Geoinf.* **2005**, *7*, 115–128.

83. Chen, X.; Ma, J.; Qiao, H.; Cheng, D.; Xu, Y.; Zhao, Y. Detecting infestation of take-all disease in wheat using landsat thematic mapper imagery. *Int. J. Remote*

Sens. **2007**, *28*, 5183–5189.

84. Barton, C.V.M. Advances in remote sensing of plant stress. *Plant Soil* **2012**, *354,* 41–44.

85. Hazaymeh, K.; K. Hassan, Q. Remote sensing of agricultural drought monitoring: A state of art review. *AIMS Environ. Sci.* **2016**, *3,* 604–630.

86. Gerhards, M.; Schlerf, M.; Mallick, K.; Udelhoven, T. Challenges and future perspectives of multi-/Hyperspectral thermal infrared remote sensing for crop water-stress detection: A review. *Remote Sens.* **2019**, *11*.

87. Calvão, T.; Pessoa, M.F. Remote sensing in food production - A review. *Emirates J. Food Agric.* **2015**, *27*, 138–151.

88. Campos, I.; González-Gómez, L.; Villodre, J.; Calera, M.; Campoy, J.; Jiménez, N.; Plaza, C.; Sánchez-Prieto, S.; Calera, A. Mapping within-field variability in wheat yield and biomass using remote sensing vegetation indices. *Precis. Agric.* **2019**.

89. Huang, Y.; Brand, H.J.; Sui, R.; Thomson, S.J.; Furukawa, T.; Ebelhar, M.W. Cotton yield estimation using very high-resolution digital images acquired with a low-cost small unmanned aerial vehicle. *Trans. ASABE* **2016**, *59*, 1563–1574.

90. Yang, C.; Odvody, G.N.; Thomasson, J.A.; Isakeit, T.; Minzenmayer, R.R.; Drake, D.R.; Nichols, R.L. Site-specific management of cotton root rot using airborne and high-resolution satellite imagery and variable-rate technology. *Trans. ASABE* **2018**.

91. Song, H.; Yang, C.; Zhang, J.; He, D.; Thomasson, J.A. Combining fuzzy set

theory and nonlinear stretching enhancement for unsupervised classification of cotton root rot. *J. Appl. Remote Sens.* **2015**, *9*, 096073.

92. Wang, T.; Thomasson, J.A.; Yang, C.; Isakeit, T.; Nichols, R.L. Automatic Classification of Cotton Root Rot Disease Based on UAV Remote Sensing. *Remote Sens.* **2020**, *12*, 1310.

93. Achanta, R.; Shaji, A.; Smith, K.; Lucchi, A.; Fua, P.; Susstrunk, S. SLIC Superpixels. *EPFL Tech. Rep. 149300* **2010**.

94. Achanta, R.; Shaji, A.; Smith, K.; Lucchi, A.; Fua, P.; Süsstrunk, S. SLIC superpixels compared to state-of-the-art superpixel methods. *IEEE Trans. Pattern Anal. Mach. Intell.* **2012**.

95. Haccius, C.; Hariharan, H.P.; Herfet, T.; Hach, T.; Cine, R.; Gmbh, T. Infrared-aided superpixel segmentation. *Int. Work. Video Process. Qual. Metrics Consum. Electron.* **2015**.

96. J. B. Wilkerson; J. H. Hancock; Moody, F.H.; M. A. Newman Design of a seed-specific application system for in-furrow chemicals. *Trans. ASAE* **2004**, *47*, 537–645.